DEVELOPMENT OF CONTROL ALLOCATION METHODS FOR SATELLITE ATTITUDE CONTROL

A THESIS SUBMITTED TO
THE GRADUATE SCHOOL OF NATURAL AND APPLIED SCIENCES
OF
MIDDLE EAST TECHNICAL UNIVERSITY

BY

TUBA ÇİĞDEM ELMAS

IN PARTIAL FULFILLMENT OF THE REQUIREMENTS
FOR
THE DEGREE OF MASTER OF SCIENCE
IN
AEROSPACE ENGINEERING

FEBRUARY 2010

Approval of the thesis:

DEVELOPMENT OF CONTROL ALLOCATION METHODS FOR SATELLITE ATTITUDE CONTROL

submitted by **TUBA ÇİĞDEM ELMAS** in partial fulfillment of the requirements for the degree of
Master of Science in Aerospace Engineering Department, Middle East Technical University by,

Prof. Dr. Canan Özgen
Dean, Graduate School of **Natural and Applied Sciences** ________________

Prof. Dr. Ȯzan Tekinalp
Head of Department, **Aerospace Engineering** ________________

Prof. Dr. Ozan Tekinalp
Supervisor, **Aerospace Engineering Dept., METU** ________________

Asst. Prof. Dr. İlkay Yavrucuk
Co-supervisor, **Aerospace Engineering Dept., METU** ________________

Examining Committee Members:

Asst. Prof. Dr. Demirkan Çöker
Aerospace Engineering Dept., METU ________________

Prof. Dr. Ozan Tekinalp
Aerospace Engineering Dept., METU ________________

Asst. Prof. Dr. Ali Türker Kutay
Aerospace Engineering Dept., METU ________________

Dr. Erhan Solakoğlu
Satellite Systems Dept., Turkish Aerospace Industries Inc. ________________

Emre Yavuzoglu
Satellite Systems Dept., Turkish Aerospace Industries Inc. ________________

Date: ________________

I hereby declare that all information in this document has been obtained and presented in accordance with academic rules and ethical conduct. I also declare that, as required by these rules and conduct, I have fully cited and referenced all material and results that are not original to this work.

Name, Last Name: TUBA ÇİĞDEM ELMAS

Signature :

ABSTRACT

DEVELOPMENT OF CONTROL ALLOCATION METHODS FOR SATELLITE ATTITUDE CONTROL

ELMAS, Tuba Çiğdem
M.S, Department of Aerospace Engineering
Supervisor : Prof. Dr. Ozan Tekinalp
Co-Supervisor : Asst. Prof. Dr. İlkay Yavrucuk

February 2010, 85 pages

This thesis addresses the attitude control of satellites with similar and dissimilar actuators and control allocation methods on maneuvering. In addition, the control moment gyro (CMG) steering with gyroscopes having limited gimbal angle travel is also addressed.

Full Momentum envelopes for a cluster of four CMG's are obtained in a pyramid type mounting arrangement. The envelopes when gimbal travel is limited to ±90°are also obtained. The steering simulations using Moore Penrose (MP) pseudo inverse as well as blended inverse are presented and success of the pre planned blended inverse steering in avoiding gimbal angle limits is demonstrated through satellite slew maneuver simulations, showing the completion of the maneuver without violating gimbal angle travel restrictions. Dissimilar actuators, CMG and magnetic torquers are used as an approach of overactuated system. Steering simulations are carried out using different steering laws for constant torque and desired satellite slew maneuver scenarios. Success of the blended inverse steering algorithm over MP pseudo inverse is also demonstrated.

Keywords: Satellite Attitude Control, Control Moment Gyro, Magnetorquer, Momentum Envelope, Steering Law

ÖZ

UYDU YÖNELİM KONTROLU İÇİN KONTROL DAĞILIM METHODLARININ GELİŞTİRİLMESİ

ELMAS, Tuba Çiğdem
Yüksek Lisans, Havacılık ve Uzay Mühendisliği Bölümü
Tez Yöneticisi : Prof. Dr. Ozan Tekinalp
Ortak Tez Yöneticisi : Yrd. Doç. Dr. İlkay Yavrucuk

Şubat 2010, 85 sayfa

Bu tezde benzer ve benzer olmayan artık eyleyiciler kullanarak uydu yönelim kontrolu ve manevra esnasındaki kontrol dagılım metodları anlatılmaktadır. Ayrıca, jiroskop limitli bir gimbal açısına sahip olduğu zaman Moment Kontrol Jiroskop (MKJ) sürüşü anlatılmaktadır.

Piramit şeklinde monte edilen MKJ kümesi için tüm momentum zarfı elde edilmiştir. Ayrıca, bu zarf gimbal hareket bölgesi $\pm 90°$olarak sınırlandırılması durumu için de elde edilmiştir. Moore Penrose (MP) sanki ters sürüşü ve karma ters sürüş teknikleri kullanılarak sürüş simulasyonları sunulmuştur ve uydu sürüş simulasyonu esnasında gimbal dönüş açısının limitlere erişmesinden kaçınarak önceden planlanmış karma sürüş tekniğinin başarısı ispatlanmıştır.

Artık eyleyicili sisteme bir yaklaşım olarak benzer olmayan eyleyiciler için MKJ ve tork çubuğu kullanılmıştır. Sürüş simulasyonları farklı sürüş yöntemleri kullanarak sabit tork ve istenen uydu yönelim manevra senoryaları için gerçekleştirilmiştir. Karma ters sürüş algoritmasının, MP sanki ters sürüşü üzerindeki başarısı gösterilmiştir.

Anahtar Kelimeler: Uydu Yönelim Kontrol, Moment Kontrol Jiroskop, Tork Çubuğu, Momentum Zarfı, Sürüş Yöntemleri

TO MY MOTHER

ACKNOWLEDGMENTS

I am heartily thankful to my supervisor, Prof. Dr. Ozan Tekinalp, whose encouragement, guidance and support from the initial to the final level enabled me to develop an understanding of the subject. He has made available his support in a number of ways, without his presence it would be impossible to finish my thesis.

I would like to thank Asst. Prof. Dr. İlkay Yavrucuk for his assistance and support and also for sharing his knowledge about control methods. I have furthermore to thank the committee members, Asst. Prof. Dr. Ali Türker Kutay, Asst. Prof. Dr. Demirkan Çöker, Dr. Erhan Solakoğlu, and Emre Yavuzoglu for joining to my presentation and sharing with me their invaluable knowledge about my work.

I would like to take the opportunity to thank those people who spent their time and shared their knowledge for helping me to complete my thesis with the best possible result: for all his help, support, interest and valuable hints, Onur Tarımcı especially on LaTeXformating. I would like to thank to my friends who worked with me in the same project Zeynep Çakır, Sinem Işık and Batu Demir for their support and enthusiasm. I also would like to thank Jaber Javanshir. I appreciate the useful discussions we had with Sharmila Kayastha. I would like to thank all my friends working in the same laboratory; Mehmet Katırcıoğlu, Deniz Yılmaz, Eser Kübalı, Emre Arslantaş for supporting me whenever I needed. Special thanks to all aerospace engineering department staff for their kind responses.

My lovely thanks goes to my sweet hearth Mina for giving me happiness and joy. Also, thanks to my friends Aslı - Cenk Çelikel for their support.

I can never thank enough my fiance Gökhan Üstün, who has supported me with such remarkable patience and sensivity. Without his love and encouragement, I could not have handled some hectic months with that much ease.

I sincerely thank to my sister Nihan for her endless love, support and energy through my life. She always encouraged me as she did in this masters program.

Last, but not least, I would like to express my deepest thanks to my mother for her love, unremitting support , understanding and patience throughout my life. She lightened all my way and made this work possible.

This thesis work is a result of projects conducted at the Simulation, Control and Avionics Laboratory of Middle East Technical University and supported by the Turkish Science and Technology Council, TUBITAK, Project No:107M346.

TABLE OF CONTENTS

LIST OF TABLES

TABLES

LIST OF FIGURES

FIGURES

LIST OF ABBREVIATIONS

$\mathbf{H}$	Spacecraft Total Angular Momentum
$\mathbf{h}$	Total Angular Momentum of Momentum Exchange Device
$\dot{\mathbf{h}}$	Angular Momentum Rate of Momentum Exchange Device
$\mathbf{I_s}$	Inertia Matrix of the Spacecraft
$\mathbf{T_{ext}}$	External Torque
$\mathbf{T_c}$	Control Torque
δ	Gimbal Angle
$\delta_\mathbf{i}$	Gimbal Angle of $i^t h$ CMG
$\dot{\delta}$	Precession of Gimbal Angle
$\mathbf{U}$	Total Gimbal Precession Rate of CMGs
$\mathbf{U_{MP}}$	Total Gimbal Precession Rate for MP-Inverse
$\mathbf{U_{SR}}$	Total Gimbal Precession Rate for SR-Inverse
$\mathbf{U_{BI}}$	Total Gimbal Precession Rate for B-Inverse
$\mathbf{J}$	Jacobian Matrix
β	Pyramid Skew Angle
$\mathbf{q}$	Blending Coefficient
ω	Angular Velocity
$\mathbf{q_e}$	Quaternion Direction Error
$\mathbf{K}$	Proportional Gain
$\mathbf{D}$	Derivative Gain
w_n	Natural Frequency
$\mathbf{M}$	Magnetic Dipole Moment
$\mathbf{B}$	Earth's Magnetic Field
$\mathbf{T_{mag}}$	Magnetic Torque
$\tau_{\mathbf{desired}}$	Desired Torque

LIST OF ACRONYMS

ADCS	Attitude Determination Control System
MW	Momentum Wheel
RW	Reaction wheel
CMG	Control Moment Gyroscope
SGCMG	Single Gimbal Control Moment Gyroscope
VSCMG	Variable Speed Control Moment Gyroscope
SSTL	Surrey Satellite Technology Ltd
MP	Moore Penrose Pseudo Inverse
SR	Singularity Robust
B	Blended Inverse
MTR 30	Magnetic Torquer Model

CHAPTER 1

INTRODUCTION

1.1 MOTIVATION

Control moment gyros (CMGs) for attitude control have been attracting the attention of many researchers since 1960's [9]. CMGs are in general can be much lighter than other momentum exchange devices like reaction and momentum wheels. Due to their inherit gyroscopic properties, CMGs can also generate higher control torques to rapidly maneuver spacecraft to the desired attitude. The direction of the angular momentum is determined by one or more motorized gimbal mechanisms. The number of controlled gimbals classifies CMGs as a single gimbal or double gimbal one. Single gimbal CMGs have many advantages of double gimbal CMGs with respect to the mechanical simplicity and ability to provide torque amplification [16].

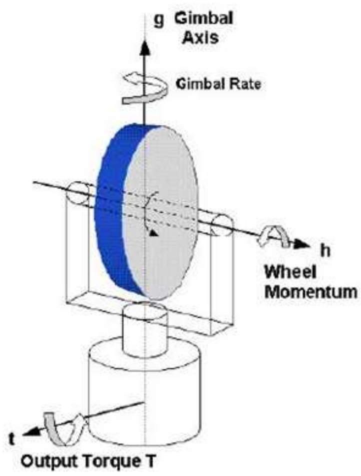

Figure 1.1: Single Gimbal Control Moment Gyroscope [16]

In this thesis single gimbal control moment gyroscopes (SGCMGs) are considered as momentum exchange devices (Figure 1.1). Originally CMGs were used in large spacecraft such as MIR, Skylab, and ISS (Figure 1.2) [33], due to the above properties, it has recently been attracting small satellite manufacturers as well. A CMG consists of a gimbaled flywheel at a continuous high spin rate (5000 rpm) and gimbal systems with high spin rates(30-90 deg/s) [15]. Torque is produced by rotating the gimbal to change the spin axis orientation of the flywheel with respect to the spacecraft [33]. Thus, mechanism complexity is the main fault of CMGs.

Figure 1.2: **I**nternational **S**pace **S**tation

CMGs with restricted gimbal travel mechanism were not extensively investigated in the past. When gimbal angle is restricted, the need for brush mechanism may be eliminated. Thus, when it is compared to the unrestricted one these features provide advantages and disadvantages to satellite depending on its mission profiles. Getting rid of the slip ring mechanism, we gain reduction in mass and reduction in noise levels in telemetry-telecommand lines. Slip ring is a complicated mechanism that is prone to wear out in time its elimination. Thus, it provides a longer service life and low mean time between failures. On the other hand, with unrestricted gimbal mechanism generated momentum envelope of CMG systems is much larger than restricted one in x and y axis. In addition, in restricted one if the satellites repeat same maneuver over and over, momentum dumping become necessary. Hence, these pros and cons should be carefully evaluated before deciding on the use of restricted gimbal travel mechanism. On the other hand, magnetic actuator is also a common attitude control device in small satellites. Magnetorquers are the magnetic actuators, also called as magnetic torquer, magnetic torque rods, are widely used for low Earth orbit, especially in small satellites and micro satellites for which number of control laws have been derived in the past [18]. Magnetorquers are designed to generate controllable magnetic dipole moments that interact with the Earth's magnetic field and generate torque for active control purposes for spacecraft [24]. CMGs and magnetorquers can provide torque without expending fuel or consumables. Other than momentum damping the use of these two actuator types together was not extensively investigated in the past.

The purpose of this thesis is to examine control allocation methods for satellites. In particular two problems are addressed; steering of CMG clusters with limited gimbal angle travel and methods of allocating controls to magnetorquers and CMGs when they are used together.

1.2 BACKGROUND

Use of CMGs as satellite attitude control actuators have been investigated since 1960's[9]. Margulies and Aubrun [19] were the first to formulate a theory of singularity and control for CMGs in 1978. They identified the geometrical properties of CMG, and properly discussed the singular surfaces of the momentum states. They also investigated the momentum envelope for different kind of CMG configurations. Nakamura and Hanafusa [21] developed the singularity to obtain approximate solution of gimbal rates allowing some torque error in the vicinity of singularity. In addition they proposed to add null motion to the particular solution to avoid singularities. Meffe [20] built up the momentum envelope for SGCMGs in pyramid configurations. The technique selected for built up envelope is cutting plane intersection with the array, as described in Stocking, et al [26]. Bedrossian et al [3, 2] presented in 1990, the steering laws for SGCMG. Moore-Penrose pseudo inverse with a null-motion algorithm was shown as an example of avoiding singularities for undirectional torque commands for which the existing algorithms fail. Singularity robust inverse was also introduced as an alternative to the pseudo inverse for computing torque - producing gimbal rates near singular states. They also recognized the similarities between the robotic manipulators and CMGs.Vadali et al [30] dealt with torque command generation using single gimbal control moment gyros and the determination of preferred initial gimbal angles for SGCMG systems to avoid internal singularities in 1991. A constrained steering law of pyramid type control moment gyros is presented by Kurukawa [12]. Then restricted workspace of angular momentum were identified and the momentum envelope was obtained. In addition, Kurukawa described the application of this method to the control of a MIR-type CMG system. Wie [33] presented the mathematical modeling of spacecraft and derivation of the kinematic equations,and identified the fundamental model of steering laws, MP-inverse Blended inverse, SR-inverse.

Lappas et al. [13] proposed a new attitude control system in their work. They properly explained the properties of CMGs and demonstrated differences between CMGs and other momentum exchange device as reaction wheel. They also designed a test bench for CMG to further understand the properties of CMG. Tekinalp and Yavuzoglu [28] developed a new inverse kinematic algorithm for redundant CMGs that provide singularity avoidance. In 2006, Lappas and Wie [15] described a robust CMG steering logic for CMGs with a mechanical gimbal angle constraint.

White et al.[31] were among the first to mention using magnetic torquers for spacecraft control in 1961. Their analysis examined the feasibility of using the interaction of the Earth's magnetic field and current-carrying coils in a fine-control attitude system. The first implementation of magnetic control was in spin-stabilized spacecraft. In 1965, Ergin and Wheeler [5] developed control laws for spin orientation control using a magnetic torque coil and discussed advantages of magnetic control. A similar analysis was also conducted by Wheeler [32] and Alfriend [1] for control laws for both error reduction and nutation damping for spin stabilized and dual-spin-stabilized satellites. The utility of magnetic torquers for satellite control has been well established for near-Earth orbits [22, 1]. Lovera et al.[18] using magnetic actuators try to solve the problem of attitude stabilization and disturbance torque attenuation for small spacecraft in 2002. Steyn [25] presented in his work a rule based on fuzzy controller and compared with an adaptive MIMO LQR controller in a low-earth-orbit small satellite attitude control system in 1994 and he controlled the attitude by gravity gradient stabilization and three-axis magnetorquer.

Rajarm and Goel [7] developed a closed-loop control law in 1979 which performed both attitude corrections and nutation damping for three-axis stabilized spacecraft with momentum bias. They used momentum wheel as a momentum exchange device. The yaw control is obtained by roll/yaw coupling established by the momentum wheel. An interesting feature of the proposed controller is that the nutational oscillations, arising due to transverse torquing, are also damped out, thus eliminating the need for half-precession cycle damping by reaction jets. They controlled the yaw by roll/yaw coupling established by the momentum wheel.

Rafal and Jacob [34] addressed the attitude control of spacecraft by applying a control synthesis for a spacecraft equipped with a set of magnetorquer coils. A linear matrix inequality-based algorithm was proposed for attitude control. They realized this by implementing the H_2 control synthesis.

1.3 ORIGINAL CONTRIBUTIONS

Main contributions of this thesis are;

a. CMG momentum envelopes for restricted and unrestricted gimbal angle travels are obtained.

b. For CMG steering while avoiding singular configurations and gimbal angle saturations is examined.

d. Using CMG and magnetorquer as dissimilar actuators, control allocation policy is developed.

1.4 SCOPE OF THE THESIS

The thesis is structured as follows:

In Chapter 2, attitude control and simulation code is described. Spacecraft dynamics model and actuator mathematical models are given. CMG cluster mounting arrangement are identified and control allocation methods for similar and dissimilar actuator types are analyzed. Next, momentum envelopes for pyramid mounting arrangement is identified. Finally, steering laws are explained to avoid system to get in the singular configuration.

In Chapter 3, gimbal angle restricted control moment gyroscope cluster is presented. First, momentum envelopes for pyramid mounting arrangement system for unrestricted and restricted gimbal angles are developed. Then, simulation models used for constant torque and satellite slew maneuver simulations are given.

In Chapter 4, steering simulations for dissimilar actuators, where CMGs and magnetorquers are used as actuators, are reported and the results are discussed.

In Chapter 5, conclusions and future works are given.

CHAPTER 2

ATTITUDE DYNAMICS AND CONTROL SYSTEM MODELS

2.1 INTRODUCTION

The primary mission of most satellites require attitude maneuvers through their entire life. The attitude control system is expected to stabilize the spacecraft and orient it to the desired directions despite the external disturbance torques acting upon it. In practice there are a lot of control examples in which the attitude control system is responsible such as;

- In orbital maneuvering and adjustment, the satellite must have a proper attitude to realize the desired $\mathbf{\Delta V}$.
- A spin stabilized satellite can be designed to keep the spin axis of its body pointed at some particular direction.
- In earth observation satellite, the satellite's payload must be pointed toward the target.

Attitude Determination Control System (ADCS) is composed of hardware and software. Hardware part is made up of actuators and sensors. Sensors provide attitude measurement in order to identify the spacecraft's attitude. Data collected from the sensors provide an attitude knowledge for the estimation algorithms of the ADCS software. On the other hand, actuators using attitude information coming from sensors provide to satellite to reach desired attitude. With respect to the momentum production, they can be distinguished between each other by internal and non-internal ones. Internal actuators are momentum exchange devices that generates torque for attitude control of a spacecraft by modifying their angular momentum. These are momentum wheels (MW), reaction wheels (RW) and control moment gyroscopes(CMG). Among them CMGs are the most powerful actuators due to their superior properties;

- They provide higher torque generation and provide high angular momentum capability which leads to a highly stable platform.
- They provide power, mass, and volume efficiency.
- Superior slew rates and also high precision tracking becomes possible with using CMGs [16, 35].

Because of these properties, in this thesis CMGs are used as an internal actuators. On the other hand, non-internal actuators produced only torque or force. These are magnetorquers and thruster. In this work, magnetorquers are used as non-internal actuators. They are also used extensively in the attitude control of spacecraft[24].

In this chapter, spacecraft dynamic equation, the control algorithm used as well as actuator models will be presented.

2.2 SPACECRAFT DYNAMICS

Total angular momentum of a spacecraft is expressed as the sum of spacecraft main body angular momentum and the angular momentum of the CMG cluster:

$$\mathbf{H_s} = \mathbf{I_s}\omega + \mathbf{h} \tag{2.1}$$

where $\mathbf{H_s}$ is the total angular momentum of the system with respect to the spacecraft's body-fixed control axis; $\mathbf{I_s}$ is the inertia tensor of the whole spacecraft including actuators, ω is the angular velocity vector of the spacecraft in the body fixed coordinate frame, and $\mathbf{h}$ is the total angular momentum of the momentum exchange devices.

According to the Newton's 2nd law, the rotational equations of motion of such a spacecraft may be written in the body fixed frame as:

$$\dot{\mathbf{H}}_{\mathbf{s}} + \omega \times \mathbf{H}_{\mathbf{s}} = \mathbf{T}_{\mathbf{ext}} \tag{2.2}$$

where, $\mathbf{T}_{\mathbf{ext}}$ is the sum of the external torques acting on the spacecraft (i.e.gravity gradient torque, solar radiation pressure). Combining Eq.2.1 and Eq.2.2, we simply obtain

$$\mathbf{I}_{\mathbf{s}}\dot{\omega} + \dot{\mathbf{h}} + \omega \times (\mathbf{I}_{\mathbf{s}}\omega + \mathbf{h}) = \mathbf{T}_{\mathbf{ext}} \tag{2.3}$$

In addition, by introducing the internal torque by momentum exchange devices, $\mathbf{T}_{\mathbf{c}}$, we get:

$$\mathbf{I}_{\mathbf{s}}\dot{\omega} + \omega \times \mathbf{I}_{\mathbf{s}}\omega = \mathbf{T}_{\mathbf{c}} + \mathbf{T}_{\mathbf{ext}} \tag{2.4}$$

where, $\mathbf{T}_{\mathbf{c}}$ is the control torque. The control torque for a spacecraft, controlled by using momentum exchange devices may be written as:

$$\mathbf{T}_{\mathbf{c}} = -\dot{\mathbf{h}} - \omega \times \mathbf{h} \tag{2.5}$$

$$\dot{\mathbf{h}} = \mathbf{T}_{\mathbf{c}} - \omega \times \mathbf{h} \tag{2.6}$$

where, $\dot{\mathbf{h}}$ is desired momentum rate of momentum exchange devices in Eq.2.6. $\mathbf{T}_{\mathbf{c}}$ is assumed to be known by using proper steering law design. With the implementation of the additional differential equations that relate body rates to the attitude parameters (i.e, quaternion, Euler angles, etc.) spacecraft attitude control are realized.

2.3 SPACECRAFT ATTITUDE CONTROL ALGORITHM

For achieving the desired maneuver proper control algorithms have to be used. In this thesis, Quaternion feedback controller is used to get desired control input $\mathbf{T_c}$ as in Eq.2.5. In this section we are analyzed to Figure 2.1 to examined that how the realized torque is obtained to steer the spacecraft to desired attitude.

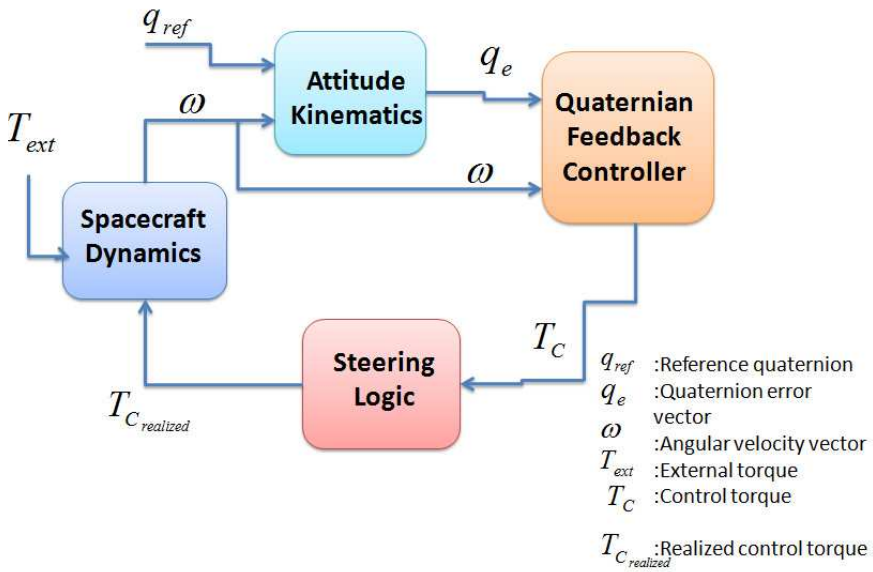

Figure 2.1: Attitude Control System Block Diagram

2.3.1 Quaternion Feedback Controller

The block diagram of the control system is shown in Figure 2.1. As it is seen in Figure 2.1 quaternion error vector $\mathbf{q_e}$ and angular rate vector ω are fed in to the feedback control system to obtain input control, $\mathbf{T_c}$. A control law with feedback terms due to the attitude error and angular rate vectors is used [33]:

$$\mathbf{T_c} = -\mathbf{K}\mathbf{q_e} - \mathbf{D}\omega \tag{2.7}$$

In the above equation, $\mathbf{q_e} = [\mathbf{q_{1e}}, \mathbf{q_{2e}}, \mathbf{q_{3e}}]^\mathbf{T}$ is the attitude quaternion error vector between the desired or commanded attitude quaternion and the current quaternion. The feedback gain matrices **K** and **D** shall be properly selected for asymptotic stability and transient performance of the system. Where **K** is the proportional controller gain matrices, with the proper selection it provides the reduces both the rise time and steady state error, and **D** is the derivative control gain matrices, it provides the increase of the stability of the system, reduces the overshoot and improves the transient response. One choice would be to use, $\mathbf{K} = \mathrm{k}\mathbf{I_s}$ and $\mathbf{D} = \mathrm{d}\mathbf{I_s}$ [28] where, $d = 2\xi\ \omega_n$ and $k = 2\omega_n^2$. ξ is the damping ratio and w_n is the natural frequency. When designing control system ξ value is commonly chosen 0.707 as a reason of optimally damped system, and also settling time t_s is taken **150s** [16].

$$t_s = \frac{4}{\xi\omega_n} \tag{2.8}$$

Thus, k and d values are easily found with respect to these common values.

$$k = 0.0016, \quad d = 0.04 \tag{2.9}$$

2.4 ACTUATOR MODEL

2.4.1 CONTROL MOMENT GYROSCOPE

A control moment gyro (CMG) system is a torquer for three axis attitude control of an artificial satellite. It consist of a spinning wheel, with constant or varying speed, gimbaled in one or two axes. If the wheel is spinning with different velocity, CMG called Variable Speed CMG (VSCMG)[16]. With respect to the gimbal axes, CMGs can be categorized as Single Gimbal CMG and Double Gimbal CMG. Depending on the mathematical modeling and cost expenditure SGCMGs is the most desired model among the other configurations. In this thesis SGCMG model is used.

2.4.1.1 Configuration Type of CMG

For full three axis control in spacecraft at least 3 CMGs are needed. However to reduce to gimbal saturation, many redundant CMG array configurations have been proposed in the past[11]. There have been different number of CMG usage for various configuration types such as pyramid, symmetric, and skew. Among them in this work, SGCMGs which have 4 CMG units are used in typical pyramid mounting type of arrangement.

The 4 pyramid type CMG system consist of 4 single gimbal CMGs (SGCMG) each positioned on one face of a 4-sided pyramid such that the momentum vector lies in this plane. Figure 2.2 shows the pyramid arrangement of 4 CMG cluster.

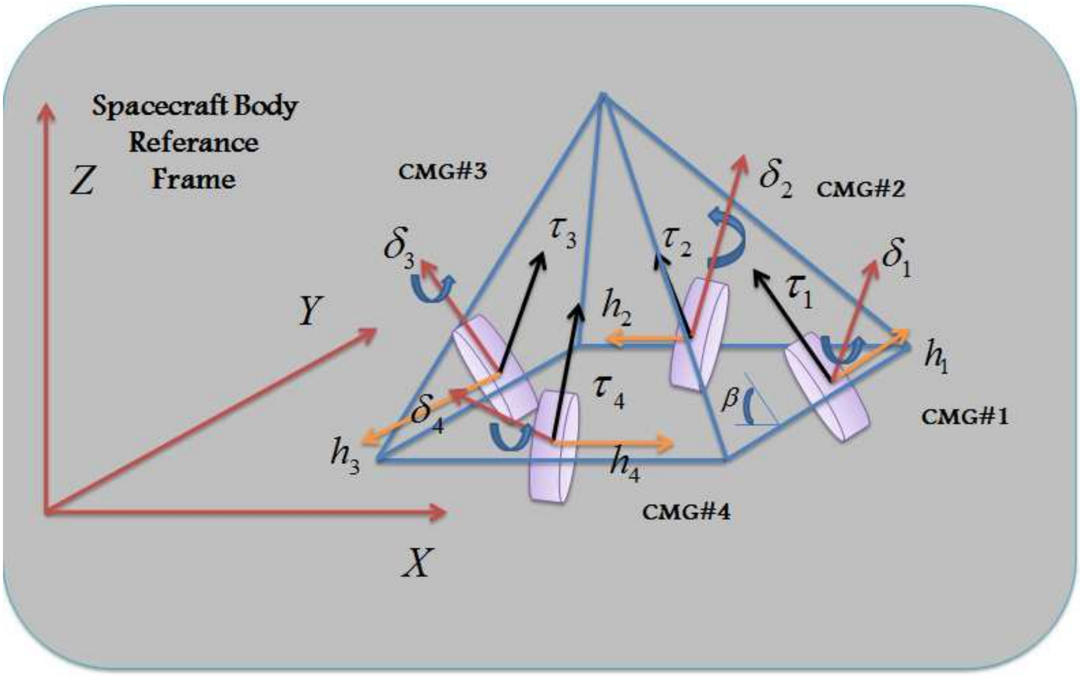

Figure 2.2: Typical pyramid configuration for 4 CMG cluster

In Figure 2.2 shows the four SGCMG cluster are constrained to gimbal on the face of a pyramid and the gimbal axes are orthogonal to the pyramid faces. Each surfaces of the pyramid is inclined with the pyramid skew angle $\beta = \mathbf{53.13}°$. This provides the fully three axis control with almost equal momentum capability in all three axes with minimum redundancy [33, 35]. Section 2.4.1.4 is fully devoted with this subject.

2.4.1.2 Formulation of Steering Laws

Steering laws are the necessary tools for satellite attitude control. With proper formulation of steering laws, satellite can achieve the desired slew maneuvers. Output of steering laws give the control torque $\mathbf{T_c}$ of satellite to realized desired attitude. Without proper steering laws set of CMGs get into the singular configurations of the momentum state, that causes no torque generation in desired direction. Formulation of the problem can be started from momentum vector. CMG angular momentum vector of h is function of CMG gimbal angle.

$$\mathbf{h} = \mathbf{h}(\delta) \tag{2.10}$$

Then time derivative of **h** can be obtained as:

$$\dot{\mathbf{h}} = \mathbf{J}(\mathbf{U})\,\mathbf{U} \tag{2.11}$$

where **U** is the gimbal precession rate vector of the CMG cluster. $\mathbf{J}(\delta)$ is the $\mathbf{3 \times n}$ matrix which is the Jacobian of the angular momentum map. n is the number of CMG actuators used to maneuver the spacecraft. Singularity condition means at the certain gimbal angle configurations the Jacobian matrix loses its rank, $rank(J) < 3$, in which case there exist a direction in space where torque production of the cluster is unavailable.

$$\mathbf{J}(\delta) = \frac{\partial \mathbf{h}(\delta)}{\partial \delta} \tag{2.12}$$

To purpose of steering law is to obtain best gimbal angle trajectories to get control torque necessary for the desired maneuver and passing through singular configurations. In actuator steering problem, inertias of gimbal and dynamics of the gimbal torquers are ignored due to their effects are negligible[28]. Steering laws are completely analyzed in Section 2.5

2.4.1.3 Control Allocation Algorithm With CMG Cluster

In this section, CMG based attitude control algorithm in a typical pyramid mounting arrangement is analyzed. Angular momentum of a cluster of four CMGs in a pyramid configuration may be written as:

$$\mathbf{h} = h_0 \left\{ \begin{array}{c} \cos\beta(-\sin\delta_1 + \sin\delta_2) - cos\delta_2 + \cos\delta_4 \\ \cos\delta_1 - \cos\delta_3 - \cos\beta(\sin\delta_2 + \sin\delta_4) \\ \sin\beta(\sin\delta_1 + \sin\delta_2 + \sin\delta_3 + \sin\delta_4) \end{array} \right\} \tag{2.13}$$

In the above equation each wheel is assumed to have an angular momentum of h_0 that is **0.1 Nm.s**, β is the pyramid skew angle and, $\delta_{\mathbf{i}}$ are the gimbal angles of each CMG in the cluster[27].

The control is to be realized through $\mathbf{T_{Crealized}}$, Eq.2.14 which we manipulate. Thus, for a satellite with four CMGs mounted in a pyramid configuration, $\mathbf{T_{Crealized}}$ can respectively be written.

$$\mathbf{T_{Crealized}} = \mathbf{JU} \tag{2.14}$$

$$\mathbf{U} = [\dot{\delta_1}\ \dot{\delta_2}\ \dot{\delta_3}\ \dot{\delta_4}] \tag{2.15}$$

$$\mathbf{J} = ho \left\{ \begin{array}{cccc} -\cos\beta\cos\delta_1 & \sin\delta_2 & \cos\beta\cos\delta_3 & -\sin\delta_4 \\ -\sin\delta_1 & -\cos\beta\cos\delta_2 & \sin\delta_3 & \cos\beta\cos\delta_4 \\ -\sin\beta\cos\delta_1 & \sin\beta\cos\delta_2 & \sin\beta\cos\delta_3 & \sin\beta\cos\delta_4 \end{array} \right\} \tag{2.16}$$

In above equations, J is the Jacobian matrix of the angular momentum whereas U is the input control matrix.

2.4.1.4 Momentum Envelope of 4 CMG Cluster

Single-gimbal control moment gyroscopes (SGCMG) have been implemented into a spacecraft to provide control torques is the design of an effective steering algorithm. These devices are mechanically installed in proper geometries to provide the necessary torque. In this thesis pyramid mounting arrangement system of Figure 2.2 is used.

The major objective for any steering approach has been the avoidance of singular states that preclude torque generation in a certain direction, the singular direction. This situation occurs when all individual CMG torque outputs are perpendicular to this direction, or equivalently, the individual momentum have extremal projections onto this direction. These conditions, if not properly addressed, it seriously prevent the usable momentum capability of the CMG system.

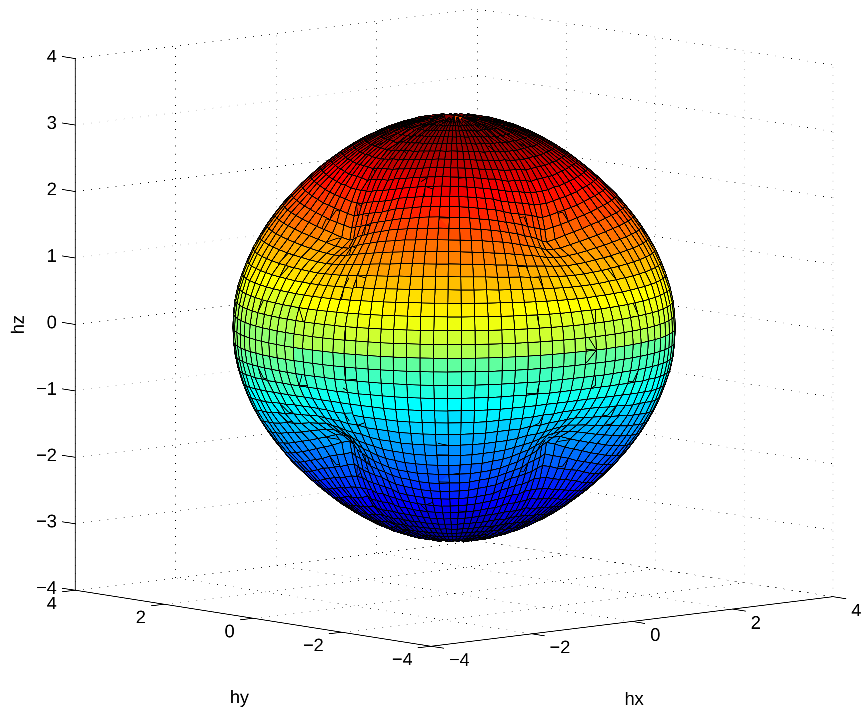

Figure 2.3: Momentum envelope for 4 CMG in the pyramid configuration

Although the extra degrees of freedom provided by adopting redundant CMG systems may reduce the possibility of encountering singular states, singular configurations cannot be eliminated. These systems, however, usually possess alternative nonsingular configurations for any given total momentum state.

The steering laws used to implement the pyramid type arrays are well understood; however the visualization of the arrays capabilities in three dimensional space is difficult. To determine the capabilities of an array, it is necessary to determine the momentum singularity surfaces produced by the array configuration. The total momentum directions of the CMG arrays in pyramid configuration gives the momentum envelope Figure 2.3. Each point of an envelope show the system momentum capability on that direction.

The gimbal axes δ_i of the pyramid arrangement of 4 CMG system are arranged normal to the surfaces of regular pyramid configuration Figure 2.2. The system input's are δ_i and the pyramid skew angle β. For nearly spherical momentum envelope β is taken 53.13 °.

While obtaining momentum envelope, singularity surfaces are identified. Each point on a singularity surfaces represents a system momentum condition for which the available system torque in some direction is zero.

2.4.2 MAGNETIC TORQRODS

Magnetic torqrods (Magnetorquers) are composed of magnetic coil and rods. When the coil is energized, rods produced input control torque for satellite maneuver. Produced torque can be written as;

$$\mathbf{T_M} = \mathbf{M} \times \mathbf{B} \tag{2.17}$$

where **M** is the generated magnetic dipole moment inside the body produced by the magnetic torqrods and **B** is the Earth's magnetic field intensity taken as a perpendicular to magnetic dipole moment[24]. Eq.2.17 can be written in matrix form as;

$$\mathbf{T_M} = \left\{ \begin{array}{ccc} 1_x & 1_y & 1_z \\ M_x & M_y & M_z \\ B_x & B_y & B_z \end{array} \right\} \tag{2.18}$$

Eq.2.18 can also be written as;

$$\mathbf{T_M} = \left\{ \begin{array}{c} T_{MX} \\ T_{MY} \\ T_{MZ} \end{array} \right\} = \left\{ \begin{array}{ccc} 0 & B_z & -B_y \\ -B_z & 0 & B_x \\ B_y & B_x & 0 \end{array} \right\} \left\{ \begin{array}{c} M_X \\ M_Y \\ M_Z \end{array} \right\} \tag{2.19}$$

Also, magnetorquer is the actuator that provide desired torque to satellite. $\mathbf{T_M}$ can also be called control torque $\mathbf{T_c}$. In this thesis, SSTL magnetorquer MTR-30 model is used, Figure 2.4. Properties of MTR-30 totally can be seen in Table 2.1.

Table 2.1: MTR-30 Properties

	MTR-30
Number of Coils	one
Mass	725 g
Length	371
Rod or width / height	60 mm × 39 mm
Resistance	62 Ω
Inductance	3.5 H
Magnetic Moment	30 Am^2 @ 200 mA
Scale factor	0.15 Am^2/mA
Magnetic Remanence	< ± 0.1 Am^2
Linearity	± 5 %
Saturation Current	> 230 mA
Connector	9 - way SD D-type

MTR-30 series are capable of providing reliable attitude control to demanding missions. The main purposes of this redundancy are extension of the generated torque level. It is designed to operate from a minimum of 5 volts and produces a magnetic moment of maximum $30Am^2$.

Figure 2.4: MTR-30 series Magnetorquer Rod[36]

Magnetic field as it can be seen from Figure 2.5 must be measured by the sensors or estimated by employing a field model in order to control the magnetorquers and model magnetorquers dynamics. It has three component of Earth's magnetic field intensity with respect to inertial frame[10].

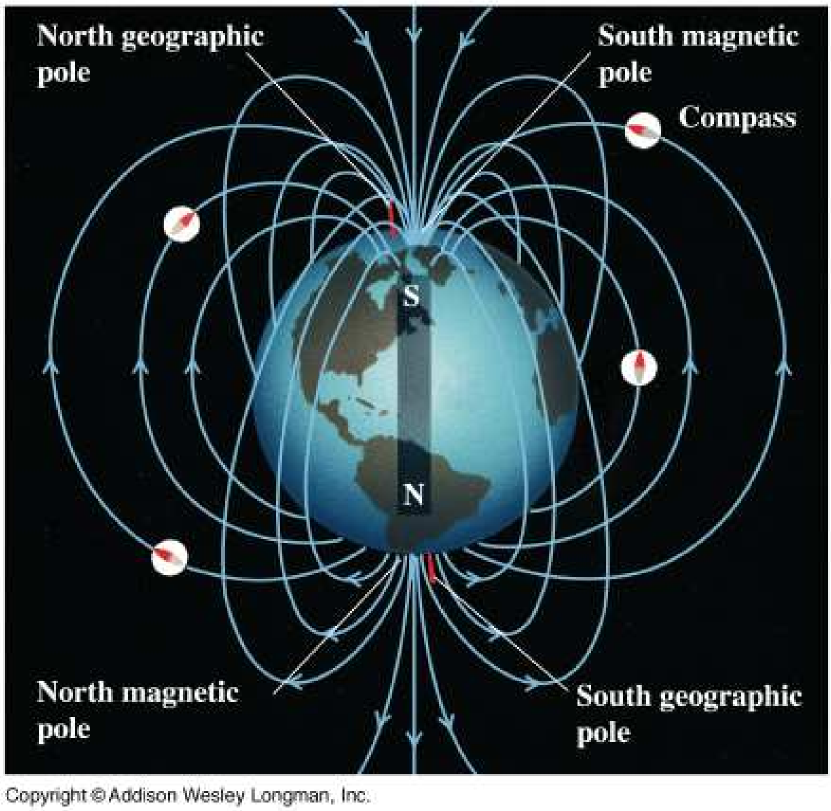

Figure 2.5: Earth's magnetic field dipole model [38]

In this thesis, magnetic field vector is taken as $[0.3; 0.8; 0.52] \times (48 \times 10^{-6})$ T. Magnetic field transformation from inertial frame to satellite body frame are calculated using quaternion rotation [6]. To apply desired torque on the satellite $\mathbf{T_M}$, magnetic moment vector $\mathbf{M}$ must be generated. However, inverse of the matrix in Eq.2.19 can not be taken since this matrix is always singular. Under this circumstances control magnetic dipole vector $\mathbf{M}$ cannot be generated from Eq.2.19. Using vector product by $\mathbf{B}$ on both sides Eq.2.17 becomes;

$$B \times T_c = B \times (M \times B) = B^2 M - B(M.B) \tag{2.20}$$

Using some simplifying assumptions, control magnetic dipole moment can be found. When applied **M** perpendicular to the Earth's magnetic field **B**, solution of $\mathbf{M} \cdot \mathbf{B}$ (which is a scalar product) gives zero. Thus, Eq. 2.20 turns to Eq.2.21;

$$M = \frac{1}{B^2} \left\{ B \times T_c \right\} \tag{2.21}$$

A control law with feedback terms due to the attitude error in terms of quaternion and angular rate vectors is as mentioned in Section 2.4.1.3.

$$T_c = -Kq_e - D\omega \tag{2.22}$$

As Section 2.4.1.3 the above equation, $q_e = [q_{1e}, q_{2e}, q_{3e}]^T$ is the quaternion direction error vector between the desired quaternion and the current quaternion. The feedback gain matrices **K** and **D** shall be again properly selected for asymptotic stability and transient performance of the system. One choice would be to use, $\mathbf{K} = k\mathbf{I}$ and $\mathbf{D} = d\mathbf{I}$ [28].

2.5 STEERING LAWS

In this section, singularity avoidance steering laws are analyzed. In the literature many steering laws have been proposed to escape the CMG cluster from singular configurations[3, 33]. A steering law is a method to find actuator inputs to obtain desired torques. For CMGs, these commands are gimbal rates whereas for magnetorquer, these are the magnetic dipole moments.

An ideal steering law is expected to avoid singularity while realizing the commanded torque. For the typical pyramid mounting arrangement of four SGCMG cluster, commanded torque, directly related with the gimbal precession rate, is obtained using steering law. torque realized as in Eq.2.14.

$$\tau_{\mathbf{realized}} = \mathbf{JU} \tag{2.23}$$

$$\dot{\mathbf{h}} = \mathbf{J}(\delta)\mathbf{U} \tag{2.24}$$

where $\mathbf{U}$ is the gimbal angle rates vector of CMG cluster. $\mathbf{J}(\delta)$ Jacobian matrix of angular momentum vector for CMG pyramid mounting arrangement. The requirement of a control torque in each of the three axis of spacecraft is expressed by the rank of the CMG system's Jacobian matrix. Since the redundant actuators of Jacobian matrix is rectangular form, it is hard to take inverse of the matrix. That means, if $rank(J) < 3$ CMG no longer produce torque in that direction. Some of the methods are investigated to overcome singularity problem.

2.5.1 Moore-Penrose Pseudo Inverse

Among the other steering laws the most basic one is Moore-Penrose pseudo inverse method (MP-inverse) to find gimbal precession rate. This inversion finds the $\mathbf{U}$ of minimum magnitude.

$$\mathbf{U_{MP}} = \mathbf{J^T}\,[\mathbf{JJ^T}]^{-1}\,\tau_{\mathbf{desired}} \tag{2.25}$$

The major drawback of MP-inverse is that it gets singular when the Jacobian matrix losses its rank in which case the singularity measure defined as Eq.2.26 becomes zero, causing the entries of $\mathbf{U_{MP}}$ reach very high values.

$$m = det(\mathbf{JJ}^T) \tag{2.26}$$

2.5.2 Singularity Robust Inverse

The Other inversion approaches is singularity robust inverse (SR) method [21]. It is presented by Nakamura and Hanafusa for over come singularities of robotic manipulator, which have many similarities with CMGs. This method can be derived from the minimization problem, Eq.2.28 that solutions give the gimbal rate.

$$U = J_{new}\tau_{desired} \tag{2.27}$$

$$\min_{U} \frac{1}{2}\left\{ U^T Q U + \tau_e^T R \tau_e \right\} \tag{2.28}$$

Q and R are the positive definite weighting matrices, respectively $\mathbf{I_3}$ and $\lambda\mathbf{I_4}$ where λ is the singularity avoidance parameter. $\tau_{\mathbf{e}} = \mathbf{JU} - \tau_{\mathbf{desired}}$ Solution of the problem gives that;

$$L_U = J(\delta)^T Q(J(\delta)U - \tau_{desired}) + RU = 0 \tag{2.29}$$

Solution of this minimization problem gives the new Jacobian matrices;

$$\mathbf{J_{new}} = \mathbf{J^T}[\lambda\mathbf{I} + \mathbf{JJ^T}]^{-1} \tag{2.30}$$

where $\mathbf{J_{new}}$ shows the new Jacobian matrix for SR inverse technique, thus for easy calculation , it can be written for SR inverse steering $\mathbf{J} = \mathbf{J_{new}}$. λ is a scalar that properly selected with respect to singularity measure, $\mathbf{m}$. When λ is taken zero, equation will close to MP inverse algorithm[21]. Then, Eq.2.27 turns that;

$$\mathbf{U_{SR}} = \mathbf{J^T}[\lambda\mathbf{I} + \mathbf{JJ^T}]^{-1}\tau_{\mathbf{desired}} \tag{2.31}$$

$$\lambda = \begin{cases} 0 & \text{for } m \geq m_0 \\ \lambda_0(1 - m/m_0)^2 & \text{for } m < m_0 \end{cases} \tag{2.32}$$

λ can also be calculated with the technique that used in ref. [30].

$$\lambda = \lambda_0 \, e^{-\mu \det(JJ^T)} \tag{2.33}$$

Disadvantage of SR inverse method is in some singularity type, the success of the algorithm is limited. Because of this failure, the recently developed algorithm which called as Blended Inverse (BI) are examined that helps through singularities while attaining desired controls at the same time.

2.5.3 Blended Inverse Algorithm

To steer the spacecraft in a stable fashion one needs to realize Eq.2.14. On the other hand to avoid singularities, one needs to specify inputs away from singular configurations, or gimbal saturations. Because of these needs Blended inverse (B-inverse) algorithm is derived as a mixed minimization problem between the desired inputs and desired torque[28].

$$\min_{U} \frac{1}{2} \left\{ \; U_e^T \, Q \, U_e + \tau_e^T \, R \, \tau_e \; \right\} \tag{2.34}$$

In this equation, $\mathbf{U_e} = \mathbf{U} - \mathbf{U_{desired}}$ where U is the realized gimbal rate vector $U_{desired}$ is the desired one, $\tau_\mathbf{e} = \mathbf{JU} - \tau_\mathbf{desired}$, while $\mathbf{Q}$ and $\mathbf{R}$ are symmetric positive definite weighting matrices. The solution of the above minimization problem gives the compromise between these two objectives:

$$U = [Q + J^T RJ]^{-1} [Q \, U_{desired} + J^T \, R \, \tau_{desired}] \tag{2.35}$$

$\mathbf{I_n}$, indicating an $\mathbf{n} \times \mathbf{n}$ unit matrix, and selecting weighting matrices as: $\mathbf{Q} = \mathbf{qI_n}$ where q is the blending coefficient and $\mathbf{R} = \mathbf{1_3}$,then the expression Eq.2.35 becomes,

$$U_B = [q 1_n + J^T J]^{-1} [q \, U_{desired} + J^T \, \tau_{desired}] \tag{2.36}$$

$$\tau_{realized} = J\, U_B \tag{2.37}$$

Eq.2.37 gives solutions of previous mentioned steering laws. Such as if $U_{desired} = 0$ equation turns the solution of SR inverse. On the other hand, if q ; blending coefficient equal to zero, this time equation turns the MP-inverse algorithm.

As it is understood from the singularity analysis that this algorithm is never singular[28]. An alternate but computationally more efficient form of the B-inverse algorithm may be given as:

$$U_B = [1_n - \beta J^T (1_3 + \beta J J^T)^{-} 1 J](U_{desired} + \beta J^T \tau_{desired}) \tag{2.38}$$

where, $\beta = 1/q$.

CHAPTER 3

GIMBAL ANGLE RESTRICTED CONTROL MOMENT GYROSCOPE CLUSTER

3.1 INTRODUCTION

Any equipment to fly in space has to be designed to withstand the harsh environment of the launch conditions as well as the orbit environment. They should also be reliable and capable to operate during the entire mission of the satellite. These conditions require the use of aerospace quality components during design and manufacturing. Brushless DC motors has attracted the attention of aerospace industry due to their long service life and low mean time between failures, primarily because they eliminated the brush mechanisms.

Figure 3.1: Slip Ring [37]

The control moment gyros have to use brush mechanisms, or slip rings (Figure 3.1), to pass the required power to the inner, gimbaled, spinning wheel together with the signals related to its control and condition monitoring. Figure 3.2 shows an element of CMG mechanism which has a slip ring. These slip-ring mechanisms can be up to ten channels depending on the number of monitoring signals that one should carry.

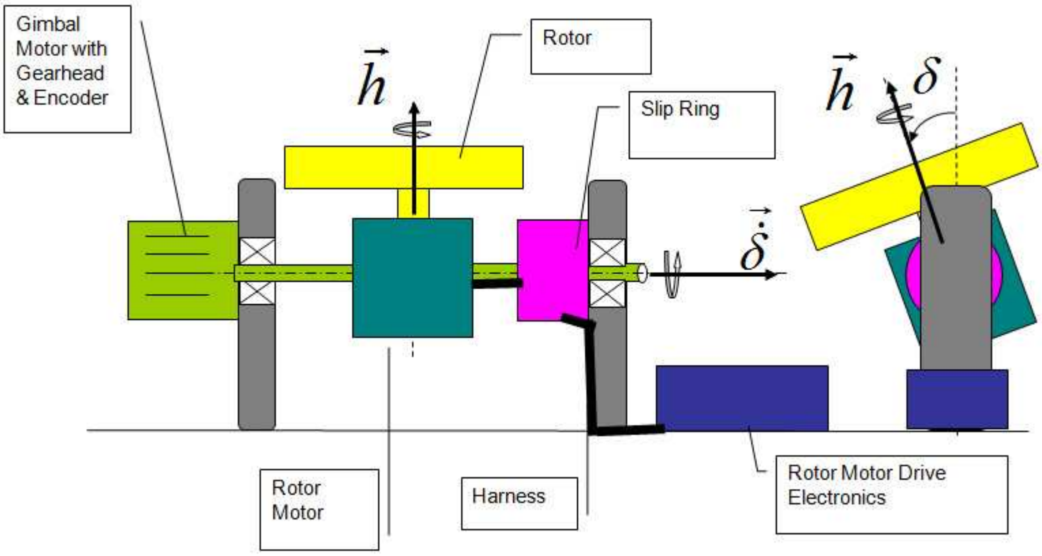

Figure 3.2: Elements of a CMG

An alternate CMG concept would be to restrict gimbal angles and pass the power and other electrical signals to the rotor using flexible cables[15]. As it is seen from the Figure 3.3 without slip ring mechanism, gimbal rotation angle becomes restricted. This shall intuitively alter, and reduce the momentum capability of the CMG mechanism in certain directions causing the cluster to reach the saturation singularity much earlier in those directions. In addition, a steering logic may require gimbal angles beyond the limitation imposed on them.

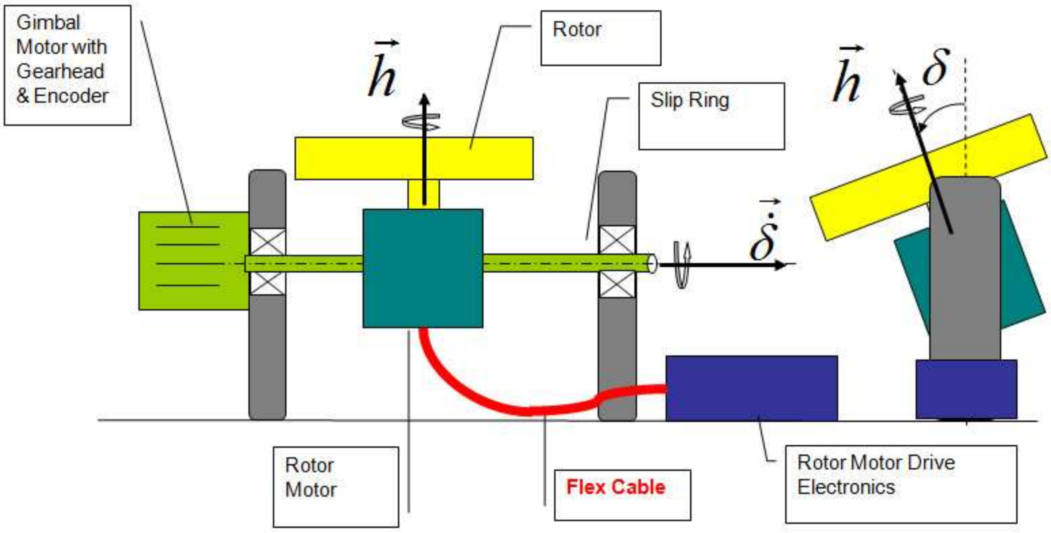

Figure 3.3: CMG mechanism without a slipring

The momentum envelope of such CMG mechanisms has not been investigated throughly in the past. The avoidance of transition through internal singularities of such clusters is also a major issue.

In this chapter, full momentum envelopes for a cluster of four CMGs in a pyramid mounting arrangement are obtained. The envelopes when gimbal travel is limited to ±90 °are also presented. CMG steering simulations using Moore Penrose pseudo inverse as well as Blended inverse (B-inverse) are presented, and success of the pre planned blended inverse while avoiding gimbal angle limits is demonstrated. Also given is a successful satellite slew maneuver example using blended inverse, showing the completion of the maneuver without violating gimbal angle travel restrictions. The purpose of this chapter is to examine the momentum envelopes when gimbal angle travels are limited and to address the issue of avoiding gimbal saturations during a maneuver.

3.2 GIMBAL ANGLE RESTRICTED MOMENTUM ENVELOPE

In this section momentum envelope for four CMG cluster in a pyramid mounting arrangement with pyramid skew angle of $\beta = \mathbf{53.13}°$are presented. Figure 3.4 shows the momentum envelope of such a cluster. It may be observed from the figure that this is a nearly spherical momentum envelope. The $h_x = 0$, $h_y = 0$, and $h_z = 0$ plane cross sections of this CMG full envelope are respectively given figures 3.5a, 3.5b and 3.5c. It may also be observed from these figures that the envelope has a nearly circular cross section along the $h_z = 0$ plane. It is possible to realize any angular momentum vector within this envelope. In fact there are infinite number of gimbal angle solutions that satisfy the angular momentum vector as it may be observed from Eq.2.13. However, at the boundary of the momentum envelope, the gimbal angle solutions are unique. In addition, there are some points where singularity measurement are zero $m = det(\mathbf{JJ^T})$ and torque production does not occur.

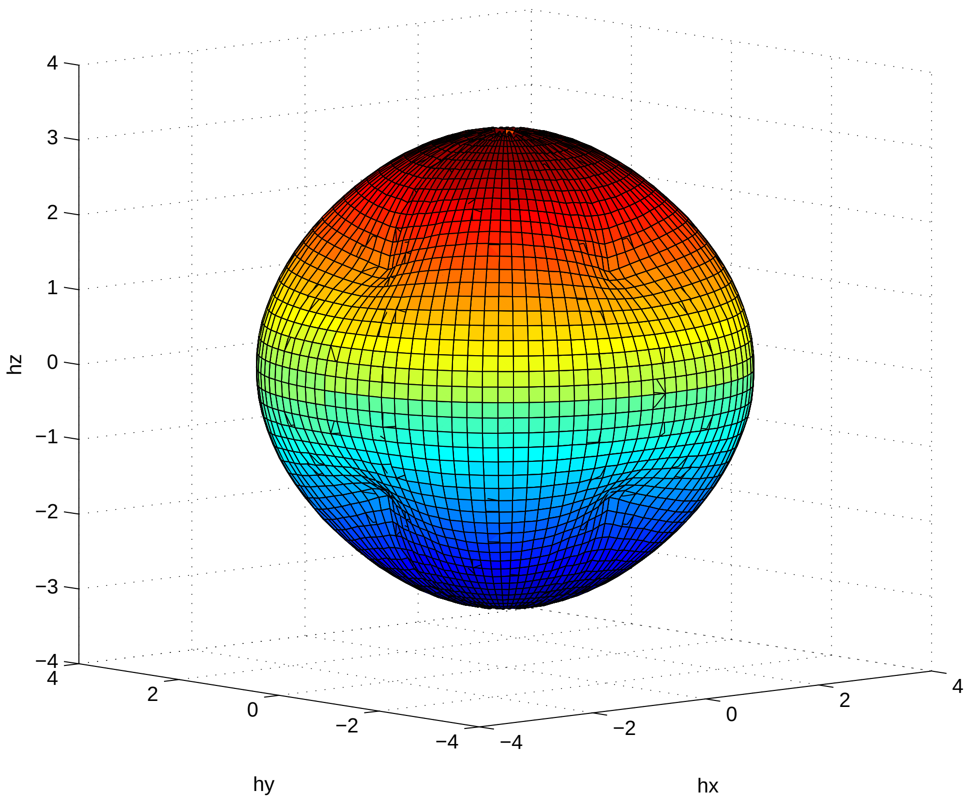

Figure 3.4: CMG momentum envelope for a cluster of four CMGs

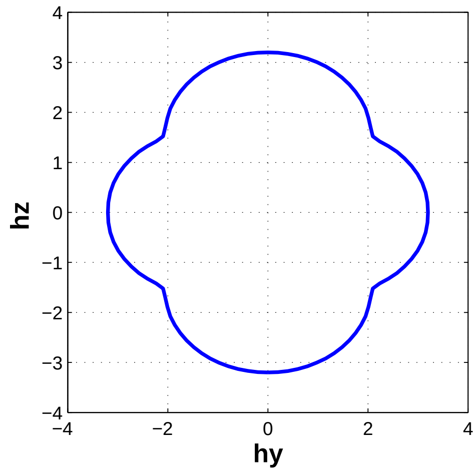

(a) Momentum Envelope cross section along $h_x = 0$ plane

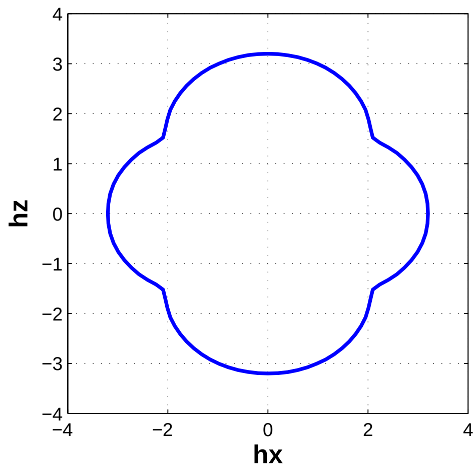

(b) Momentum Envelope cross section along $h_y = 0$ plane

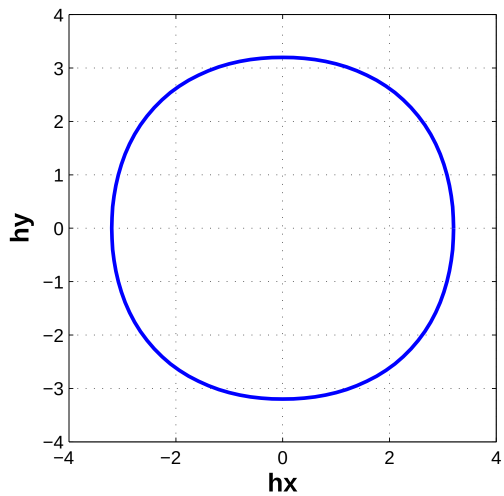

(c) Momentum Envelope cross section along $h_z = 0$ plane

Figure 3.5: Momentum envelope cross section areas along $h_x = 0, h_y = 0 and h_z = 0$ planes

When the gimbal angles are restricted, the envelope will no longer be spherical. Figure 3.6 shows the momentum envelope of the previous cluster when the gimbal travel is restricted to -90°< δ_i <90°interval. The vertical and horizontal plane cross sections of this envelope is presented in figures 3.7a, 3.7b, and 3.7c.

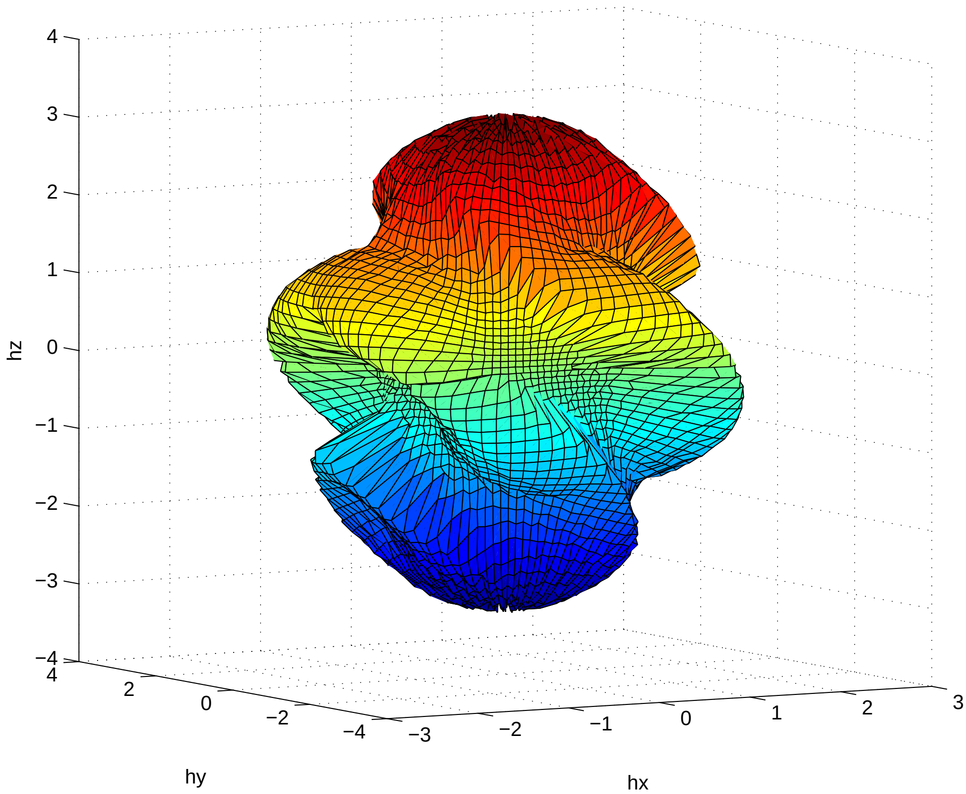

Figure 3.6: CMGs momentum envelope with gimbal travel is restricted ±90 °

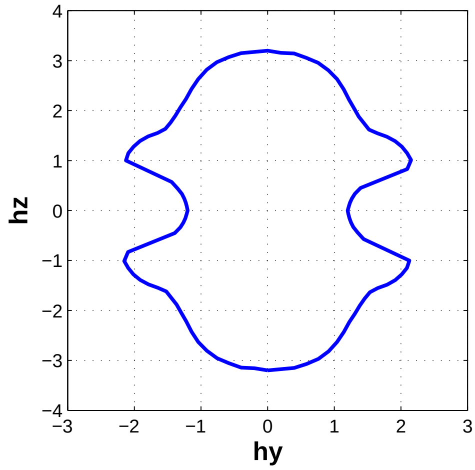

(a) Restricted momentum envelope cross section along $h_x = 0$ plane

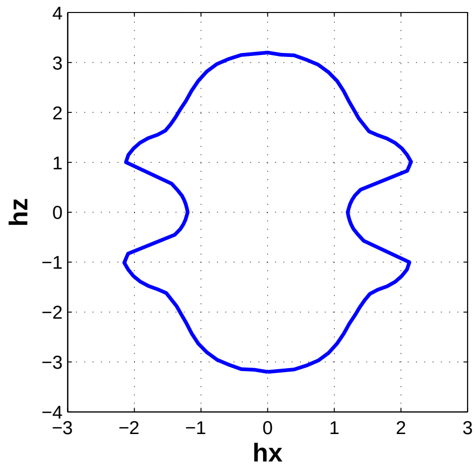

(b) Restricted momentum envelope cross section along $h_y = 0$ plane

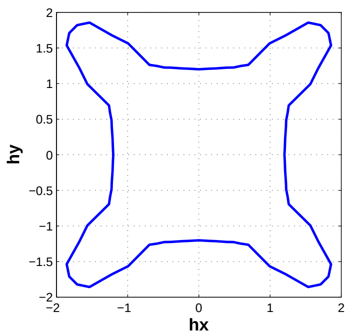

(c) Restricted momentum envelope cross section along $h_z = 0$ plane

Figure 3.7: Restricted momentum envelope cross section areas along $h_x = 0, h_y = 0$ and $h_z = 0$ planes.

From these figures, it may be observed that the envelope has shrunk considerably, especially along h_x and h_y directions. In the vertical direction (i.e., h_z) the envelope still reaches the same high value. This is because the corresponding gimbal angles, [90°, 90°, -90°, -90°], are possible with the given restrictions. In a regular momentum envelope, singularity measure is zero at the momentum envelope boundary. In this envelope on the other hand, the singularity measure is not necessarily zero at the momentum envelope boundary since the boundary is created by restricting the gimbal travel.

3.3 SIMULATION RESULTS

In this section simulation results on the application of MP-inverse and B-inverse algorithm for such a gimbal angle restricted CMG clusters are presented, and discussed. Since SR-inverse and MP-inverse give same results, we will not discussed the solutions of SR-inverse in this thesis. Respectively, constant torque simulation and then spacecraft simulation are presented. During simulation actuator dynamics are not taken into account.

3.3.1 CONSTANT TORQUE SIMULATION

In this section for a desired constant torque steering simulations are presented. The gimbal angles are started from: δ= [83°;70°;-90°;-90°]. At these gimbal angles, angular momentum of the CMG cluster is $\mathbf{h_0}$=[-1.493,-0.998,-0.055] Nm.s which is close to the restricted momentum envelope boundary.

A constant torque of $\tau_{\mathbf{desired}}$ =[1,0,0]^T Nm is required to carry this momentum to the other end of the boundary, around $\mathbf{h_f}$=[1.493,-0.998,-0.055]^T Nm.s in less than 3s.

3.3.1.1 Constant Torque Simulation Results Using MP-inverse

Simulation block for the MP-inverse algorithm is given Figure 3.8.

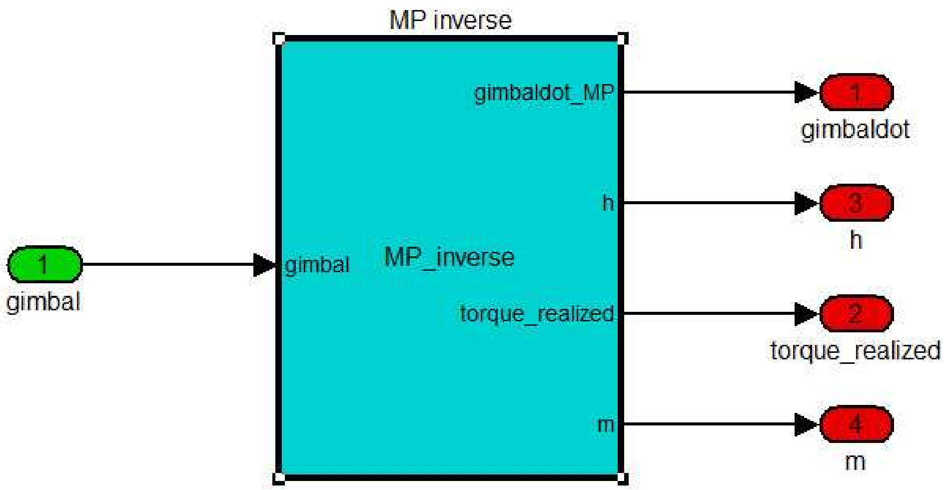

Figure 3.8: Constant torque simulations with MP-inverse

The following figures show the solutions of MP-inverse simulation. As it is seen in the Figure 3.9 and Figure 3.10 that desired torque and angular momentum are not realized. This is because of the fact that the second gimbal reached its limit Figure 3.11 and this is also cause the torque error (Figure 3.12) become very large. Figure 3.13 shows that the system is away from singularity during simulations.

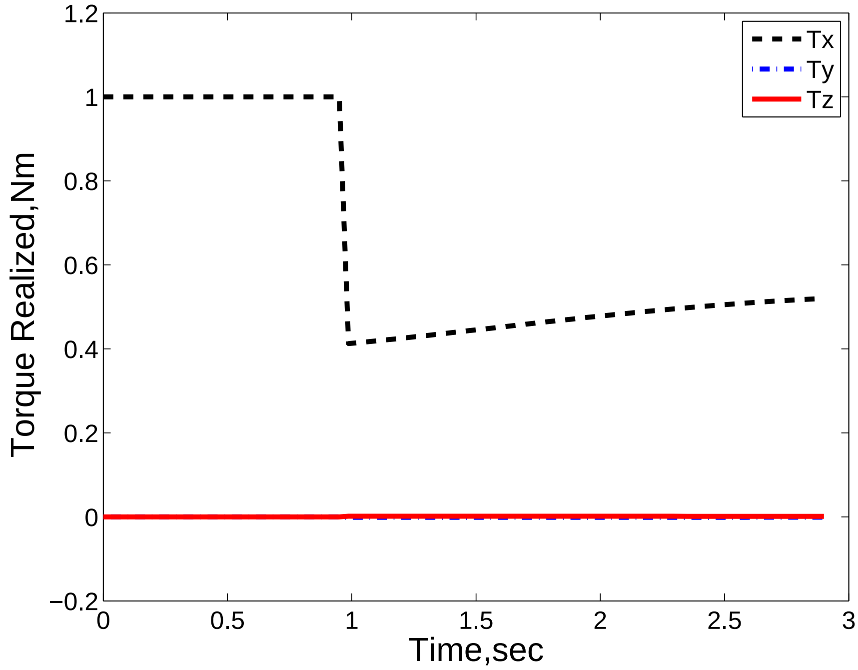

Figure 3.9: Realized torque history during MP-inverse algorithm

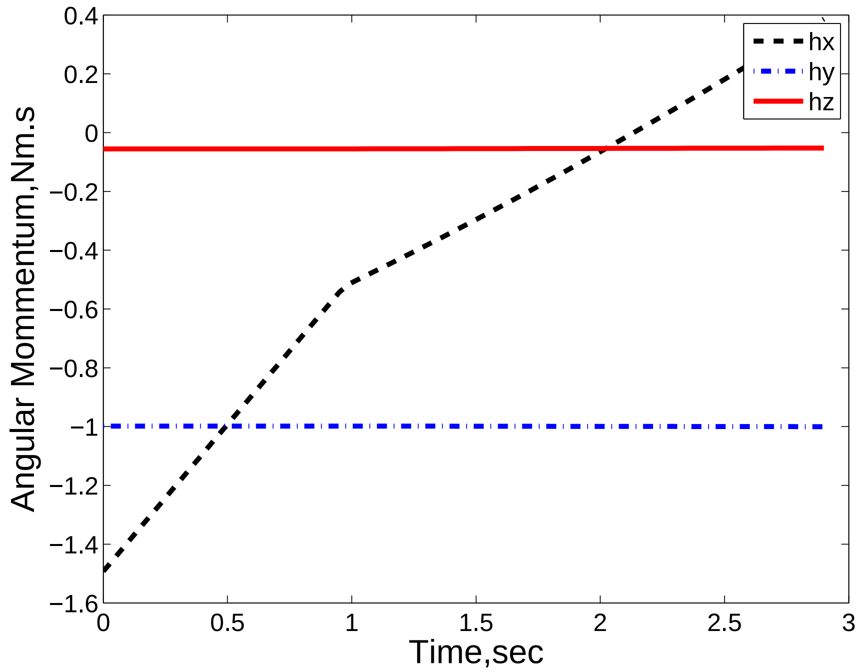

Figure 3.10: Realized angular momentum history during MP-inverse algorithm

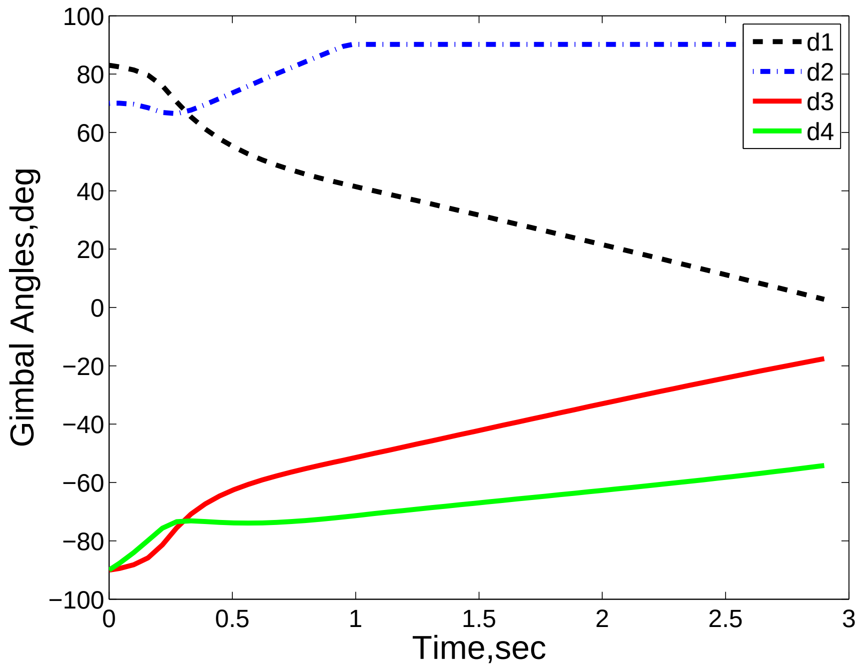

Figure 3.11: History of gimbal angles during MP-inverse algorithm

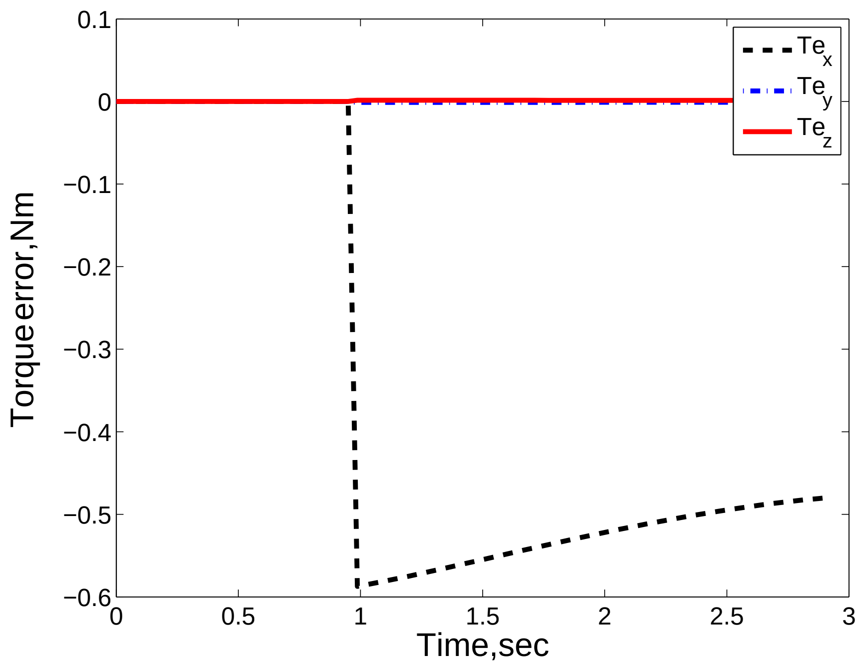

Figure 3.12: Error between realized and desired torque using MP-inverse algorithm

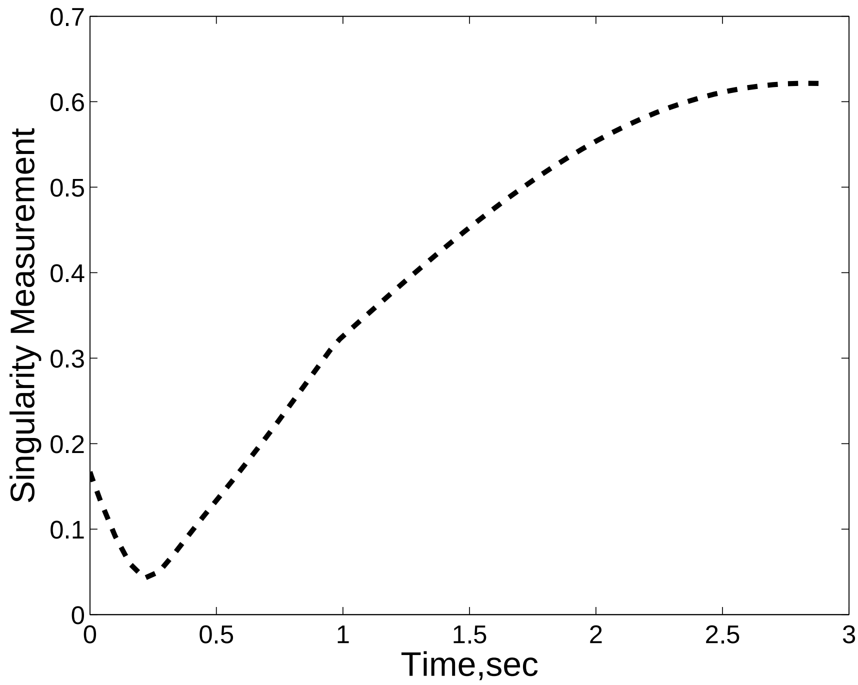

Figure 3.13: Singularity measurement for MP-inverse algorithm

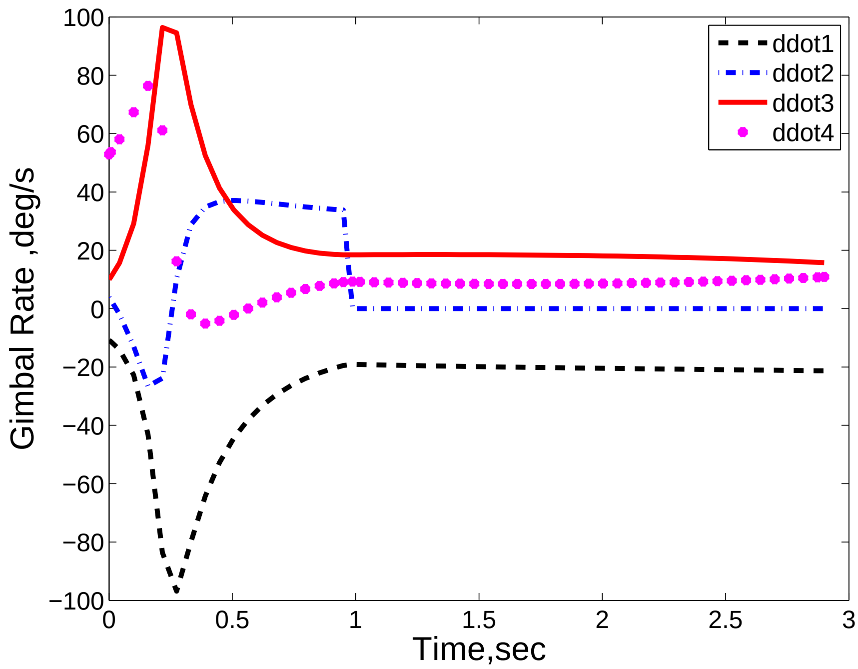

Figure 3.14: History of gimbal rates during MP-inverse algorithm

3.3.1.2 Constant Torque Simulation Results Using Blended inverse

In this section same simulation is repeated to get the required constant torque but this time by applying Blended inverse algorithm. Block diagram of this simulation is shown in Figure 3.15.

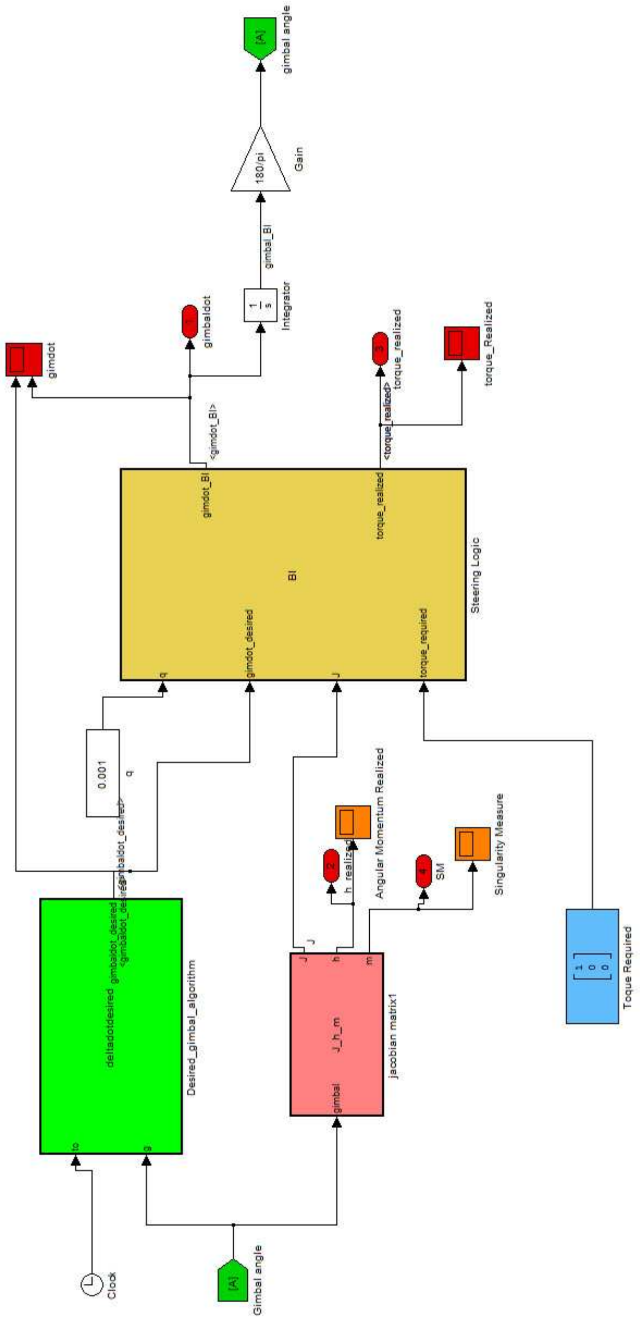

Figure 3.15: Block diagram of a constant torque simulation

In B-inverse algorithm, both the desired torque and desired gimbal rates are required. Thus, a proper trajectory is needed to steer gimbals. First, the angular momentum trajectory of the CMG cluster during a slew maneuver is obtained through a computer simulation. Then, the desirable gimbal angles at the discrete instants (nodes) of the angular momentum trajectory are calculated by solving the following optimization problem[28]:

$$\min_{U}(h_p - h(\delta_p)) \qquad p = 1, ..., P \tag{3.1}$$

Where, p is the node number. Once the nodal gimbal values are found, the gimbal rate may easily be calculated using,

$$\delta = \frac{\Delta_p - \Delta}{p\Delta t - t} \tag{3.2}$$

$$(p-1)\Delta t - \epsilon < t < p\Delta t - \epsilon, \qquad p = 1, ..., P \tag{3.3}$$

Where, t is the current time, and Δ t is the temporal distance between two nodes. The blending coefficient, q in Eq.2.37 is taken 0.001 and ϵ as 0.05 in the simulations presented in this thesis.

From Figure 3.16 it may be observed that the desired constant torque is very well realized. Angular momentum history shown in Figure 3.17 is as desired. The system did not encounter any singularities (Figure 3.18) and gimbals did not reach saturation limits (Figure 3.19). The gimbal angles pass through the node points very closely, shown in Table 3.1 and the realized gimbal rates shown in Figure 3.20 are also reasonable. Moreover, error which occurs between desired and realized torque became smaller than MP-inverse method since desired torque is realized (Figure 3.21).

Table 3.1: CONSTANT TORQUE MANEUVER PLAN

Nodal Locations (s)	Desired Gimbal Angles(deg)	Realized Gimbal Angles(deg)
0.0	[83, 70, -90, -90]	[83, 70,-90,90]
0.5	[60.5, 88.1,-70.2, -85.1]	[60.6, 87.6, -70.3, -84.4]
1	[38.4, 87.5,-48.2, -69.9]	[36.2, 87, -46.5, -68.8]
1.5	[12.6, 82, -24.8, -58.9]	[12.8, 82.6, -25.1, -58.9]
2	[-2.5, 89.8, -14.1, -51.2]	[-3.70 89.8 -13.32, 50.5]
2.5	[-24.3, 90, -4.4, -35.5]	[-24, 90, -4.4, -35.8]
3	[-50.4, 90, -4.5, -6.1]	[-46, 90, -7.6, -12.4]

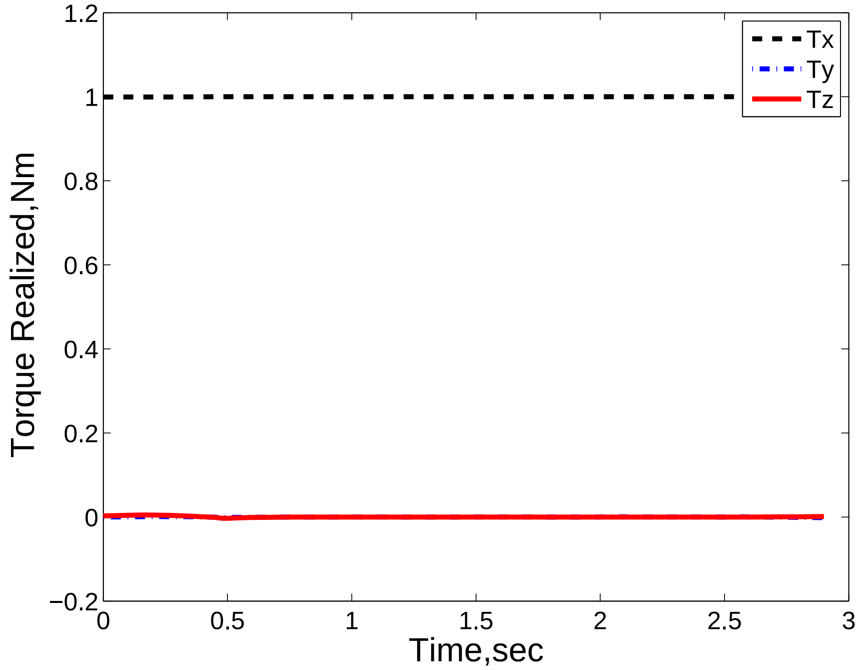

Figure 3.16: Constant torque simulations with B-inverse

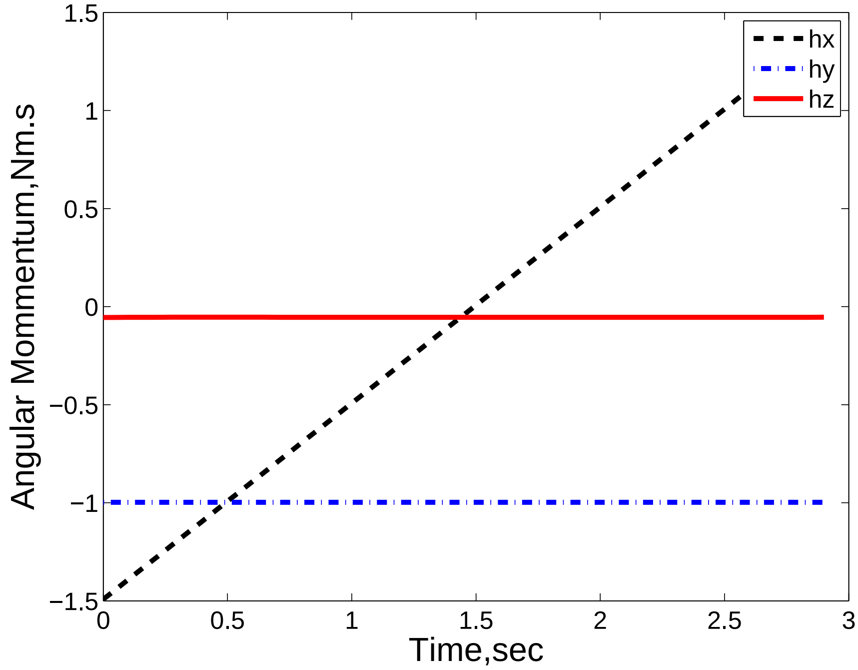

Figure 3.17: Realized angular momentum history during B-inverse simulation

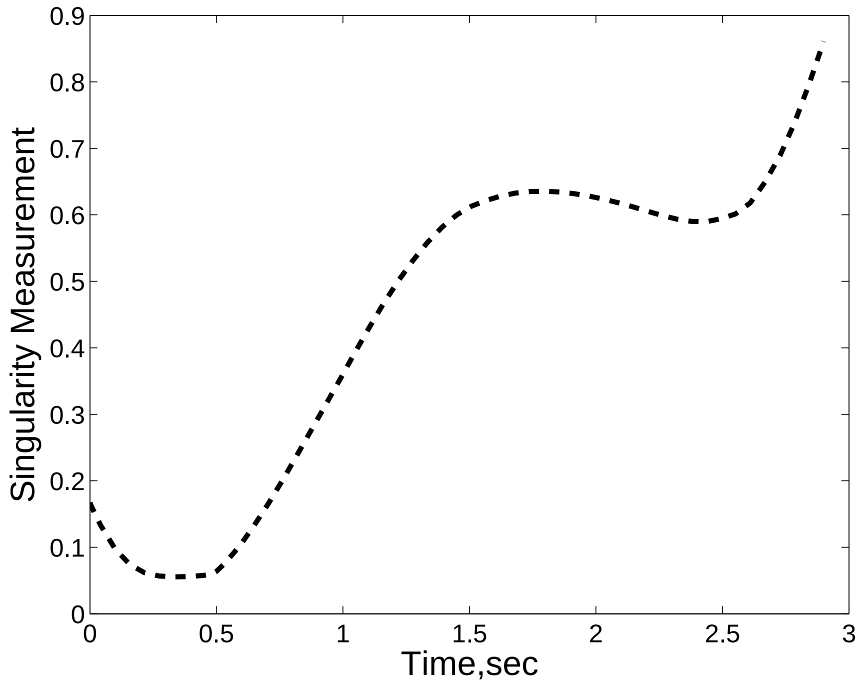

Figure 3.18: Singularity measurement for B-inverse simulation

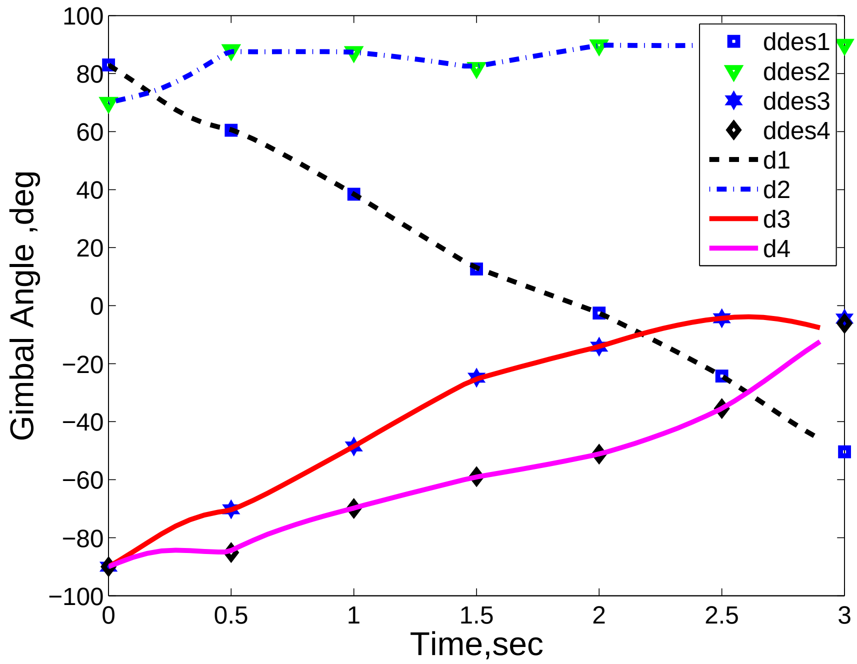

Figure 3.19: History of gimbal angles during B-inverse simulation

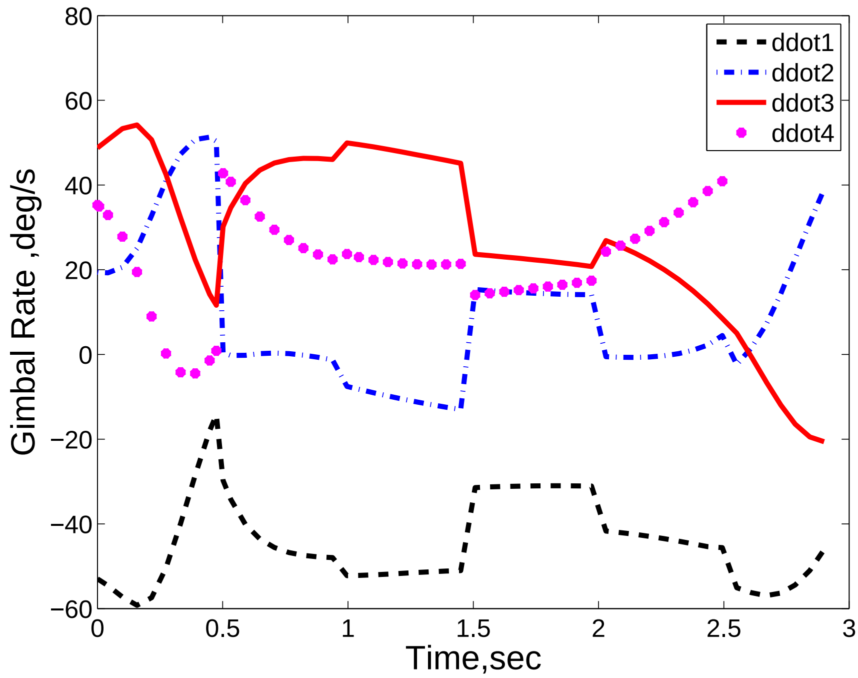

Figure 3.20: Gimbal rate history during B-inverse simulation

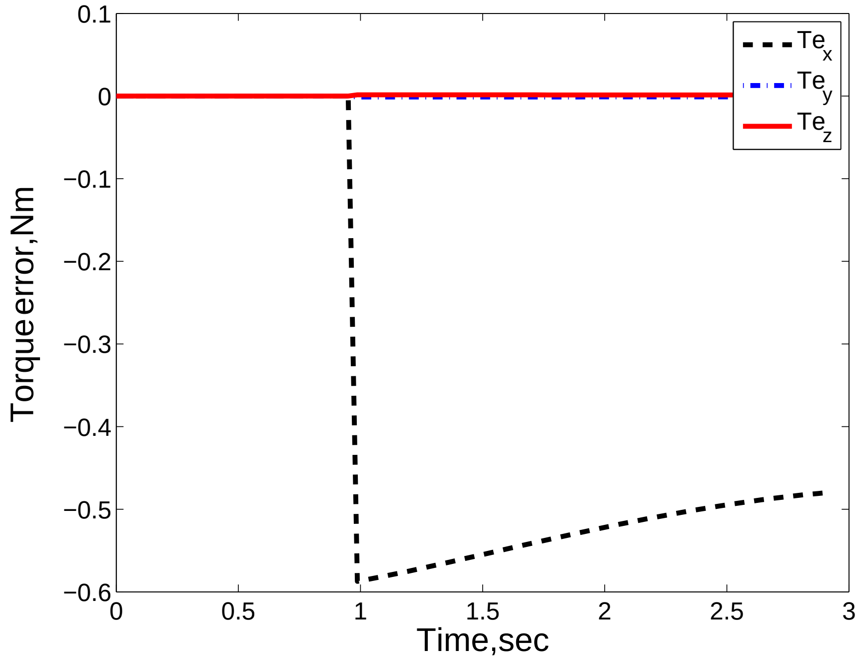

Figure 3.21: Error between realized and desired torque using B-inverse

3.3.2 SATELLITE SLEW MANEUVER SIMULATION

In this section satellite slew maneuver is carried out using MP-inverse and the B-inverse algorithm. During simulations, a satellite with a diagonal moment of inertia ($10kg.m^2$ in all axes) is used(I_s).

$$\mathbf{I_s} = \left\{ \begin{array}{ccc} 10 & 0 & 0 \\ 0 & 10 & 0 \\ 0 & 0 & 10 \end{array} \right\} \tag{3.4}$$

To carry out maneuver planning, again, the satellite slew maneuver with feedback control law given in Eq.2.7, together with a perfect momentum exchange device is simulated for 300 s. Figure 3.22 shows the block diagram of the spacecraft simulation:

3.3.2.1 Satellite Slew Maneuver Simulation Using MP-inverse Algorithm

In this section satellite slew maneuver are realized by MP-inverse algorithm. During 300 sec, model is simulated. The acquired results are seen from the graphics. Desired achievement from satellite that to do -65°roll maneuver. As it is seen from Figure 3.23 that by using MP-inverse control algorithm, satellite did not reach the desired state. Moreover, the satellite do not reached the desired attitude. It may easily be observed from the Figure 3.24 that the system became singular within 4.56 seconds. That means there is not enough torque generation to bring the satellite to the desired attitude (Figure 3.25). The effects of singularity may be seen from figures 3.26, 3.27, 3.28 and 3.29.

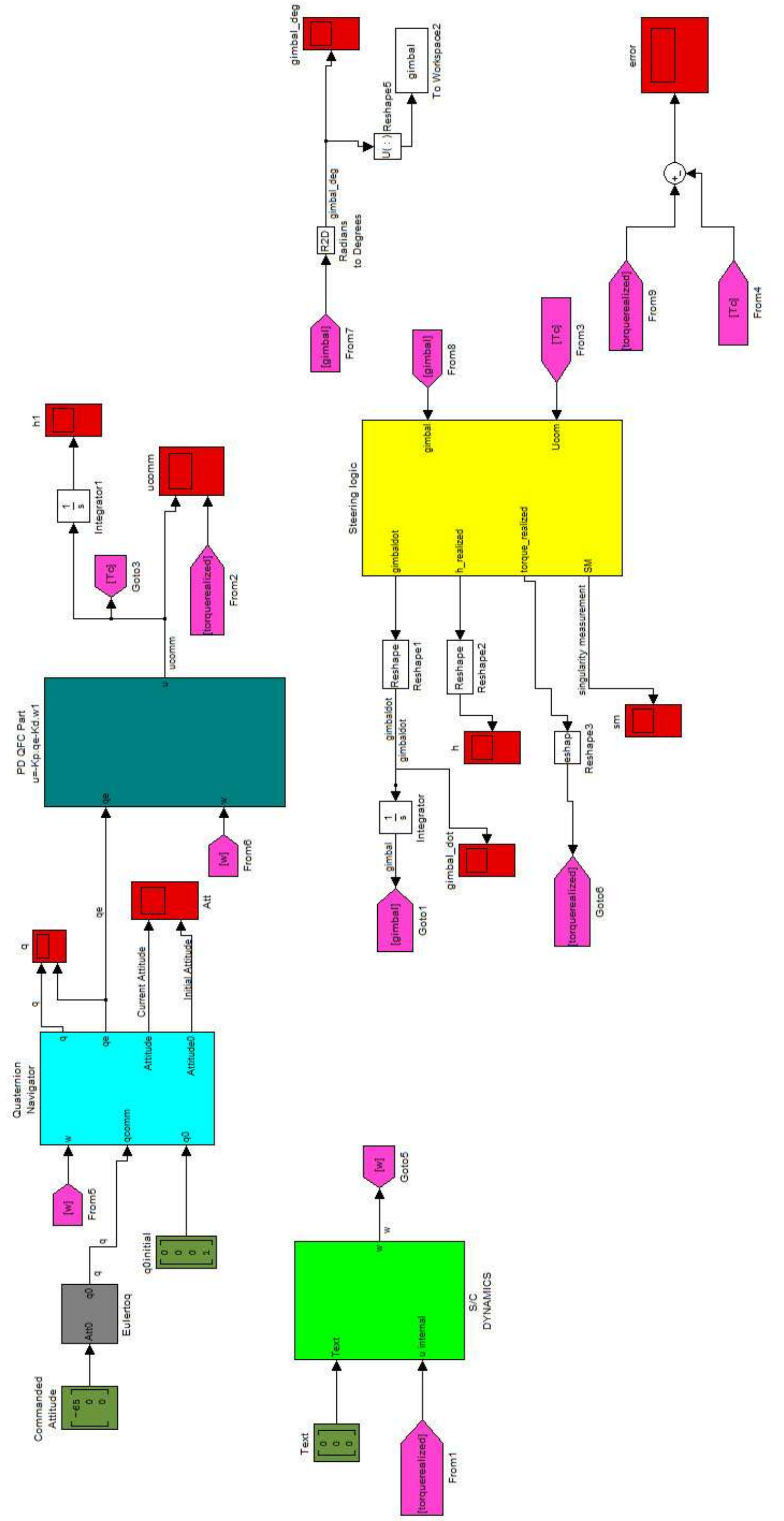

Figure 3.22: Spacecraft simulation model in Simulink

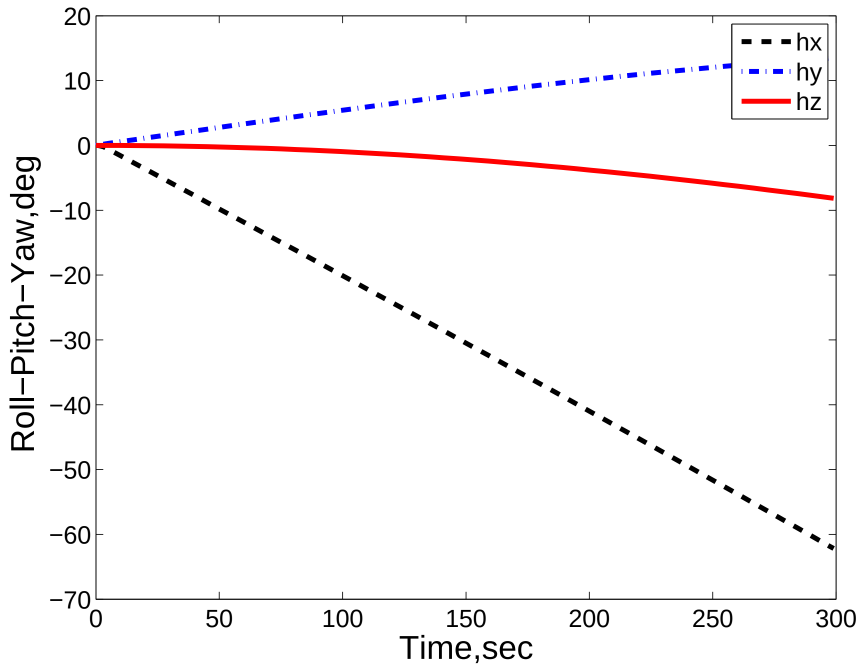

Figure 3.23: Satellite attitude during a -65°roll maneuver

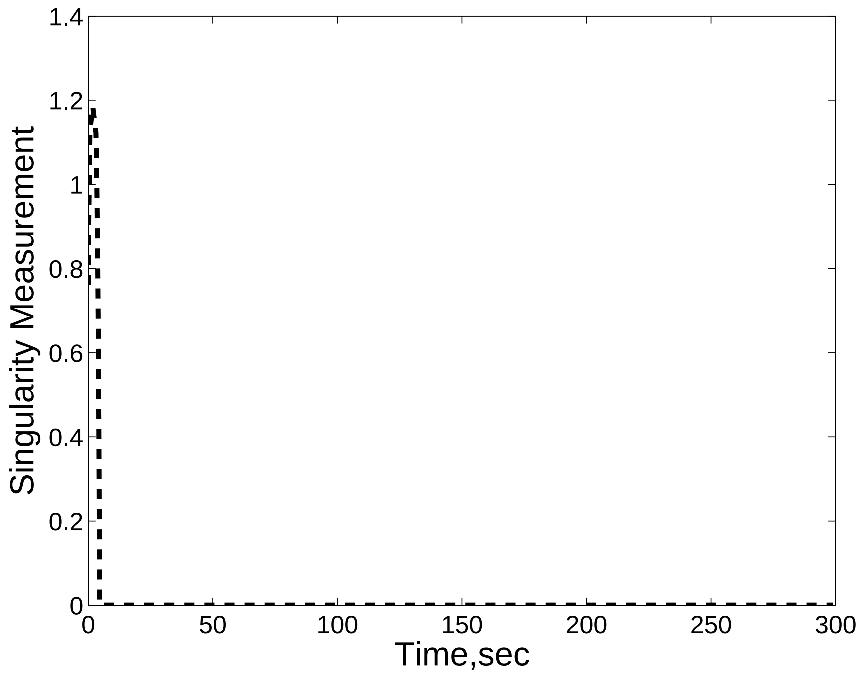

Figure 3.24: Singularity measurement for MP-inverse simulation

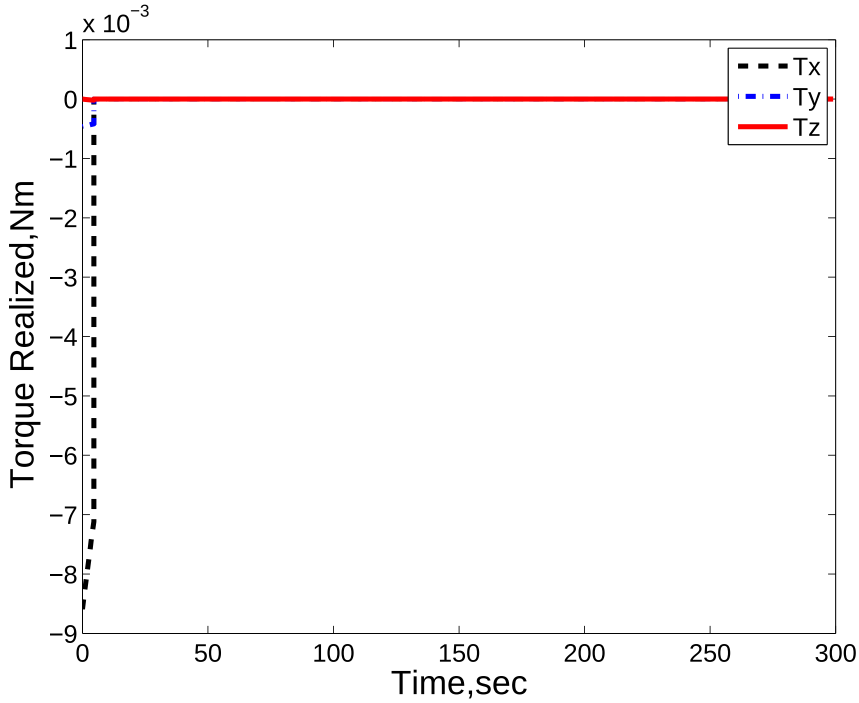

Figure 3.25: Torque history during spacecraft simulation using MP-inverse algorithm

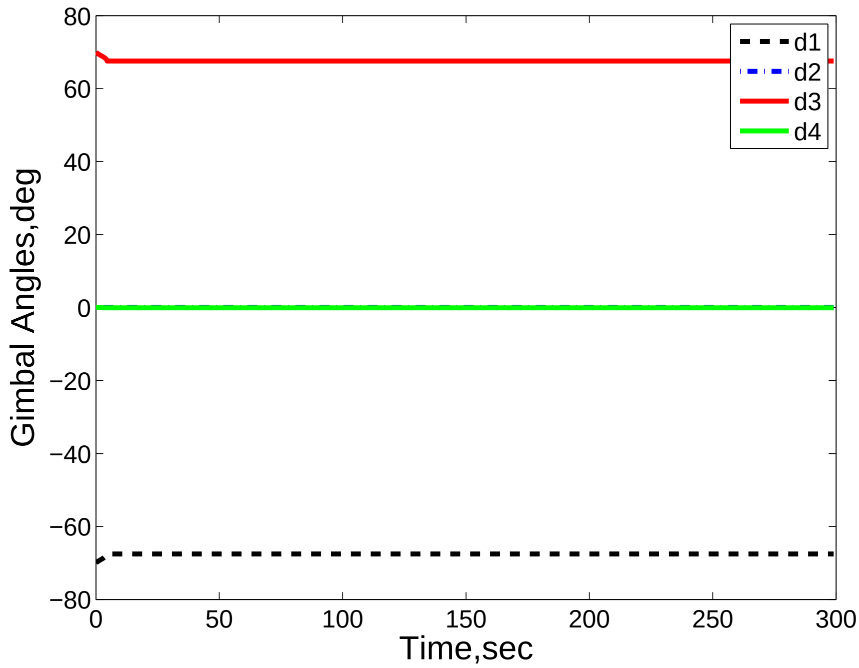

Figure 3.26: History of gimbal angles during MP-inverse simulation

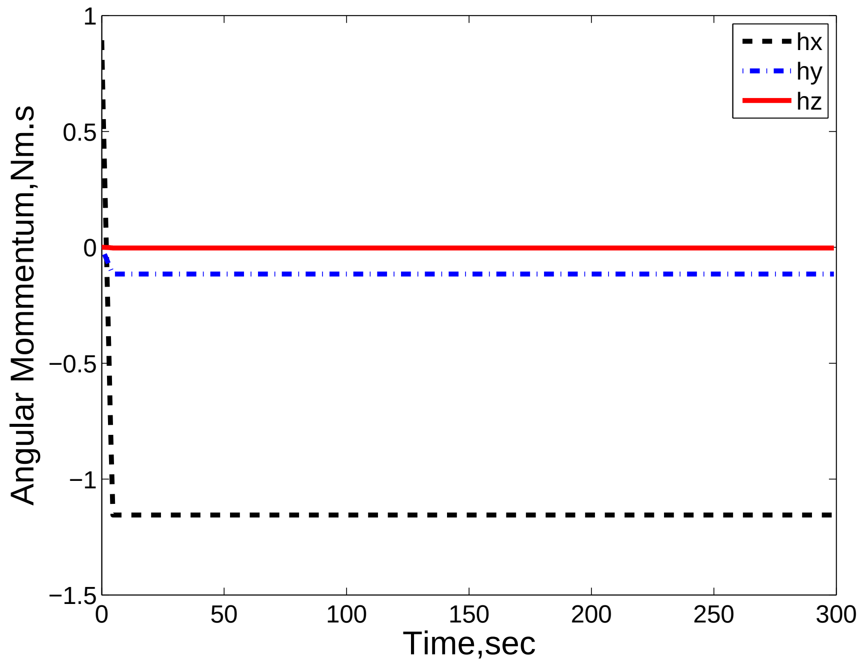

Figure 3.27: Realized angular momentum history during spacecraft simulation by MP-inverse

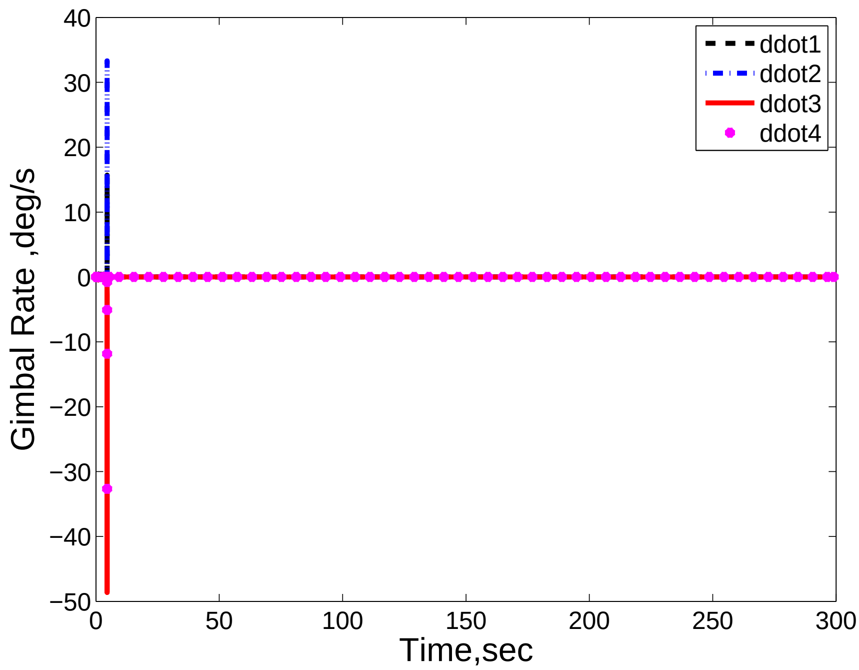

Figure 3.28: Gimbal Rate history during MP-inverse simulation

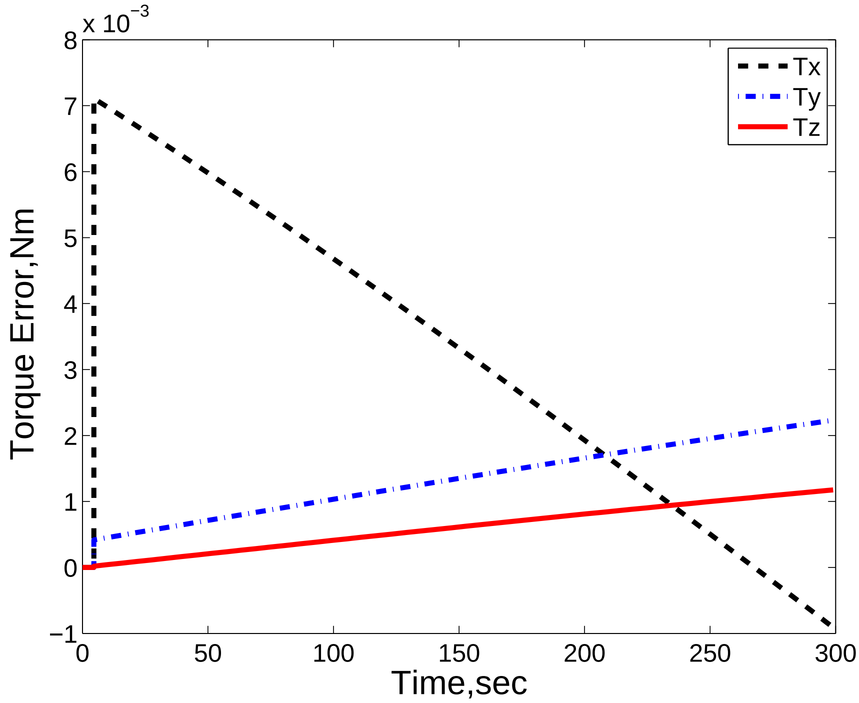

Figure 3.29: Torque error between realized torque and commanded torque using MP-inverse algorithm

3.3.2.2 Satellite Slew Maneuver Simulation Using Blended inverse algorithm

In this section satellite slew maneuver is realized by using B-inverse algorithm. The desired gimbal angles corresponding to the angular momentum values at the selected nodes are again calculated using the optimization routine,based on the restricted momentum envelope requirements Eq.3.1. The temporal values of the nodes, desired gimbal angles, and realized gimbal angles at these nodes are presented in Table 3.2.

Table 3.2: SATELLITE -65°MANEUVER PLAN

Nodal Locations (s)	Desired Gimbal Angles (deg)	Realized Gimbal Angles(deg)
0.0	[-70, 0, 70, 0]	[-70, 0, 70, 0]
51.647	[-55.1, 0.6, 55.3, -0.8]	[-55.2, 0.6, 55.4, -0.8]
99.647	[-62.6, 0.7, 62.8, -0.9]	[-62.3, 0.7, 62.5, -0.8]
300	[-70.8, -0.3, 69.4 0.8]	[-70.8, -0.3, 69.4, 0.8]

The satellite attitude control simulation is given in Figure 3.30. Figure 3.33 presents the realized gimbal angles and together the desired ones during the maneuver. It is clear from these figures that the maneuver is realized perfectly without violating the gimbal angle restrictions. In fact, the realized gimbal angles at the nodes are very close to those planned initially (Table 3.2). The gimbal rates, presented in Figure 3.34, show that they are quite small. Where it is seen from the Figure 3.32 that system is far from the singularity limits. Figure 3.35 and Figure 3.31 shows the realized torque and the angular momentum history. As it is seen from the graphics that angular momentum and also torque realized as expected.

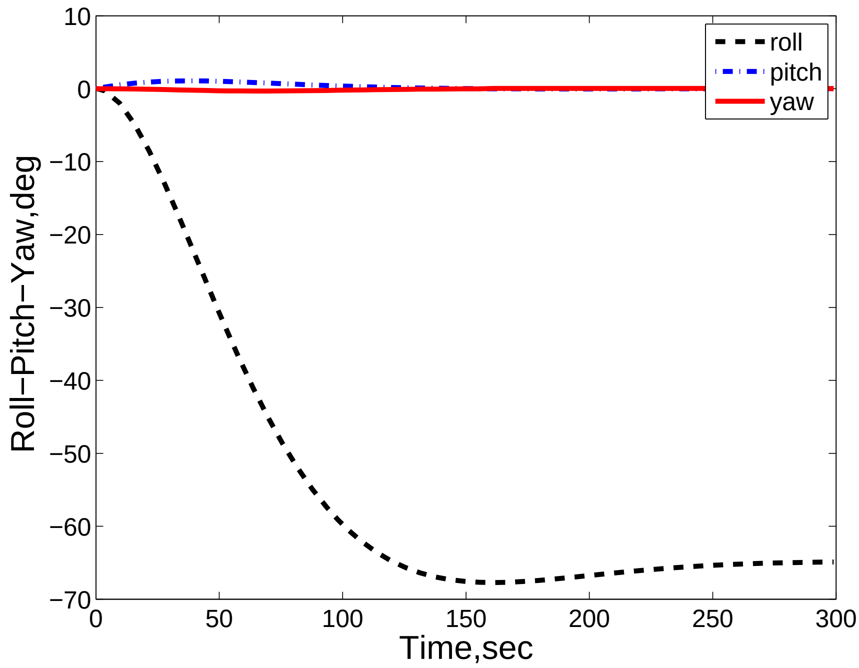

Figure 3.30: Satellite attitude during a -65°roll maneuver

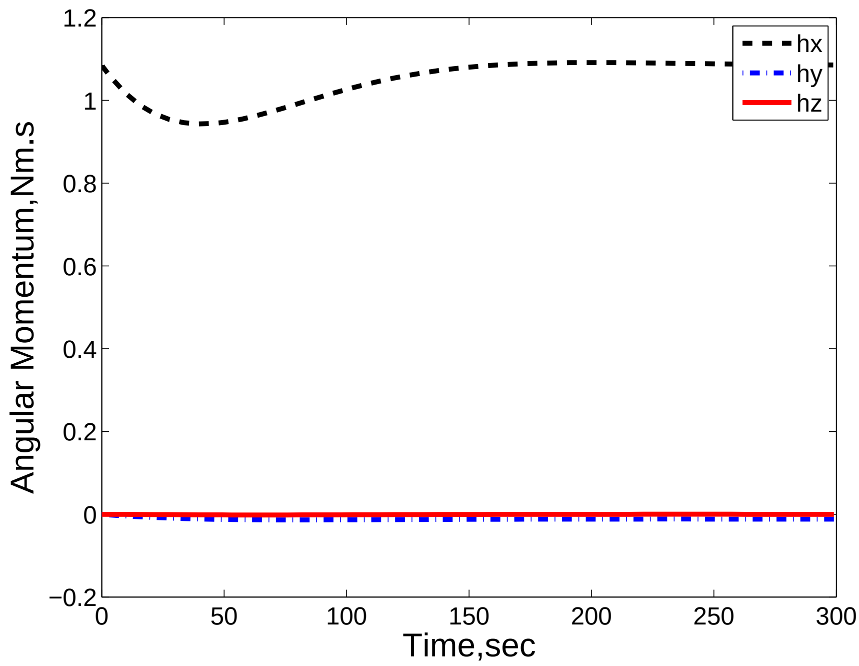

Figure 3.31: Realized angular momentum history during spacecraft simulation by B-inverse

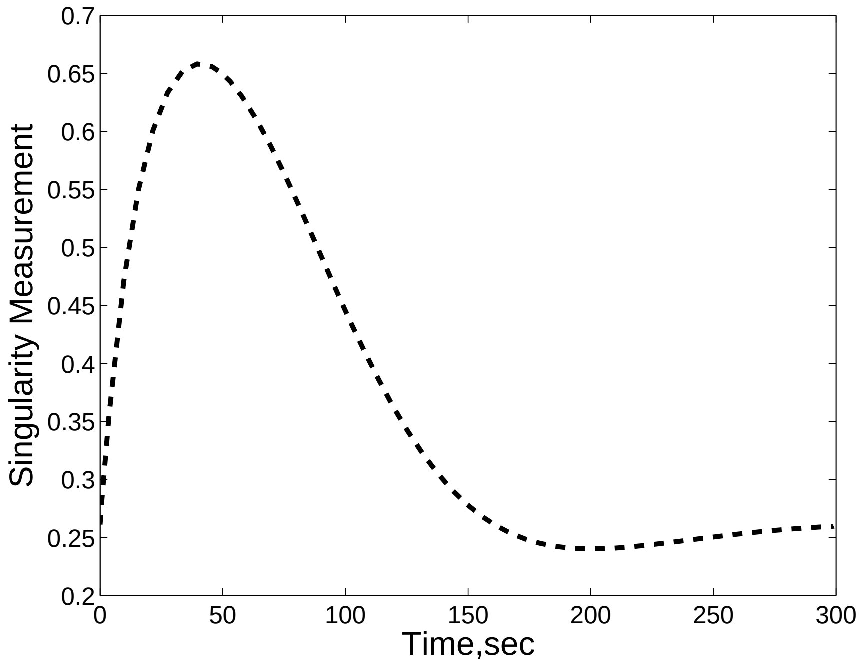

Figure 3.32: Singularity measurement for B-inverse simulation

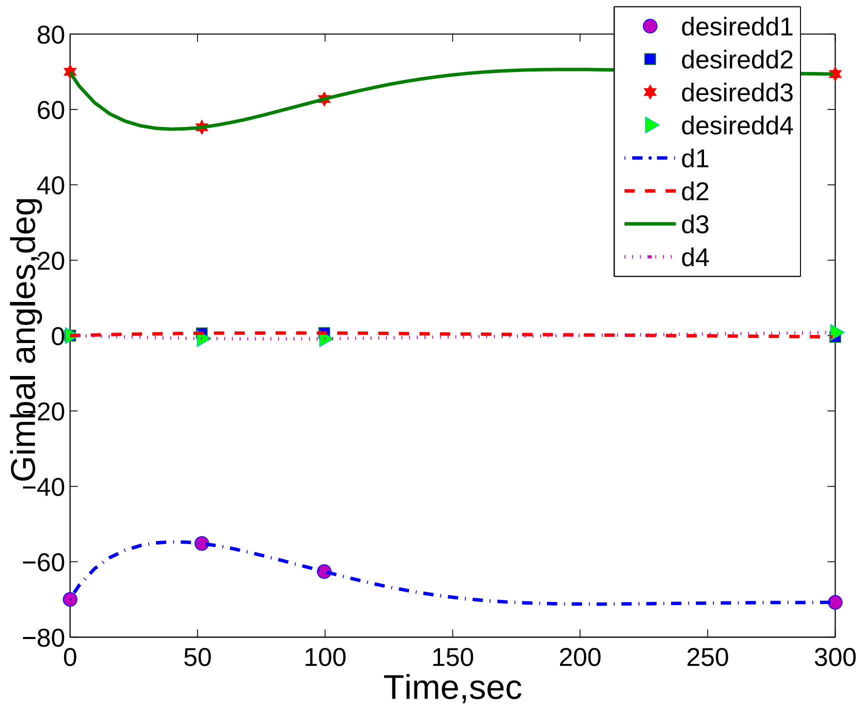

Figure 3.33: History of gimbal angles during B-inverse simulation

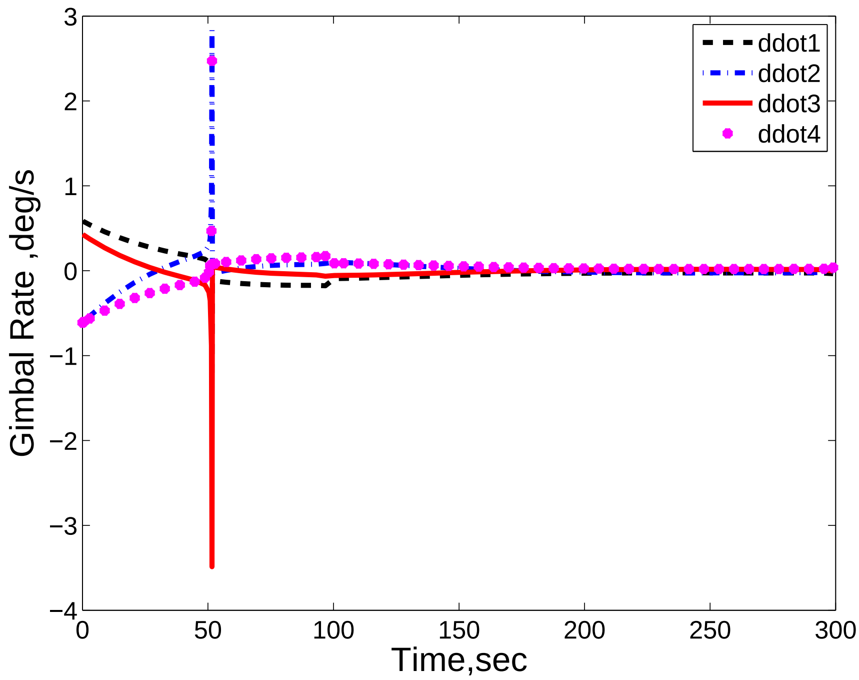

Figure 3.34: Gimbal rate history during B-inverse simulation

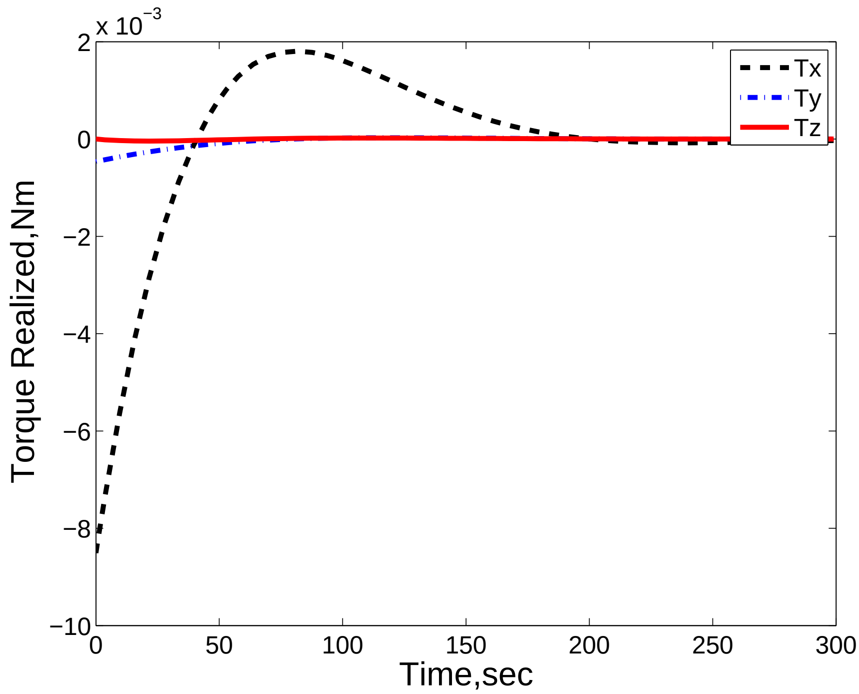

Figure 3.35: Torque history during spacecraft simulation using B-inverse algorithm

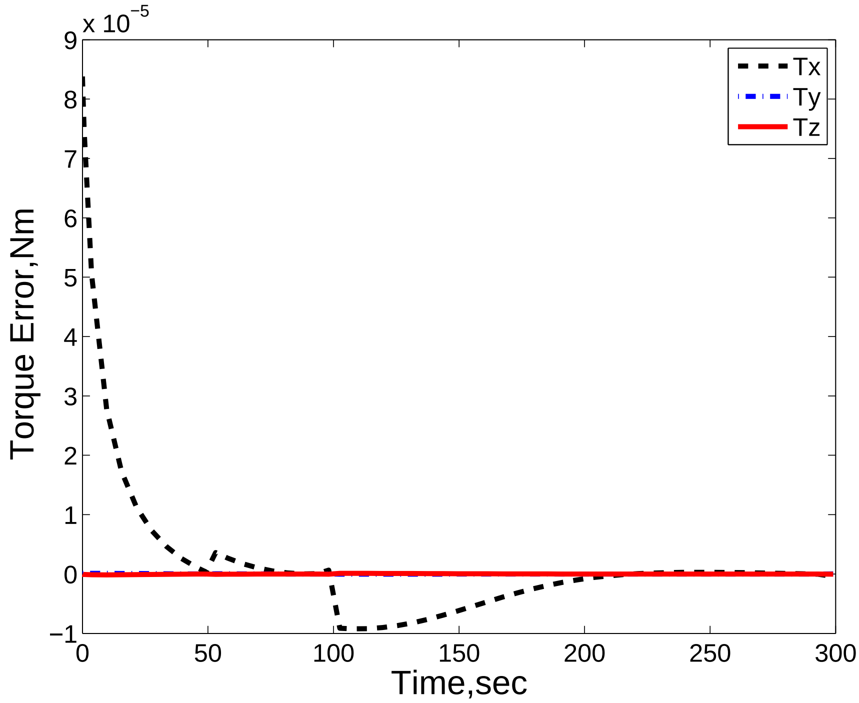

Figure 3.36: Torque error between torque realized and commanded torque using B-inverse algorithm

CHAPTER 4

SATELLITE CONTROL USING REDUNDANT DISSIMILAR ACTUATORS

4.1 INTRODUCTION

The purpose of this chapter is to examine how dissimilar actuators, magnetorquer and CMGs, used together. This mixed usage of these actuators can prevent actuator saturation and can allow fast maneuver capability to achieve desired attitude of the satellite.

4.2 MODEL

In this section satellite attitude models with magnetorquers and CMGs as actuators are presented. Four CMGs in a pyramid configuration and three magnetorquers aligned in each axis are considered. As it is mentioned in Section 2.4.1.3 rotational equations of motion a given spacecraft may be written in the body fixed frame as:

$$\mathbf{I_s}\dot{\omega} + \omega \times \mathbf{I_s}\omega = \mathbf{T_c^*} + \mathbf{T_{ext}} \tag{4.1}$$

Where, $\mathbf{T_c}^*$, is the total control torque, and $\mathbf{T_{ext}}$, is the sum of other external torques acting on the spacecraft. This time, spacecraft is controlled using CMGs and magnetorquers. Control torque may be written as:

$$\mathbf{T_c^*} = -\dot{\mathbf{h}} + \mathbf{T_{magnetic}} - \omega \times \mathbf{h} \tag{4.2}$$

$$\tau^* = -\dot{h} + T_{magnetic} \tag{4.3}$$

where $\dot{h}$ angular momentum rate of CMGs and $\mathbf{T_{mag}}$ is the magnetic torque produced by magnetorquer. In this chapter, Quaternion feedback controller is used, as well section 2.4.1.3.

Angular momentum of a cluster of four CMGs in a pyramid configuration may be written as Eq.2.13. In this equation each wheel is assumed to have an angular momentum of $\mathbf{h_0}$, β is the pyramid skew angle and, $\delta_\mathbf{i}$ are the gimbal angles[27].

The control torque is to be realized using actuators through τ^* , Eq.4.3 which we manipulate. Thus, for a satellite with 3 magnetorquers aligned in three axes of the satellite body frame and four CMGs mounted in a pyramid configuration, $\tau_\mathbf{realized}$ (Eq.4.4) may be written as:

$$\tau_{realized} = J^* U^* \tag{4.4}$$

$$U^* = [M_x \;\; M_y \;\; M_z \;\; \dot{\delta}_1 \, \dot{\delta}_2 \, \dot{\delta}_3 \, \dot{\delta}_4]^T \tag{4.5}$$

$$J^* = ho \left\{ \begin{array}{ccccccc} 0 & B_3/h_0 & -B_2/h_0 & -\cos\beta\cos\delta_1 & \sin\delta_2 & \cos\beta\cos\delta_3 & -\sin\delta_4 \\ -B_3/h_0 & 0 & B_1/h_0 & -\sin\delta_1 & -\cos\beta\cos\delta_2 & \sin\delta_3 & \cos\beta\cos\delta_4 \\ B_2/h_0 & -B_1/h_0 & 0 & -\sin\beta\cos\delta_1 & \sin\beta\cos\delta_2 & \sin\beta\cos\delta_3 & \sin\beta\cos\delta_4 \end{array} \right\} \tag{4.6}$$

This time Eq.2.16 is turn to 3×7 matrixes and $\mathbf{U}$ is the control command composed of magnetic dipole vector $\mathbf{M}$ and gimbal angle rates vector $\dot{\delta}$. For stable and precise satellite attitude control, control torque assumed to be known using quaternion feedback controller and the desired torque shall be found from:

$$\tau^*_{desired} = -Kq_e - D\omega + \omega \times h \tag{4.7}$$

To steer the actuators without encountering singularities, $\mathbf{U}$ must be found. Eq.4.4 can only be solved by calculating inverse of rectangular Jacobian matrix using Moore-Penrose pseudo inverse. However, when Jacobian matrix loses its rank system becomes singular. Thus, proper steering laws must be implemented to pass trough singularities as already mentioned in Section 2.4.1.

4.3 SIMULATION RESULTS

In this section two case studies on the application of MP-inverse and B-inverse algorithm for redundant actuator systems which use 4 CMGs and 3 magnetorquers are presented. First case actuator steering simulation by using a pre-specified torque history and the second case spacecraft simulation are presented. During simulation Dormand-Prince method is chosen as a solver.

4.3.1 PRE-SPECIFIED TORQUE SIMULATION

In this section pre-specified torque simulation results are presented. Angular momentum of each CMG is taken 0.1 Nm.s. Desired torque is taken to implement as $[-10^{-3}; 0; 0] \times \sin(t)$ Nm and initial gimbal angles are taken $\delta_{\mathbf{0}}$ =[60 °;0°; 13.84°;-30°]. Figure 4.1 shows the block diagram of the simulation.

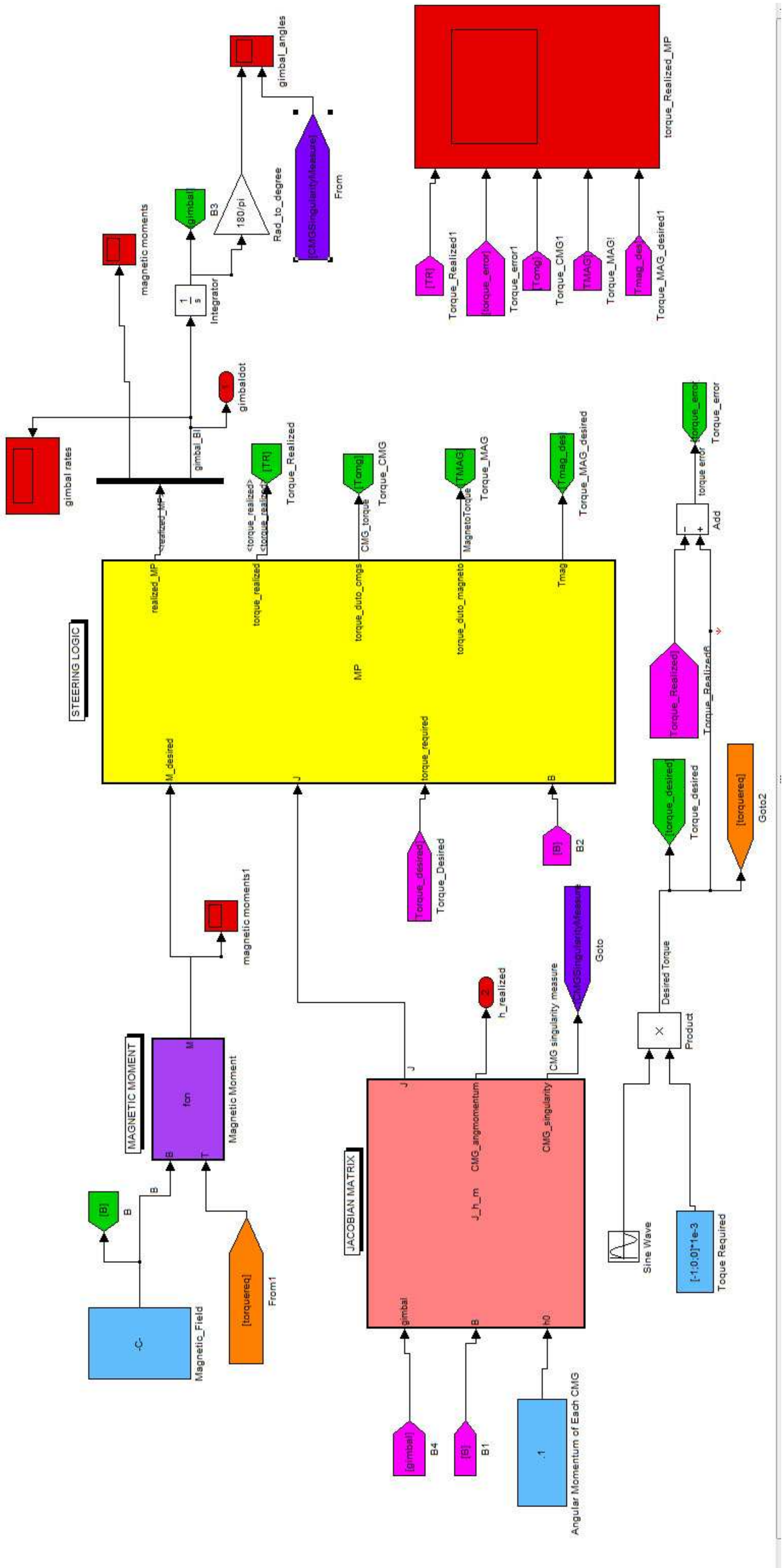

Figure 4.1: Block Diagram of a Constant Torque Simulation for Dissimilar Redundant Actuator System

At the sea level, the field is horizontal and the field strength is about 30 μT near the equator, while it becomes vertical with field strength of 60 μT around the poles [10]. In this thesis, magnetic field is taken as $[0.3; 0.8; 0.52] \times 48\mu$T in Earth fixed frame. Transformation is considered from Earth fixed frame to satellite body frame.

4.3.1.1 Simulation Using MP-inverse Algorithm

In this section control allocation with dissimilar actuator is first realized by MP-inverse method. Realized torque during 10 sec simulation with MP-inverse method is presented in Figure 4.2. This torque comes out to be very close to the desired torque specified above.

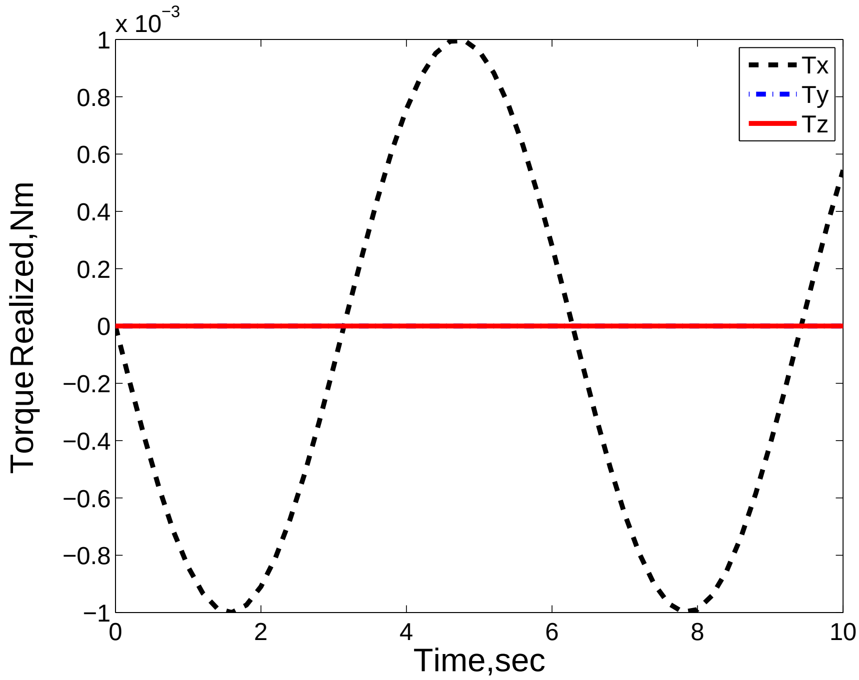

Figure 4.2: Torque history during simulation with MP-inverse

Figure 4.3 and Figure 4.4 shows the torques generated by CMG and magnetorquer clusters. It is clear from these figures that torque is mainly by the CMGs. During the simulation,the contribution of the torque rods is very small. Since most of the desired torque is generated using CMGs, difference between desired and realized torque came out to be very small as expected, Figure 4.5.

In Figure 4.6 shows gimbal rates required by the steering algorithm and Figure 4.7 shows gimbal angles. Normally we would like to use torque rods during the maneuver to prevent CMG's from reaching their saturation limits, or accumulating momentum. Thus, it is desirable to have as small gimbal activity as possible. In the simulation code the saturation limits are also included. From simulation results it is observed that these limits are not exceeded.

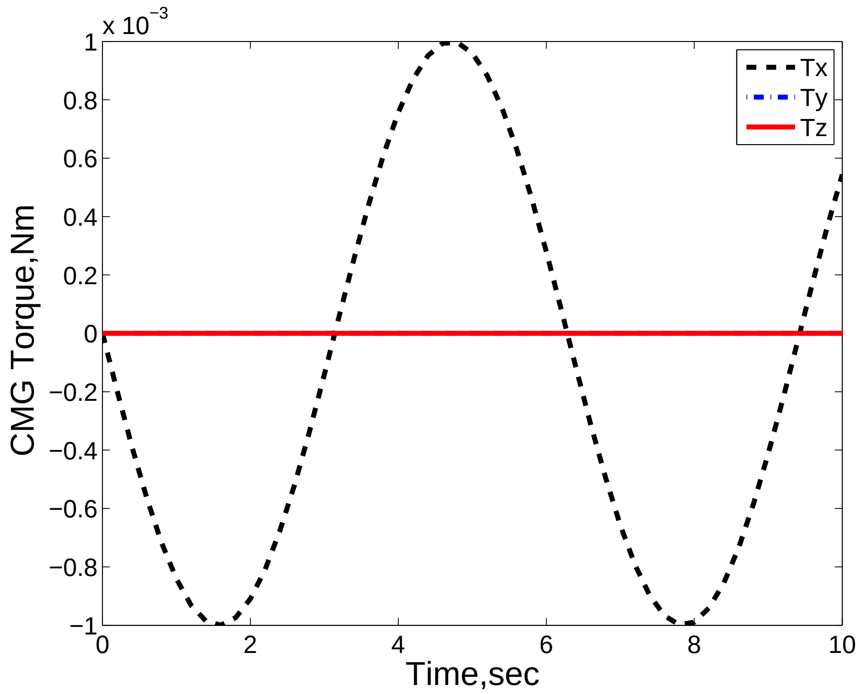

Figure 4.3: Control torque generated by the CMG cluster

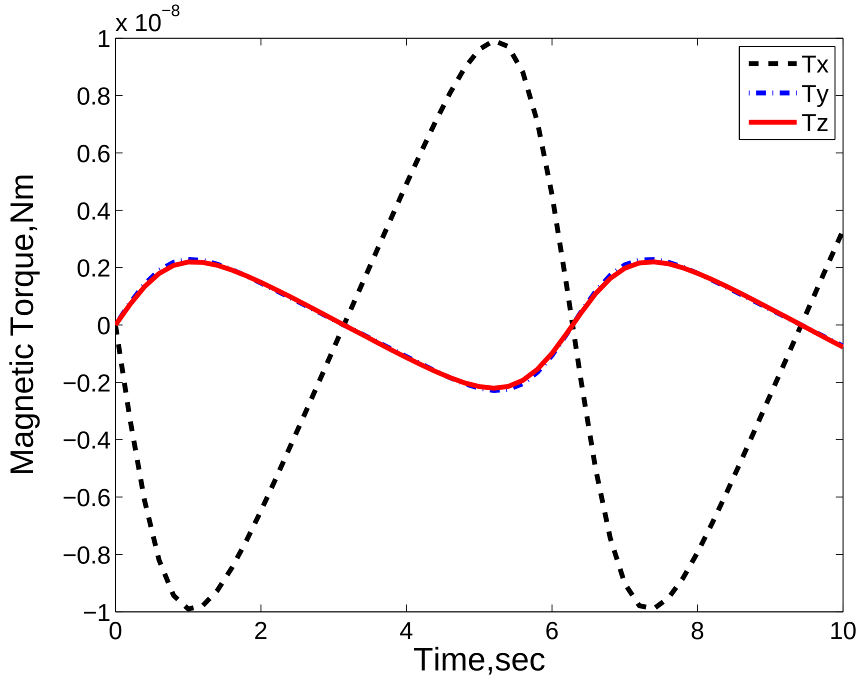

Figure 4.4: Control torque generated by magnetic torqrods

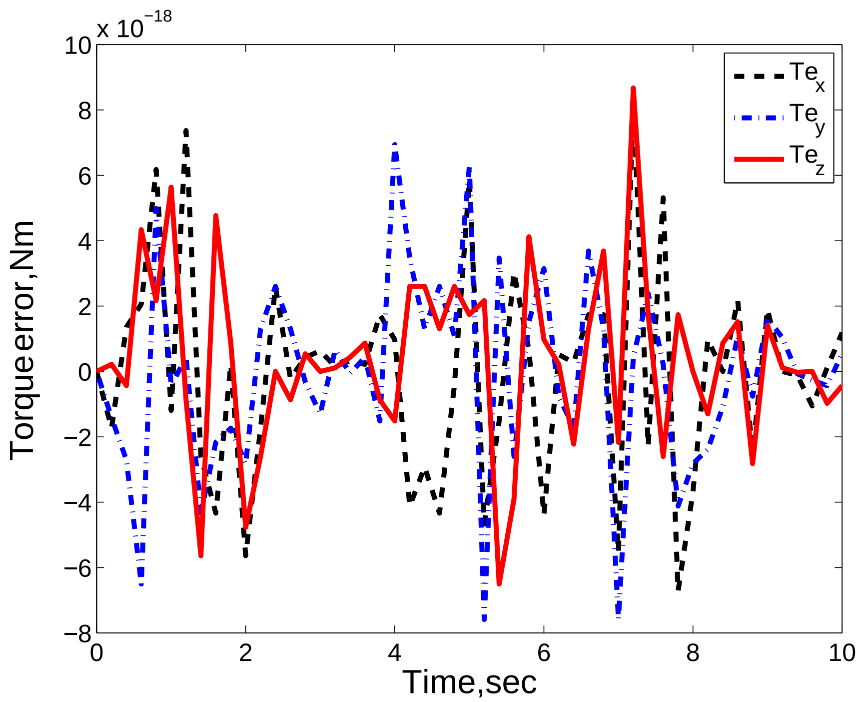

Figure 4.5: Torque error between desired and realized torque

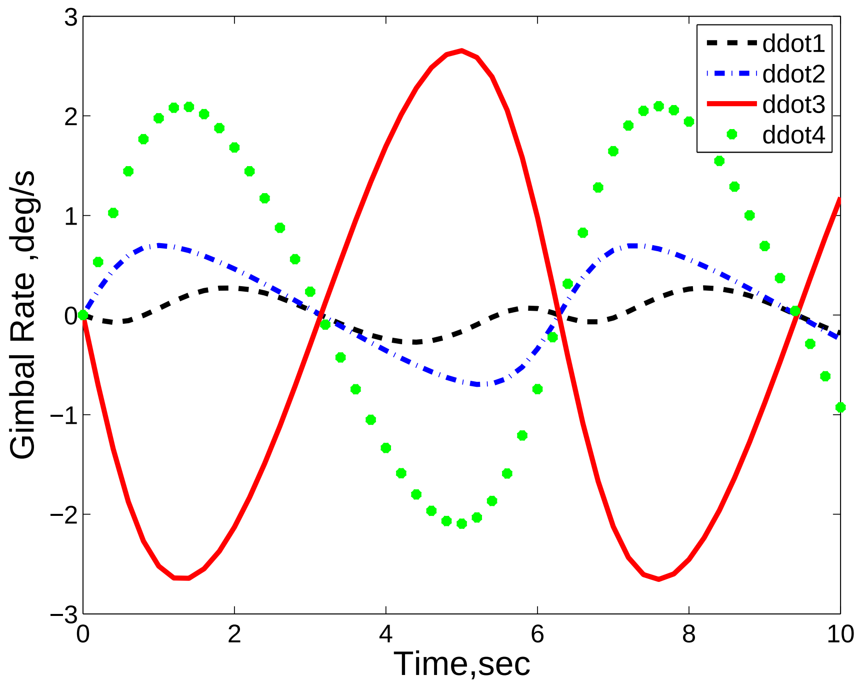

Figure 4.6: Gimbal rate history while steering using MP-inverse

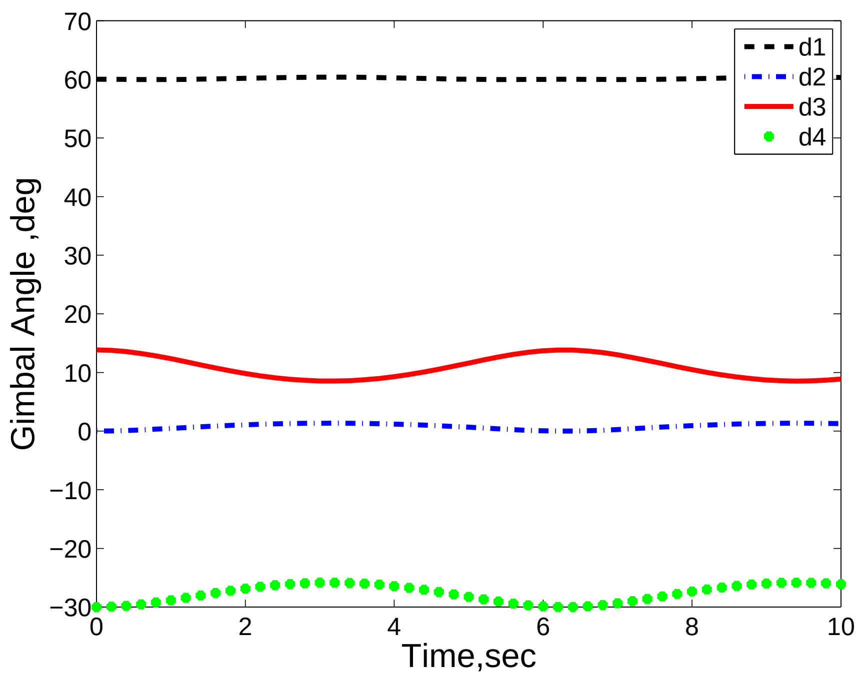

Figure 4.7: Gimbal angle history while steering using MP-inverse

4.3.1.2 Simulation Using Blended Inverse Algorithm

In this section same simulation given in the previous section is repeated this time using Blended inverse (B-inverse) method. Blending co-efficient q is taken as 1×10^{-12} and angular momentum of each CMGs h_0 is taken as 0.1 Nm.s. To implement B-inverse algorithm, the desired values for gimbal rates and magnetic moments are needed. In this simulation study, the desired gimbal rates are taken as zero. The desired magnetic moment are calculated from[24]:

$$M = \frac{1}{B^2} \left\{ B \times T_c \right\} \tag{4.8}$$

Realized torque during 10 sec simulation with B-inverse method, presented in Figure 4.8, shows that the desired torque is very accurately realized. Figure 4.9 and Figure 4.10 shows the torque obtained from the magnetorquers and the CMG cluster. This time in contrast previous section most of the torque is generated by the magnetorquers and also Figure 4.11 shows generated torque error between desired and realized torque. It can be seen from Figure 4.10 that most of the torque is realized providing that using magnetorquer that is close to the calculated by Eq.4.8. There is no noticeable change in gimbal angle (Figure 4.13). Figure 4.14 shows that gimbal rates are also very small. The magnetic moment history of the simulation shows that the saturation limits of MTR-30 magnetorquer model are not exceeded Figure 4.15.

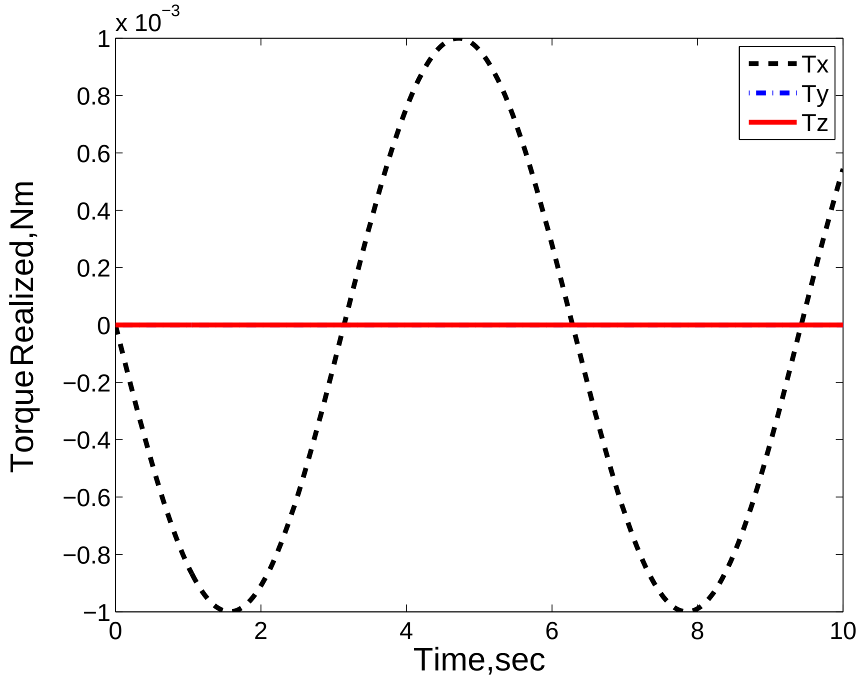

Figure 4.8: Torque history during simulation with B-inverse

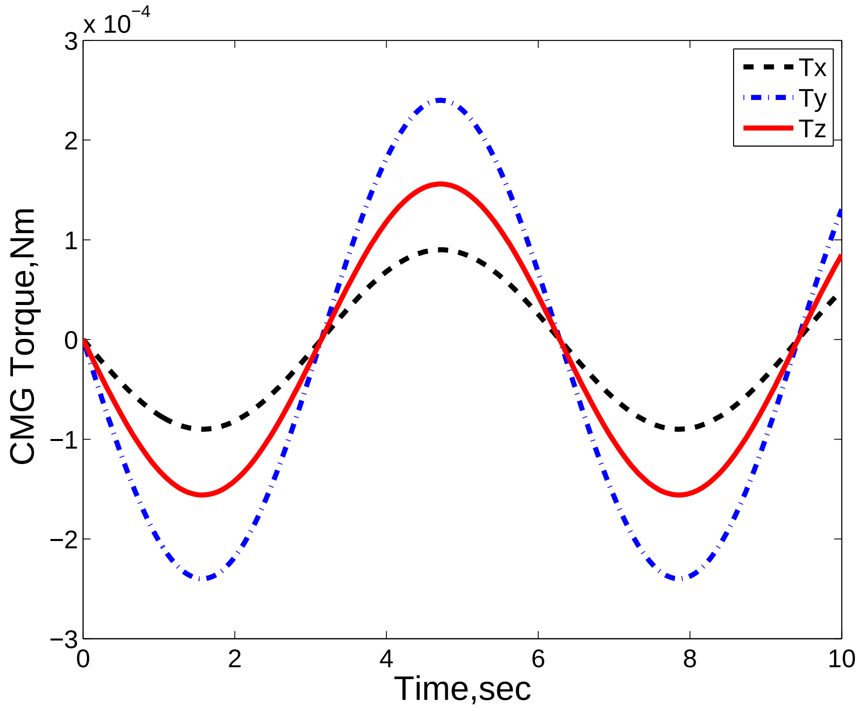

Figure 4.9: Control torque generated CMG clusters during B-inverse simulation

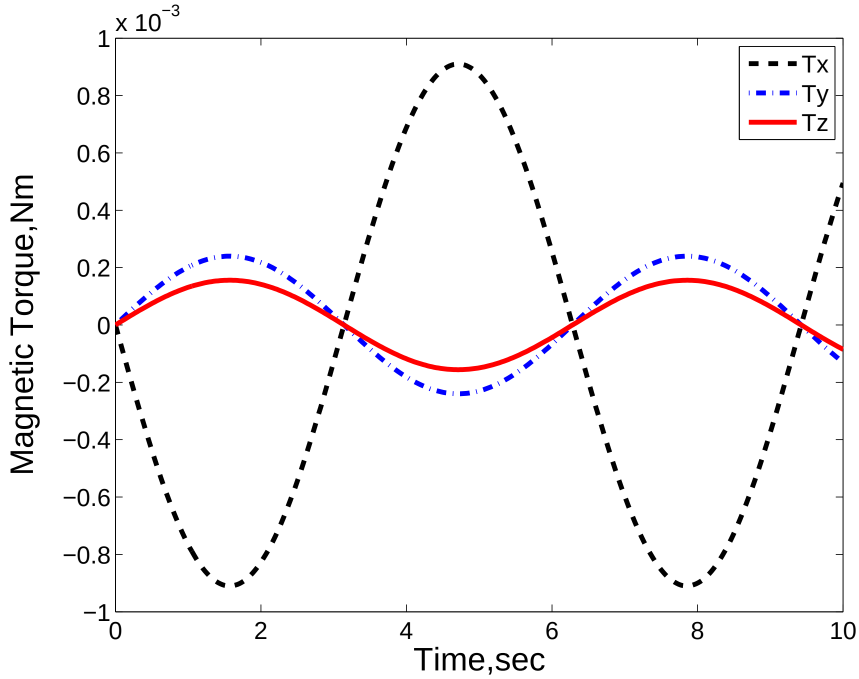

Figure 4.10: Control torque generated by magnetic torqrods during B-inverse simulation

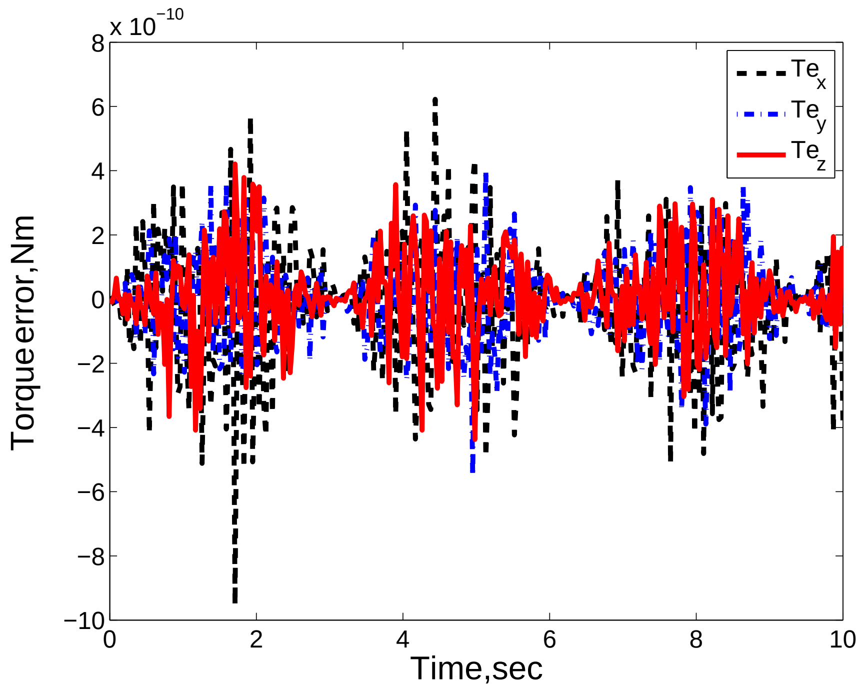

Figure 4.11: Error between desired and realized torque during B-inverse simulation

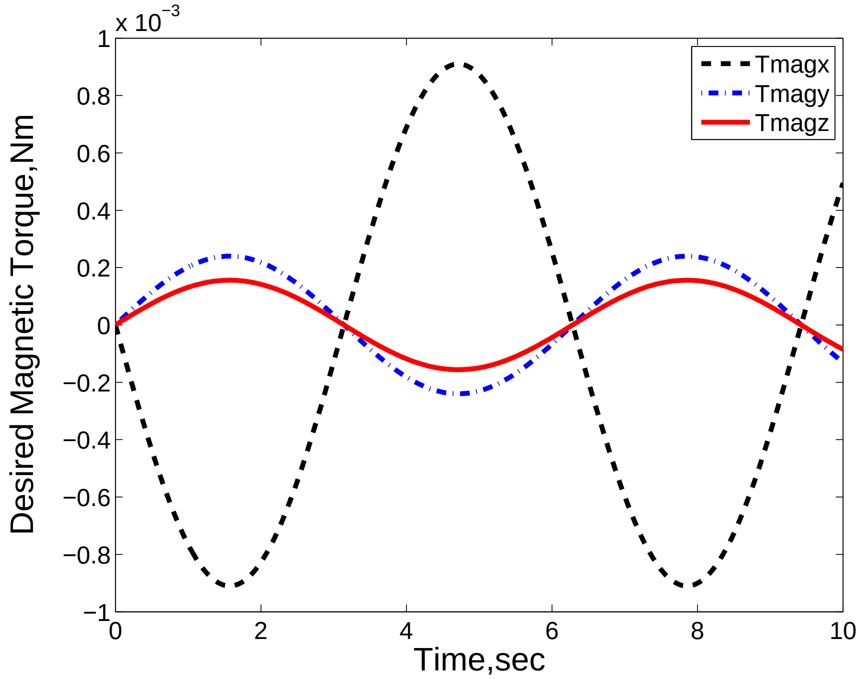

Figure 4.12: Desired magnetic torque generated during B-inverse simulation

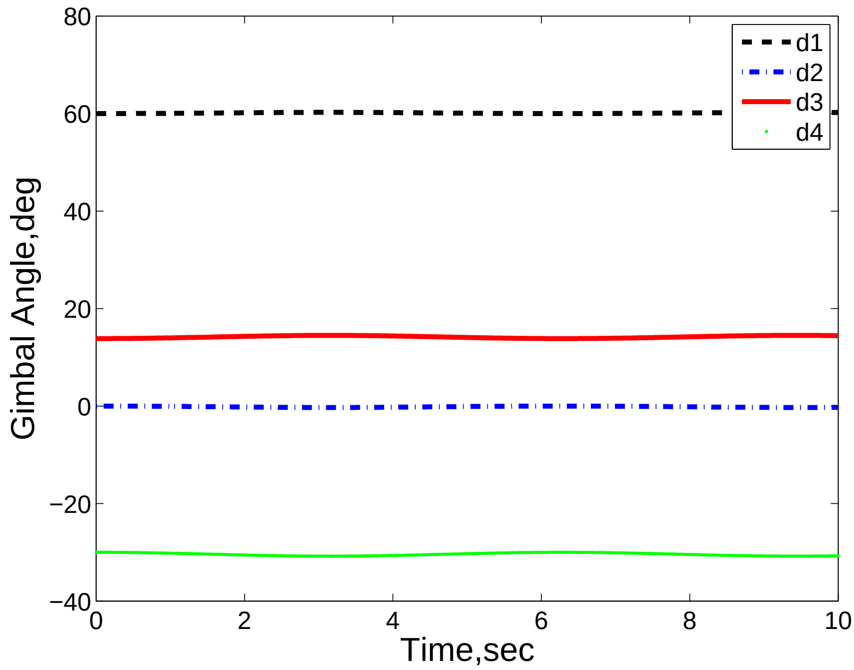

Figure 4.13: Realized gimbal angle history during simulation by B-inverse

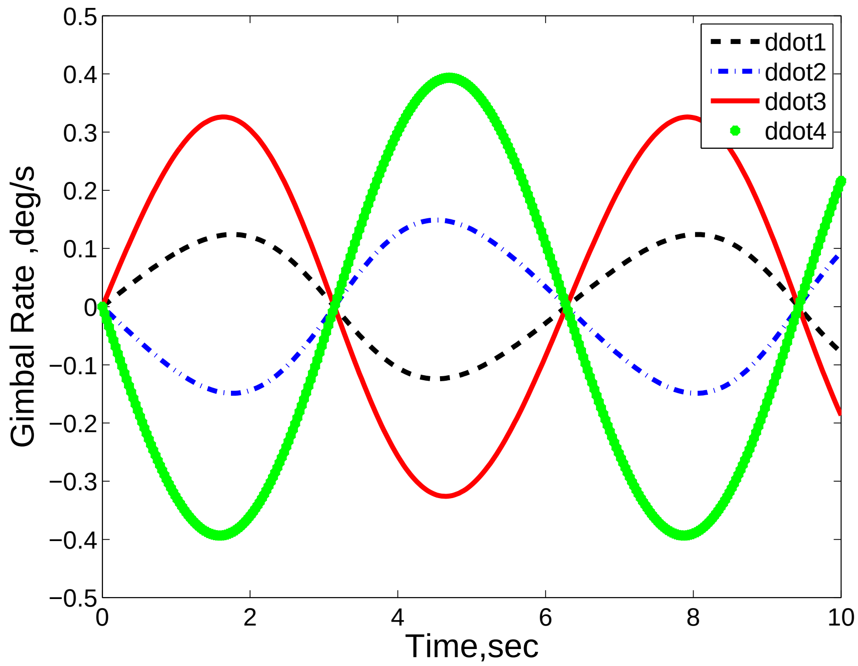

Figure 4.14: Gimbal rate history while steering algorithm using B-inverse

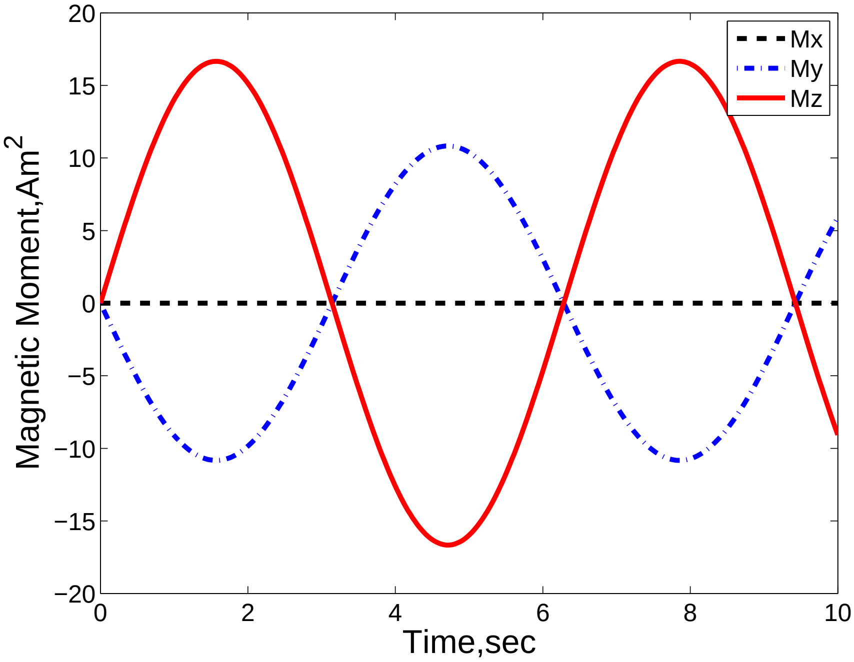

Figure 4.15: Magnetic moment history during pre-specified torque simulation by B-inverse

4.3.2 SATELLITE SLEW MANEUVER SIMULATION

This section satellite slew maneuver is carried out using MP-inverse and B-inverse algorithms. Figure 4.16 shows the spacecraft simulation code written in Simulink environment.

During simulations, a satellite with a diagonal moment of inertia matrix ($10kg.m^2$ in all axes) is used. To achieve commanded attitude, satellite slew maneuver with feedback control law given in Eq.2.7 is employed (Figure 4.17). Commanded attitude is chosen [-65 °; 0°; 0°] and it is implemented in code with a pre-filter to prevent saturations in the actuators at the beginning of the simulation (Figure 4.18) . Initial gimbal angles are taken $\delta_{\mathbf{0}}$ = [90°; 0°; -90 °;0°] which causes singularity in the CMG cluster employed.

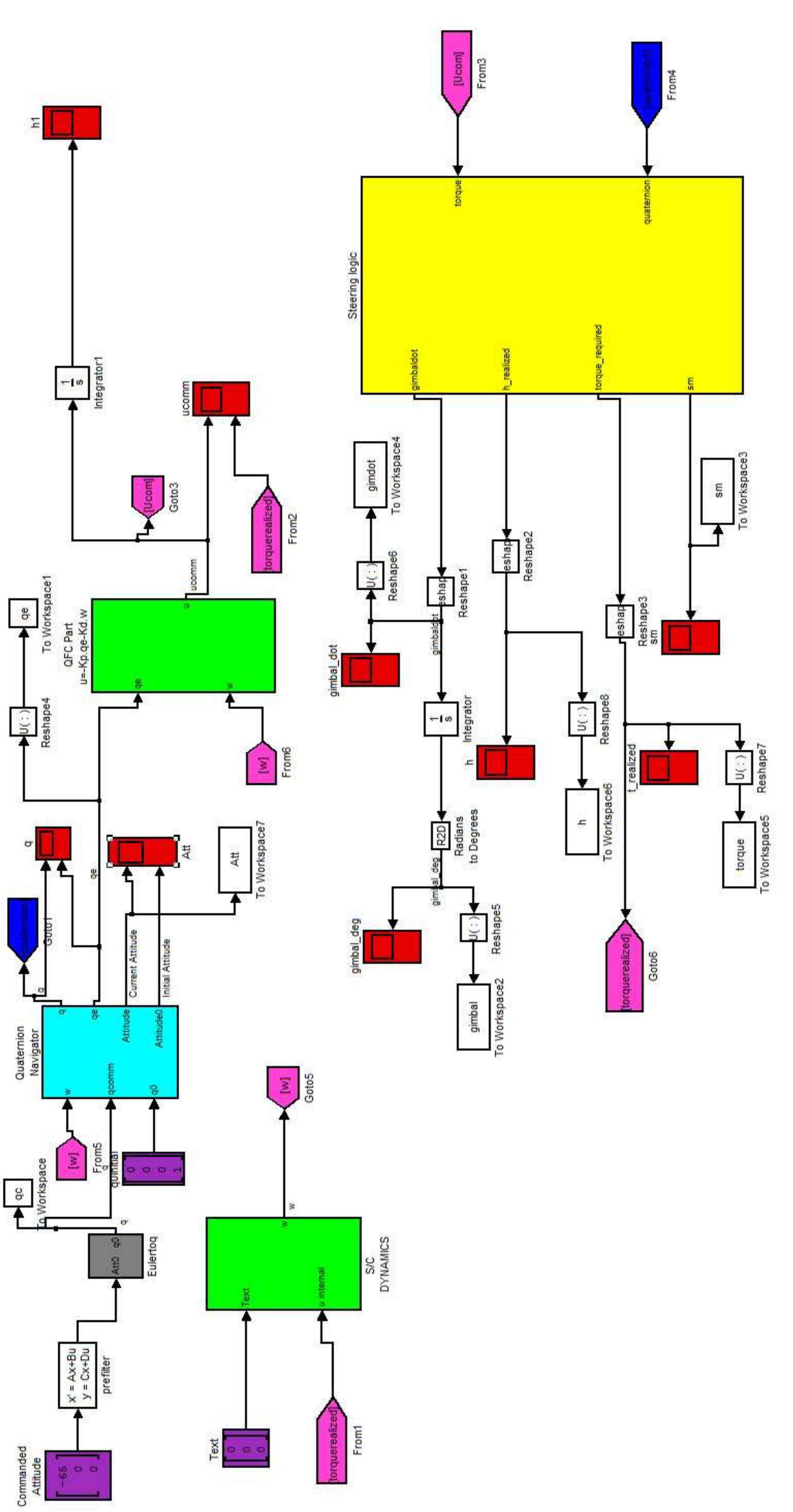

Figure 4.16: Spacecraft simulation using dissimilar actuators

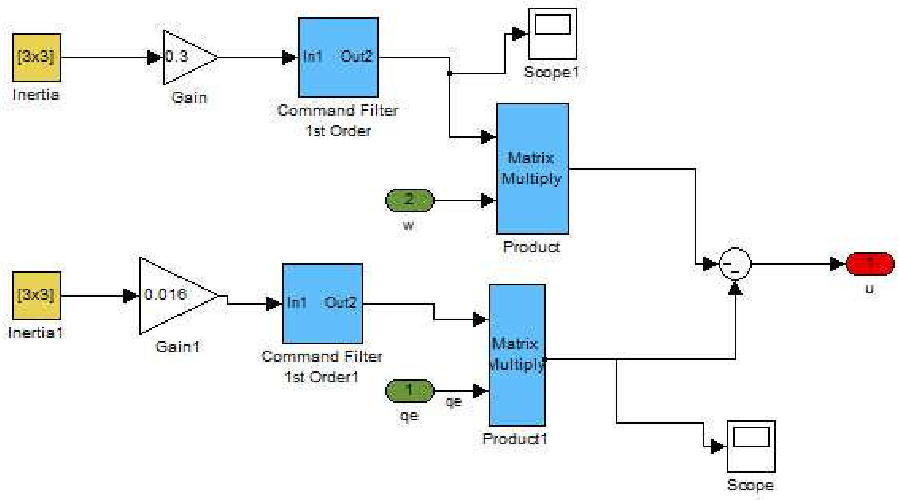

Figure 4.17: Quaternion feedback controller diagram in spacecraft simulation

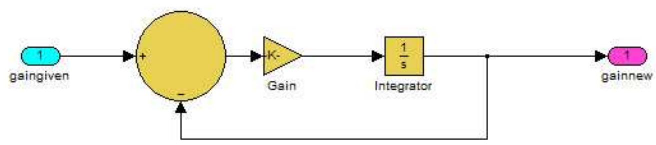

Figure 4.18: Command filter used in quaternion feedback controller

Magnetic field is taken as $[0.3; 0.8; 0.52] \times 48\mu\text{T}$ in Earth fixed frame as before.

4.3.2.1 Satellite Slew Maneuver Simulation Using MP-inverse Algorithm

In this section spacecraft simulation is realized as MP-inverse algorithm. Figure 4.19 shows the configuration of the steering logic part in the spacecraft simulation for MP-inverse algorithm.

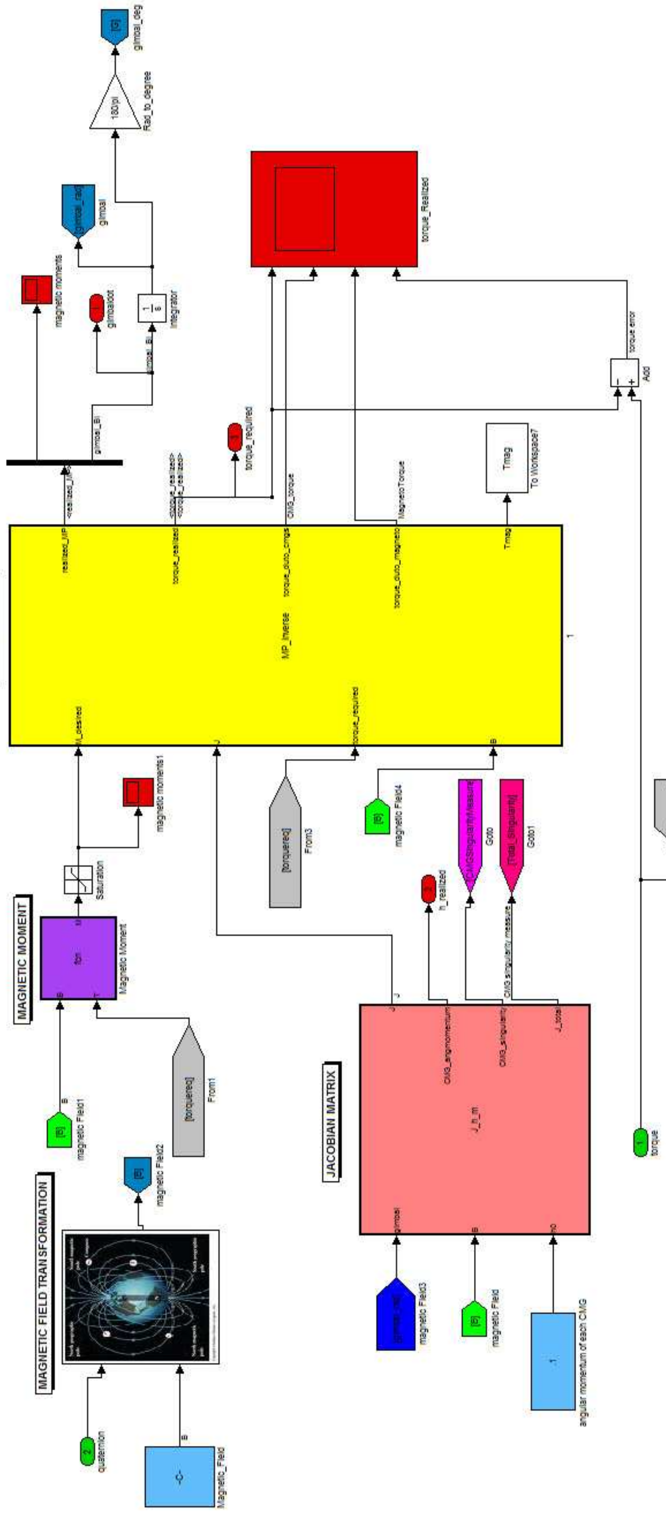

Figure 4.19: Steering logic part for MP-inverse algorithm

Figure 4.21 and Figure 4.22 shows the torque produced by the CMGs and magnetorquers respectively. From these figures it may be observed that most of the torque is realized by the CMGs. Observed error between desired and realized torque is very small since desired torque is realized without using two actuator at the same time (Figure 4.23). Figure 4.24 shows the singularity measure graphics. Since the CMG cluster is singular the total singularity measure becomes very small. This results in chattering in both the actuators and the gimbal rate history (Figure 4.25) as if the Jacobian matrix is rank deficient. However, the system recovers and satellite attitude maneuver is successfully completed (Figure 4.26).

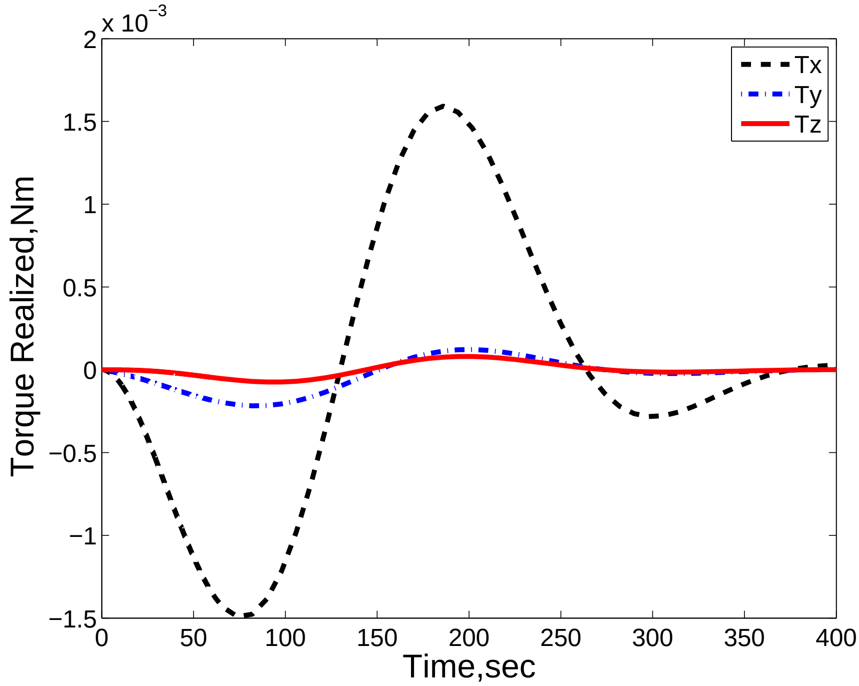

Figure 4.20: Torque realized during satellite simulation using MP-inverse

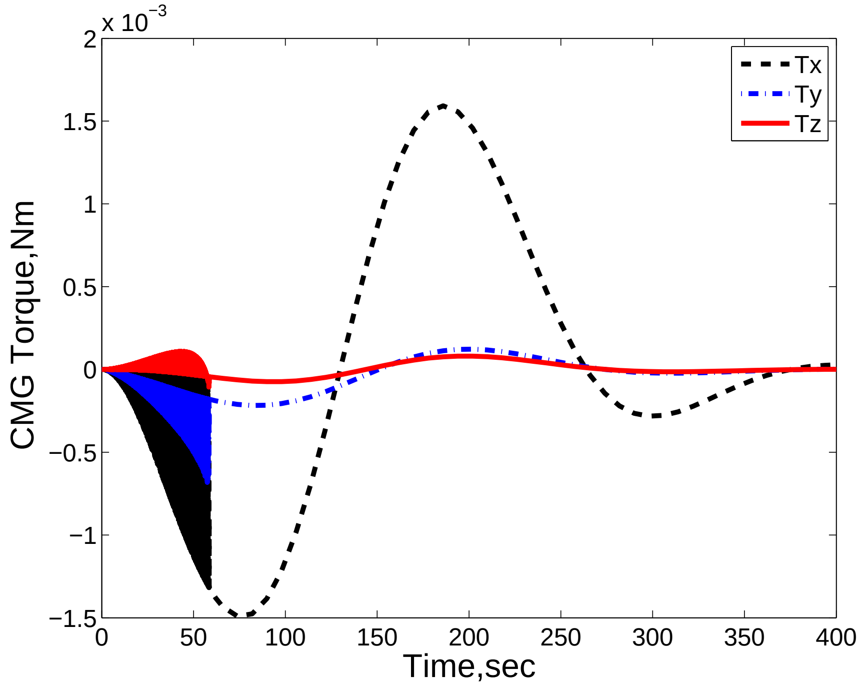

Figure 4.21: During satellite simulation CMG torque history for MP-inverse algorithm

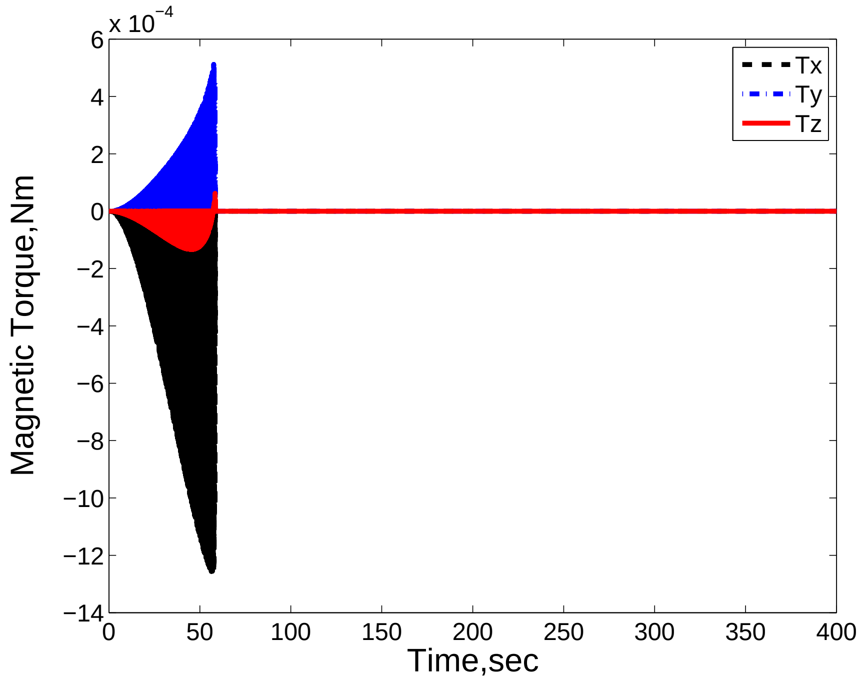

Figure 4.22: During satellite simulation magnetic torque history for MP-inverse algorithm

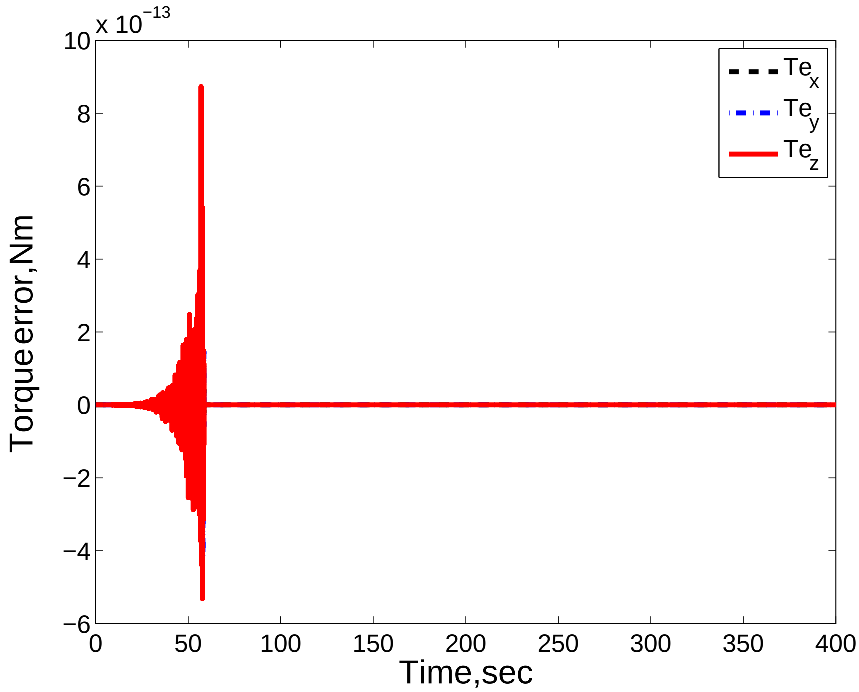

Figure 4.23: During satellite simulation torque error history between desired and realized one for MP-inverse algorithm

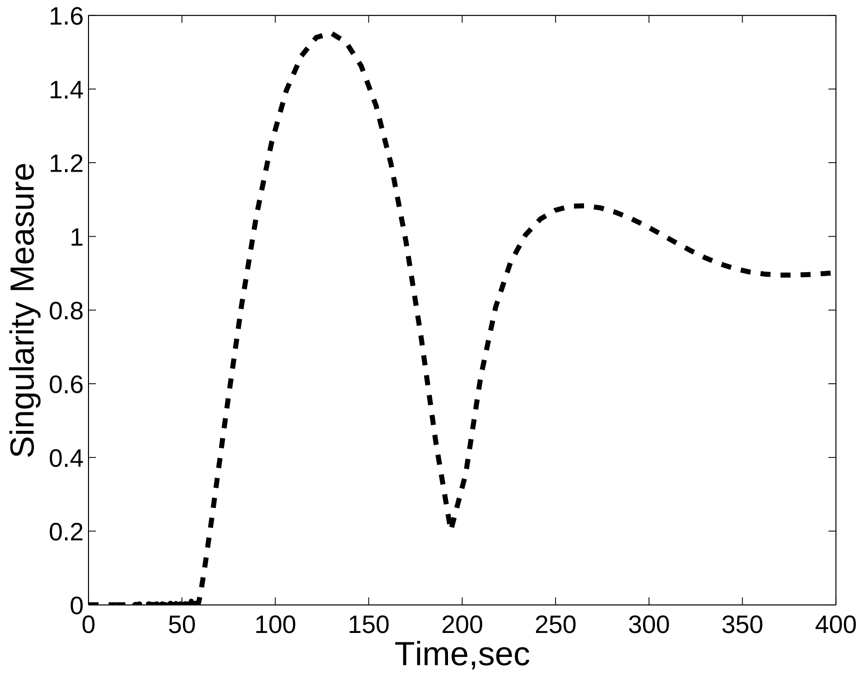

Figure 4.24: Singularity measurement using MP-inverse algorithm during spacecraft simulation

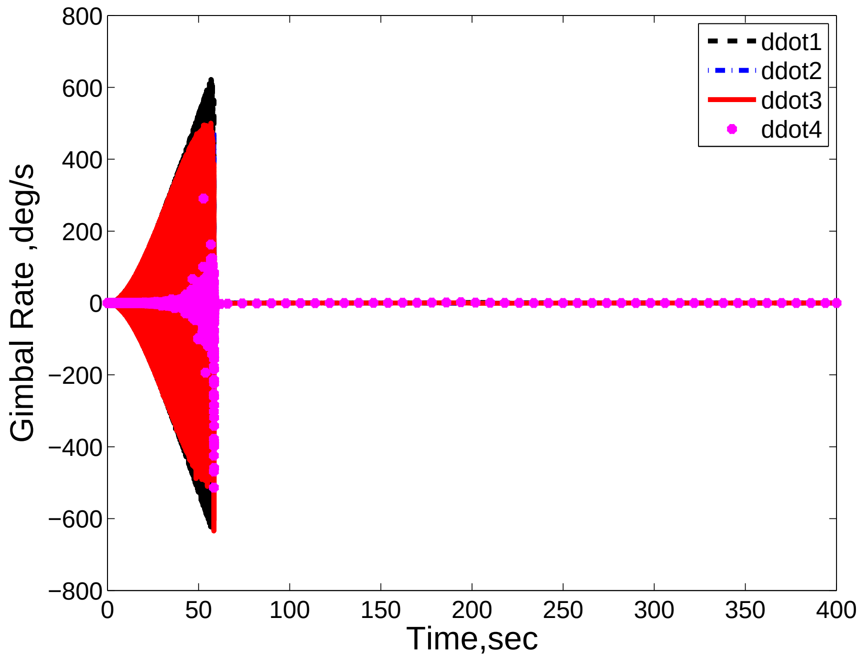

Figure 4.25: Gimbal rate history during simulation

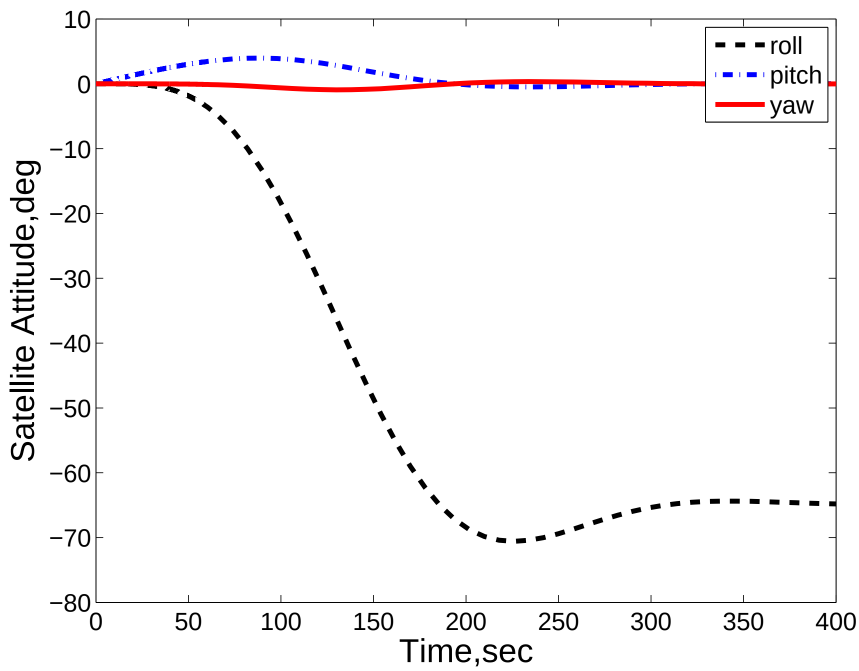

Figure 4.26: Spacecraft attitude during 400 sec simulation time with MP-inverse method

4.3.2.2 Satellite Slew Maneuver Simulation Using Blended Inverse Algorithm

In addition to the previous section, satellite simulation is also repeated this time using B-inverse algorithm. During simulations gimbals are again started from the CMG cluster singularity (i.e. [+90°; 0°; -90 °;0 °]). The blending coefficient is selected as $q = 1 \times 10^{-6}$. In general large blending coefficient causes too much torque error, while as very small blending coefficient will give a performance similar to the MP-inverse. Again the desired attitude [-65°; 0 °; 0 °] is commanded. As it may be observed from Figure 4.27. Torque realized is presented in Figure 4.28. Figure 4.29 and Figure 4.30 shows the torque produced by CMGs and magnetorquers respectively. Since using blended inverse algorithm, difference between realized and desired torque comes around 10^{-5} as expected (Figure 4.31). The desired gimbal rates are selected zero and desired magnetic moments are obtained from magnetic moment formula given above Eq.4.8.

Figure 4.32 shows the desired magnetic Torque history. Thus torque history is successfully realized. CMG on the other hand compensates this torque to achieve the overall desired resultant torque commanded by the feedback system. It may also be observed from these figures that the chatter is no longer present in the actuators. That is the end result of the B-inverse.

Figure 4.33 shows the singularity measure. Since gimbal angles start from the internal singularity point, at the first stages of simulation Eq.2.26 gives results close to zero. However, actuators are easily steering through non singular states. It is also seen from the gimbal angles history (Figure 4.34). In addition control magnetic dipole moment is not exceed the saturation limit as it is implemented to the code (Figure 4.35). Figure 4.36 shows the variations of gimbal angle history, also magnetic moment and gimbal rates are the inputs for achieving desired torque. With respect to torque that is generated from actuators, these variations of magnetic moment and gimbal rates are normal as we expected.

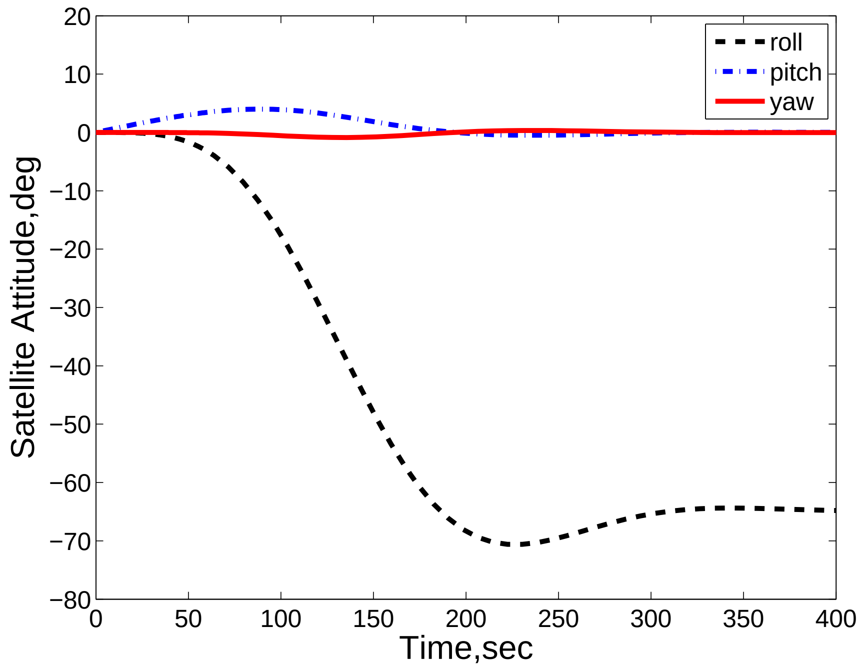

Figure 4.27: Spacecraft attitude during 400 sec simulation time with B-inverse method

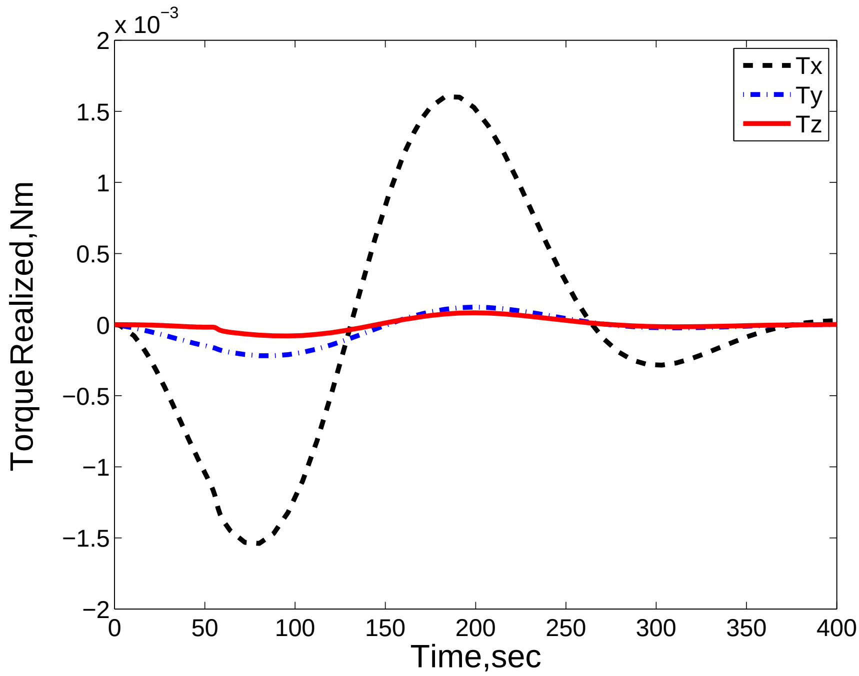

Figure 4.28: During satellite simulation realized torque history for B-inverse algorithm

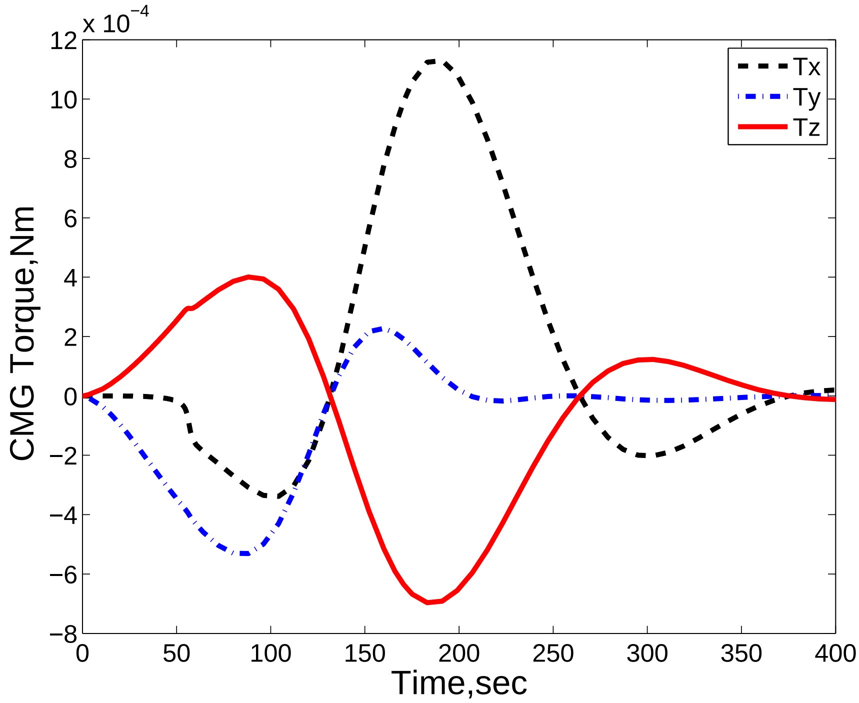

Figure 4.29: Realized torque history generated by CMGs using B-inverse algorithm

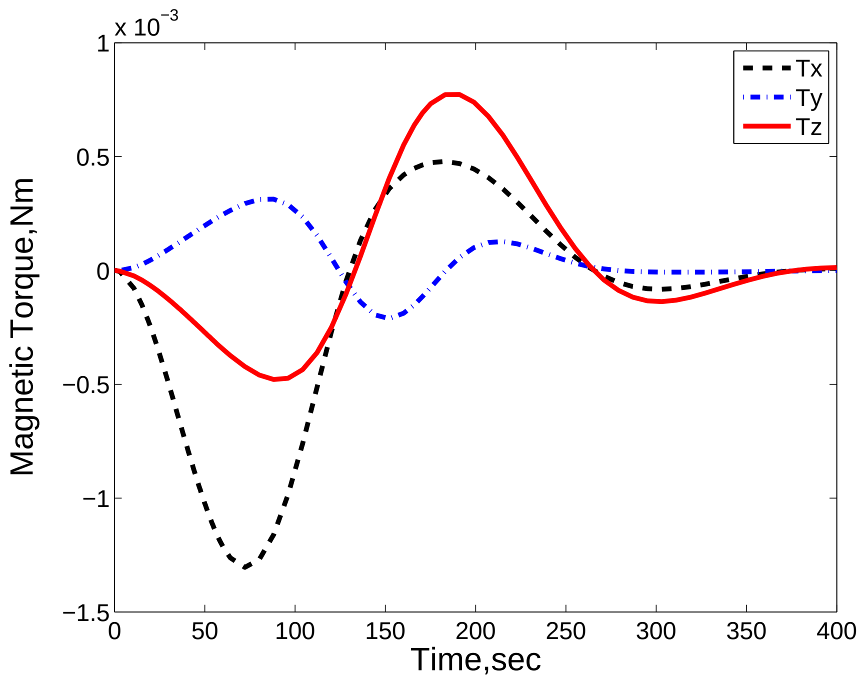

Figure 4.30: Realized torque history generated by magnetorquer using B-inverse algorithm

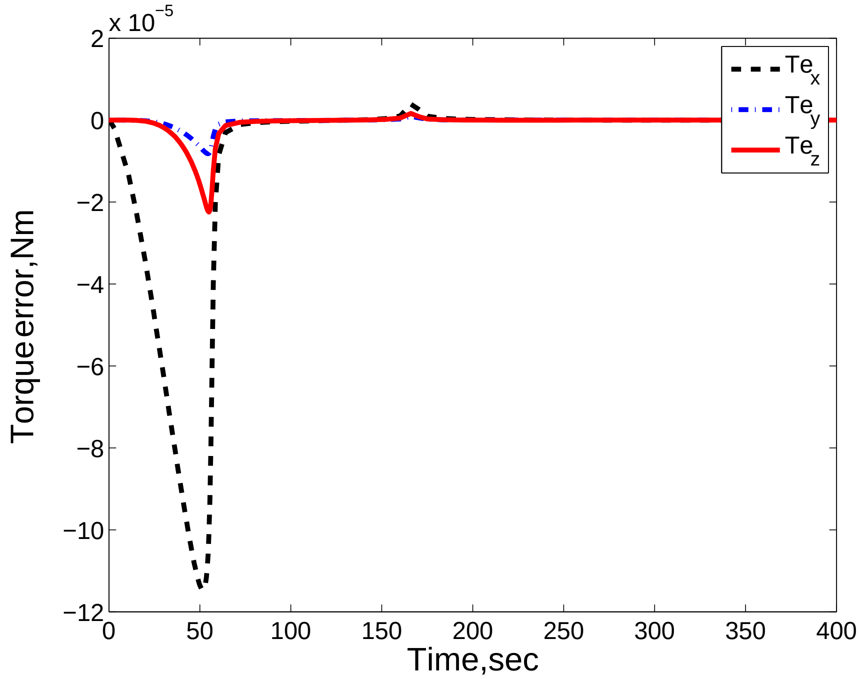

Figure 4.31: Torque error between desired and realized one

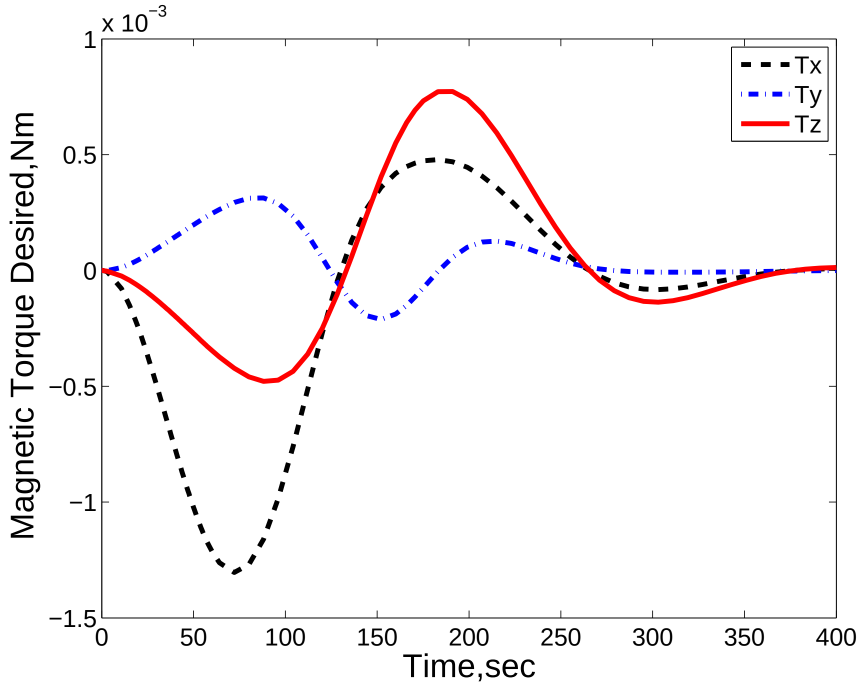

Figure 4.32: During satellite simulation desired magnetic torque history using B-inverse algorithm

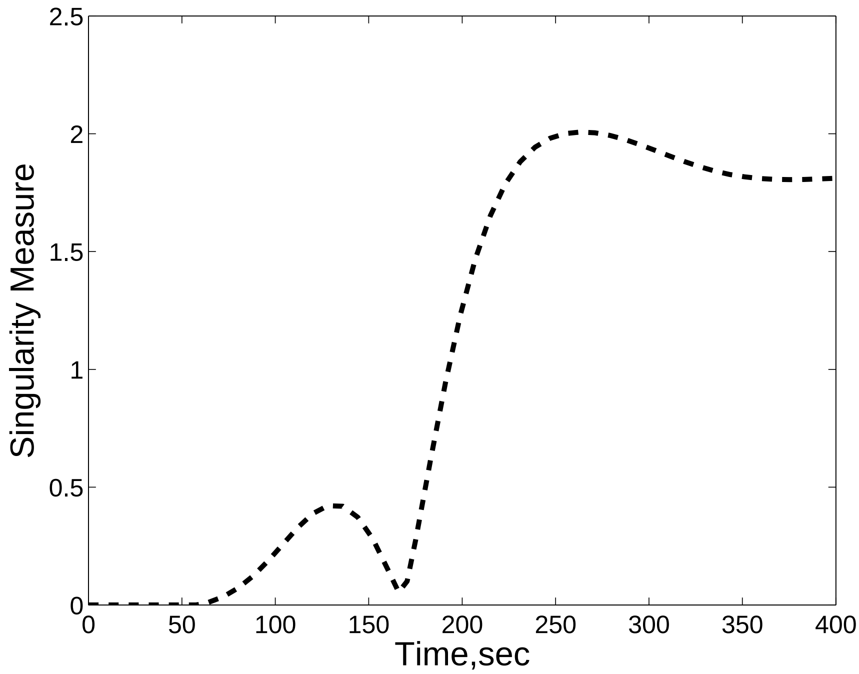

Figure 4.33: Singularity measure during spacecraft simulation using B-inverse

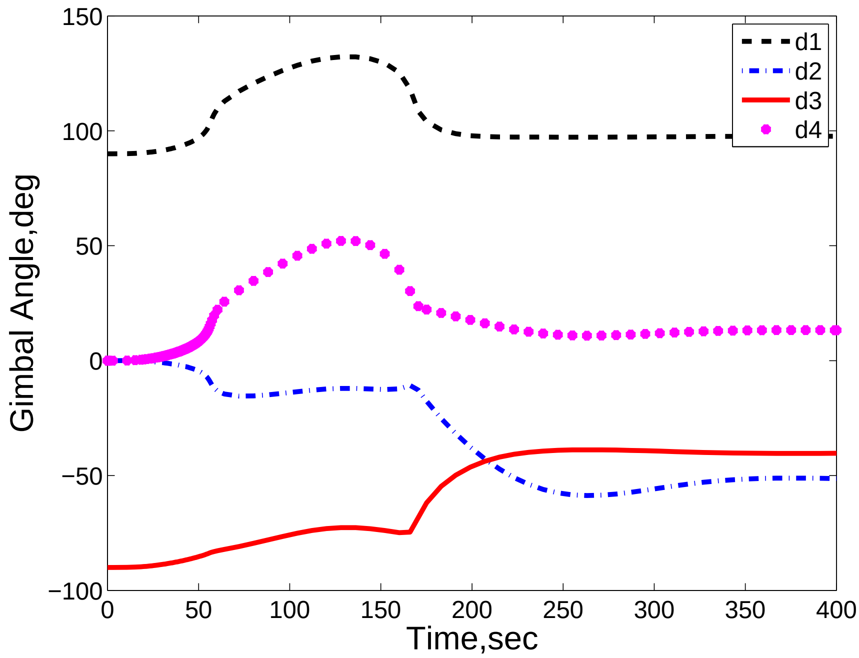

Figure 4.34: Gimbal angle history during spacecraft simulation using B-inverse method

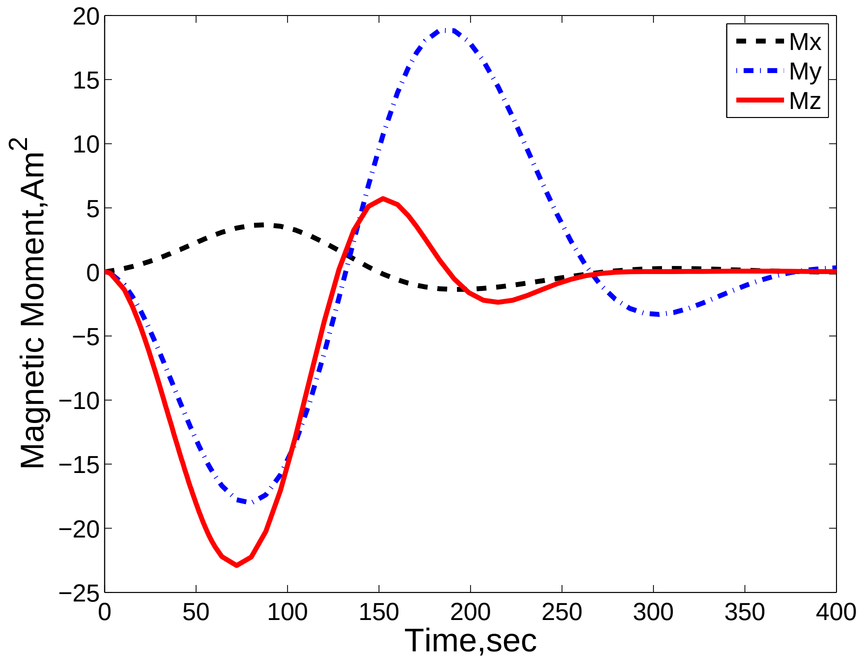

Figure 4.35: During satellite simulation magnetic moment history for B-inverse algorithm

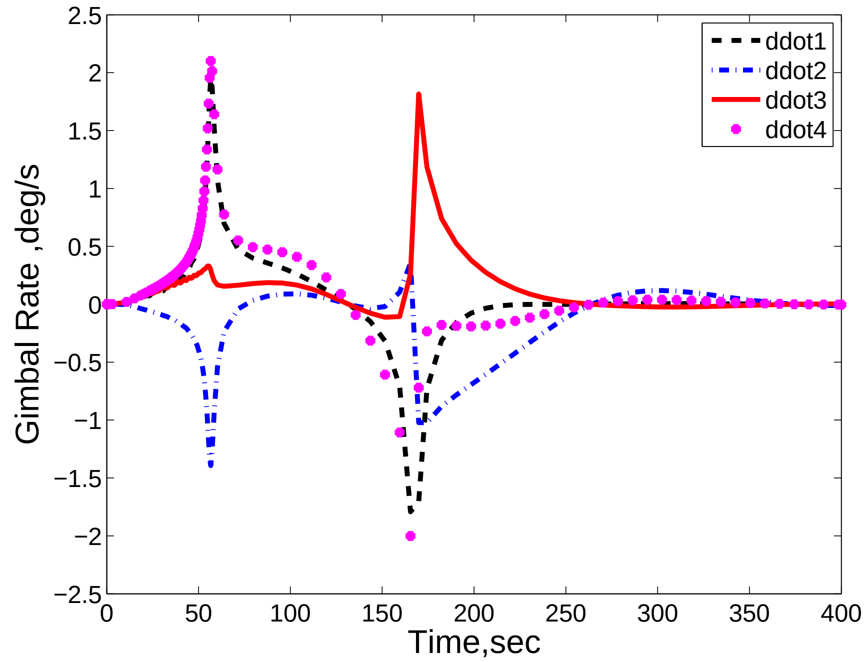

Figure 4.36: Gimbal rate history during satellite simulation using B-inverse

CHAPTER 5

CONCLUSION

In this thesis, the use of redundant actuators for satellite attitude control is investigated. Two problems are addressed.

In the first problem the steering of pyramid mounted CMGs with restricted gimbal angle travel is examined. First, momentum envelope is obtained for a CMG cluster with restricted gimbal angle travel. The steering with the shrunk momentum envelope is investigated by using both MP and Blended inverse steering algorithms, through simulations. Simulations has shown that with the MP inverse method is not successful. Thus, the desired torque could not be realized since the gimbal angles were saturated. On the other case, using blended inverse method and proper planing the desired torque is realized without encountering any gimbal angles saturation. Next, satellite slew maneuvers with restricted gimbal angle simulations is tested. During MP inverse simulations, as expected gimbal angles saturated. Thus satellite did not realize the desired maneuver. In contrast to the MP inverse simulation, blended inverse simulation, satellite slew maneuver successfully realized, showing the success of the B-inverse algorithm.

In the second problem steering with dissimilar redundant actuators is addressed. Using pre-specified torque and then satellite slew maneuver simulation again using Moore-Penrose Pseudo inverse and Blended inverse steering algorithm are employed. In pre-specified torque simulation using MP-inverse method, most of the torque is realized by the CMGs. On the other hand, using B-inverse algorithm it was possible to command magnetorquers to supply most of the torque. Then, satellite slew maneuver is examined. The CMG cluster gimbal angles are started from a singular configuration. Using MP-inverse algorithm desired attitude is realized with the excessive chattering of the gimbals and the magnetorquer whereas using B-inverse commanded attitude is generated without any chatter. In addition desired magnetic torque and realized magnetic torque that obtained using B-inverse simulation give same torque history.

In conclusion, using redundant actuator systems, the superiority of B-inverse algorithm above MP-inverse is demonstrated .

As a future work,

- The combined use of constrained gimbal angle CMG cluster and magnetorquer shall be considered.
- There is another study case that one should also consider to analyze the condition where one of the actuators is lost during the flight period which might help to assure the satellite investment is sale and secure.

REFERENCES

[1] Alfriend, K.T., *Magnetic Attitude Control System for Dual- Spin Satellites*, AIAA Journal, Vol. 13, June 1975, pp. 817-822.

[2] Bedrossian, N.S., Paradiso, J., Bergman,V., Rowell, D.,*Redundant Single Gimbal Control Moment Gyroscope Singularity Analysis*, Journal of Guidance, Vol.13, No.6., Nov-Dec 1990.

[3] Bedrossian, N.S., Paradiso, J., Bergman, E.,*Steering Law Design For Redundant Single-Gimbal Control Moment Gyroscopes*, Journal of Guidance, Vol. 13, No.6, Nov.-Dec.1990.

[4] Bedrossian, N.S., *Steering Law Design For Redundant Single Gimbal Control Moment Gyro Systems*, MS Thesis, Massachusetts Institute of Technology, 1987.

[5] Ergin, E.I., Wheeler P.C., *Magnetic Control of A Spinning Satellite*, Journal of Spacecraft and Rockets, 2, 6, NOv.-Dec. 1965.

[6] Elmas, T.C. ,Tekinalp , O. ,*Attitude Control Allocations Using Dissimilar Redundant Actuators*, IFAC ASME Symposium, ASME Dynamic System and Control Conference, Sep. 13-15 2010, Submitting.

[7] Goel, P.S., Rajarm, S., *Magnetic Attitude Control of a Momentum-Biased Satellite in Near-Equatorial Orbit*, Journal Guidance and Control ,Vol.2,NO.4, July-August 1979.

[8] Horri, N.M., Hodgart, S., *Large Angle Maneuver of Under Actuated Small Satellites Using Two Wheels*, 4th IAA Symposium on Small satellites for Earth Observation, Berlin, Germany, April 7-11, 2003.

[9] Jackot, A.D., Liska, D.J.,*Control Moment Gyros in Attitude Control, Journal of Spacecraft and Rockets*, 3(9), 1966, pp. 1313-1320.

[10] Kahraman, Ö.,*Control Allocation Against Actuator Failures In Overactuated Small Satellites*, M.S. thesis,Middle East Technical University,2007.

[11] Kurokawa, H.,*A Geometric Study of Single Gimbal Control Moment Gyros*, Report of Mechanical Engineering Laboratory, No. 175, p.108, 1998.

[12] Kurokawa, H.,*Constrained steering Law of Pyramid-Type Control Moment Gyros and Ground Tests*, Journal of Guidance, Control ,and Dynamics,Vol.20, No.3 ,May -June 1997.

[13] Lappas,V.J., Steyn W., Underwood C.I.,*Attitude Control For Small Satellites Using Control Moment Gyros*, 52nd IAF,2001.

[14] Lappas V. J., Steyn W., Underwood C., *Control Moment Gyro Gimbal Compensation Using Magnetic Control During External Disturbances*, AIAA Guidance, Navigation and Control Conference and Exhibit, Montreal, Canada, 6-9 August 2001.

[15] Lappas, V.J., Wie,B., *Robust CMG Steering Logic with Gimbal Angle Constraints*, Proceedings of the AIAA/AAS Astrodynamics Specialist Conference, Paper No: AIAA-2006-6651, Keystone, Colorado, August 21-24, 2006.

[16] Lappas, V.J.,*A Control Moment Gyro Based Attitude Control System For Agile Satellites*, PhD. Thesis,University of Surrey, Guilford, Surrey, United Kingdom, October 2002.

[17] Lorenzo, S., Bruno, S.,*Modeling and Control of Robot Manipulators*, McGraw Hill, New York, 1996.

[18] Lovera, M., De Marchi, E., Bittanti, S.,*Periodic Attitude Control Techniques for Small Satellites With Magnetic Actuators*, IEEE Transactions on Control Systems Technology,Vol.10,N0.1,January 2002.

[19] Margulies, G., Aubrun J.N., Geometrical Theory of Single Gimbal Control Moment Gyro System, The Journal of the Astronautical Sciences, Vol.XXVI, No.2, pp .159-191 , April-June 1978.

[20] Meffe, M. Stocking, G., *Momentum Envelope Topology of Single-Gimbal CMG Arrays for Space Vehicle Control*, Proceedings of AAS Guidance and Control Conference, Keystone, CO, Jan.-Feb. 1987, AAS Paper 87-002.

[21] Nakamura, Y., Hanafusa, H.,*Inverse Kinematic Solutions with Singularity Robustness for Robot Manipulator Control* Journal of Dynamic Systems, Measurement, and Control, Vol. 108, 1986, pp. 163- 171.

[22] Renard, M.L.,*Command Laws for Magnetic Attitude Control of a Spin-Stabilized Earth Satellites*, Journal of Spacecraft and Rockets, Vol. 4, Feb. 1967, pp. 156-163.

[23] Robert, B.A., Kurk, J.W., Englar, T.S.,*Three-axis Attitude Control with Two Reaction Wheels and Magnetic Torquer Bars*, AIAA Guidance, Navigation, and Control Conference and Exhibit, Providence, Rhode Island, 16-19 August 2004.

[24] Sidi, M.J.,*Spacecraft Dynamics and Control, a Practical Engineering Approach*, Cambridge University Press, 1997.

[25] Steyn, W.,*Comparison of Low-Earth-Orbit Satellite Attitude Controllers Submitted to Controllability Constraints*, Journal of Guidance, Control, and Dynamics, Vol.17, No.4, July-August 1994.

[26] Stocking, G.,*Design Study Report Momentum Control System Study*, Sperry Flight Systems, November 1978.

[27] Tekinalp, 0., Elmas, T., Yavrucuk, I., *Gimbal Angle Restricted Control Moment Gyroscope Clusters*, RAST 2009, Recent Advances in Space Technologies, Istanbul, Turkey, 11-13 June, 2009.

[28] Tekinalp, O., Yavuzoglu, E., *A New Steering Law for Redundant Control Moment Gyroscope Clusters*, Aerospace Science and Technology, Vol. 9, No. 7, October 2005, pp. 626-634.

[29] Tsiotras, P., Doumtchenko, V.,*Control of Spacecraft Subject to Actuator Failures: State-Of-Art and Open Problems*, R. H. Battin Astrodynamics Symposium, Texas A&M, College Station, TX, AAS paper 00-264, March 20-21, 2000.

[30] Vadali, S. R., Oh H., and Walker, S., *Preferred Gimbal Angles for Single Gimbal Control Moment Gyroscopes*, Journal of Guidance, Control and Dynamics, Vol. 13, No. 6, 1990, pp. 1090-1095.

[31] White,J.S., Shigemoto, F.H. ,and Bourqin, K., *Satellite Attitude Control Utilizing the Earth's Magnetic Field*, National Aeronautics and Space Administration, Technical Report Nasa TN-D1068, Aug. 1961.

[32] Wheeler, P.C., *Spinning Spacecraft Attitude Control via The Environmental Magnetic Field*, Journal of Spacecraft and Rockets, 4,12, Dec. 1967, 1631-1637.

[33] Wie, B.,*Space Vehicle Dynamics and Control*, AIAA Education Series, AIAA Inc. Reston, VA, 1998.

[34] Wisniewski, R., Stoustrup, J.,*Periodic H_2 Synthesis for Spacecraft Attitude Control with Magnetorquers*, Journal of Guidance, Control, and Dynamics, Vol.27, No.5, September -October 2004.

[35] Yavuzoglu, E.,*Steering Laws For Control Moment Gyroscope Systems Used In Spacecrafts Attitude Control*, MS Thesis, Middle East Technical University, 2003.

[36] MTR 30 Magnetorquer, *http://centaur.sstl.co.uk/datasheets/Subsys_MTQ.pdf* as accurate as 19.January.2010.

[37] SLIPRING.COM, *http://www.slipring.com/images/Thru_Hole_25mm_ID.pdf* as accurate as 27.January.2010.

[38] Magnetic Field, *http://www.physics.sjsu.edu/becker/physics51/mag_field.htm* as accurate as 2.January.2010